Studies on the short term planetary wave activity in the MLT region over Southern Hemisphere using SuperDARN HF radar.

by

Ntlakanipho Ngwane

Submitted in fulfilment of the academic requirements for the MSc degree in the School of Chemistry and Physics, University of KwaZulu-Natal Durban

June 2016

As the candidate's supervisor I have/have not approved this thesis/dissertation for

submission

Signed:_____________ Name:____________________ Date:_______

Signed:______________ Name:___________________ Date:_______

Abstract

The atmospheric vertical pressure profile, chemical composition and temperature distribution, together, define a set of conditions governing the manifestation of atmospheric dynamics. Observations and extensive research shows that lower atmospheric layers play host to the formation of forced atmospheric waves such as atmospheric planetary waves and solar tides. These waves serve as transportation modes for energy budgets and ascend to upper atmospheric layers where they induce significant meteorological processes. Planetary waves, tides and gravity waves often dissipate energy in the mesosphere lower-thermosphere (MLT) region.

This dissertation presents a study of the planetary wave variability in the MLT region using the South African National Antarctic Expedition High Frequency (SANAE HF) radar data, a component of the Super Dual Auroral Radar Network (SuperDARN). The focus is on short term planetary waves with periods ranging from 2 to 6 days. This planetary wave variability in the MLT is investigated during the occurrence of minor sudden stratospheric warming (SSW) events. The study also investigates the assertion that there is a non-linear interaction between planetary waves and atmospheric tides.

The mesospheric wind data considered stretched from year 1998 to year 2008. The criterion towards a conclusive investigation of short term planetary waves included determining years within the said interval (1998 to 2008) with minor SSW events. The 11 year long temperature data from the NCEP/NCAR reanalysis project was used for this. The study managed to show the previously stated finding that mesospheric wind reversal occurs a week prior the stratospheric wind reversal linked with the warming. Years 2002, 2003 and 2007 were shown to host minor SSW events. In year 2002, minor SSW events occurred in days 235, 243 and day 255. In year 2003, the minor SSW event occurred in day 280. The minor SSW for year 2007 occurred in day 263. This meant that the planetary wave variability and the non-linear interaction between planetary waves and tides is investigated in the said years only. The short time Fourier transform technique (STFT) was used to reveal the tidal wave behaviour in the MLT region. It was observed that the semi-diurnal tide (SDT) is the most active tide at high latitudes.

The wavelet transform was used to show the planetary wave variability in the MLT region. Along the zonal component, the activity in year 2002 was shown to be the most robust compared to the activity in years 2003 and 2007. In the meridional component, the planetary wave behaviour in year 2007 was the most active compared to years 2002 and 2003.The wavelet transform was simultaneously used to implement the first phase towards asserting the non-linear interaction between planetary waves and atmospheric tides. This phase is termed SDT modulation. In year 2002, 2 day and 3 day p-waves possibly modulated an SDT along the zonal component while 3 day and 6 day p-waves possibly modulated an SDT in the meridional component. In 2003, both along the zonal and the meridional

components, the 4 day p-wave possibly modulated an SDT. In year 2007, a 6 day and a 4 day p-wave possibly modulated an SDT along the zonal and meridional components respectively.

The proposition that there is a possible non-linear interaction between p-waves and tides was further reinforced using the bispectrum analysis. This method revealed the interaction predicted by the modulation phase. Peaks signifying p-wave SDT wave interaction were observed. These peaks were all consistent with the modulation that was said to have occurred between p-waves and SDTs. The third step in validating the stated assertion involved looking for secondary waves that may have formed due to a possible primary wave (p-waves and SDTS) interaction. This step was conducted on periods suggested by the SDT modulation. In every p-wave SDT wave suspected interaction as per the SDT modulation, secondary waves were shown to exist.

Preface

The experimental work described in this thesis was carried out at the School of Physics, University of KwaZulu-Natal, Durban, from February 2014 to June July 2016 under the supervision of Professor Sivakumar Venkataraman, and under the co-supervision of Dr. Sibusiso H. Mthembu. These studies represent original work by the author and have not otherwise been submitted in any form for any degree or diploma to any other tertiary institution. Where use has been made of the work of others it is duly acknowledged in the text.

Ntlakanipho Ngwane

Declaration – Plagiarism

I, Ntlakanipho Ngwane, declare that

1. The research carried out in this dissertation, except where otherwise stated, belongs to the author.

2. This research has not been forwarded for any qualification to any other institution of higher learning.

3. All the data, pictures and plots included in this dissertation belong to the author unless or otherwise mentioned and duly acknowledged.

4. Every text or writing included in this dissertation has been written by the author unless stated otherwise or duly acknowledged. In cases where text has been quoted, statements have been reworded and ownership through referencing has been given to the original author. In instances where words have been used as they are, the text has been placed in italics with quotation marks and referenced.

5. This work contains no information of any form copied and pasted directly from the internet unless duly acknowledged.

Signed: _____________________________

Acknowledgements

- I would like to extend my sincere gratitude to my supervisory team, Professor V. Sivakumar who is the primary supervisor and Dr. S. Mthembu my co-supervisor. Under your wings, I felt rare comfort and security as your expertise guided me to where we are today.

- I would also like to thank the University of KwaZulu Natal for all the facilities they offered me.

- My utmost gratitude goes to my sponsor, the South African National Space Agency (SANSA) for their support financially and through motivation. This journey would not have been possible without your assistance and patience.

- I would like to thank all my friends for their unwavering support throughout this journey. Ninginike ithemba lapho ngizizwa ngikhathala. Kuwena Phephelani Zondi, Sam Gasa, Bongs Ndlovu, Mzamo Zondi nawe Mbalenhle Thusi ngibonga kakhulu.

- My heartfelt gratitude goes to the love of my life Nokuphiwa Khumalo. You were with me since the beginning of this journey and you were the source of strength when I felt I could not go on. Mzilikazi kaMashobane, Mntungwa, Mbulazi!

- My sisters Nomzamo and Bongekile Ngwane will always serve as motivation for me to achieve greater heights. Your constant and consistent belief in your brother will be rewarded one day.

- To my nieces Amanda, Hlengiwe, Sbahle and my nephew Buhle and every other African child, may you draw inspiration from this work and seek to achieve even greater things.

- Ngalencwadi ngamukela umafungwase wakwaNgwane, indodakazi yami uNtandokazi Kuhlekonke Ngwane. Uyathandwa ntombazane.

I dedicate this dissertation to my parents, ***Ncediwe L. Ngwane*** *my mother and the late* ***Albert K. Ngwane*** *my father. May this document reflect the amount of effort you put towards shaping a man that I am today. This is your legacy.*

Table of Contents

Chapter 1

Introduction and Background Theory

The Earth's atmosphere is a multi-layered gas, which fills its immediate environment extending upwards from the surface of the Earth. Relative to the heliosphere, the Earth's atmosphere can be thought of as the Earth's thin blanket which facilitates life. It has no upper limit but blends in an unconstrained manner with interplanetary space. It constitutes several gases with varying concentrations. These gaseous constituents contribute to the health of the Earth's atmosphere and their chemistry has an influence on the physical dynamics that different layers exhibit. Nitrogen and oxygen molecules account for about 99 percent of the total gas content in the atmosphere. They (nitrogen and oxygen molecules) are referred to as permanent gases due to their low variability with time (Saha, 2008). Other gases making up the Earth's atmosphere include carbon dioxide, argon, water vapour, ozone and other anthropogenic particles which are all variable with time. Anthropogenic particles may include smoke, dust particles, chlorofluorocarbons (CFCs) and other human deposits onto the atmosphere. A bar graph on Figure 1.1 is a representation of the atmospheric molecular concentration. The molecular concentration is measured in parts per million by volume (ppmv). Molecular concentrations shown in Figure 1.1 were measured from the mean sea level (see Schlatter, 2009).

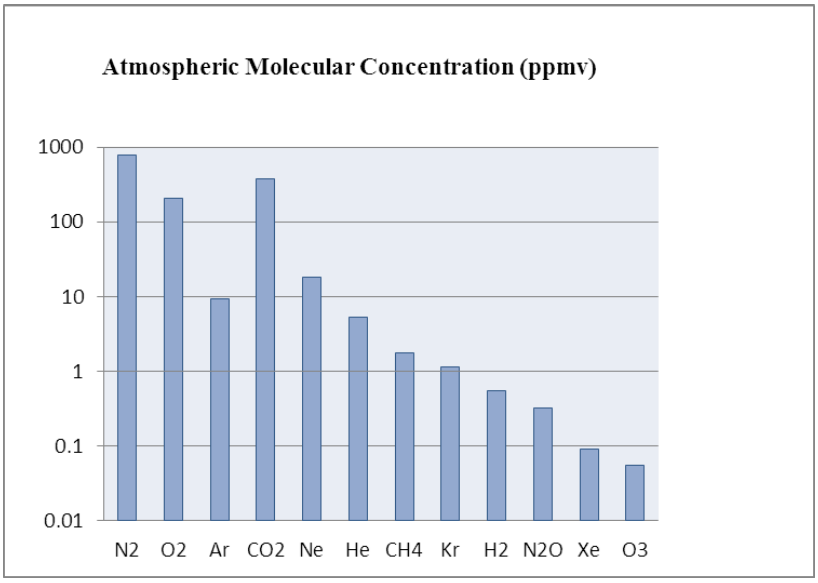

Figure 1.1: A bar graph showing atmospheric gas composition in dry air using molecular concentration. The ozone molecule (O3) varies between 0.01 and 0.1 ppmv. Source: Schlatter (2009)

On a molecular scale, the Earth's atmosphere can be thought of as an infinite space consisting of independent particles that exhibit negligible interactions with each other; hence it can be treated as an ideal gas (Saha, 2008). The ideal gas assumption reduces significant properties in the physics of the atmosphere to pressure, temperature and density. A brief discussion of each of these properties in terms of their variability, how they are measured and their influence on the state of the atmosphere is given.

Atmospheric pressure is defined as the weight of the overlying air per unit area of the surface at that level (Saha, 2008). It is therefore a maximal value at the surface of the Earth and decreases with increasing height. Pressure is significant in atmospheric dynamics in that it dictates wind propagation. Wind propagates from high to low pressure regions. Disturbances and fluctuations during wind propagation lead to the formation of atmospheric waves which then serve as a transport for heat, momentum and time varying particles (Walterscheid et al., 2000). This explains the dynamic ascendance of planetary waves from tropospheric heights to the upper atmospheric layers. The atmospheric vertical pressure profile can be produced using a formulation given as

$$p(z) = p_0 e^{\frac{-z}{H}}, \tag{1.1}$$

where $p(z)$ is the pressure at any atmospheric height z, H is the scale height equalling RT_0/g and p_0 is the pressure at Earth's surface. R is the universal gas constant, T_0 is the temperature at the Earth's surface and g is the gravitational acceleration at Earth's surface. Atmospheric pressure also varies horizontally along the Earth's topography. The horizontal pressure distribution dynamically forces air to be displaced from high to low pressure regions. This motion is described by the relation given as

$$F = \frac{1}{\rho}\frac{\nabla p}{d}, \tag{1.2}$$

where F is the pressure gradient force, ∇p is the pressure gradient, d is the distance between two points and ρ is the air density.

Density in the atmosphere is the quantity that measures the amount of matter per unit volume. It is defined as the mass per unit volume. The existence of some particles in the Earth's immediate space is what sustains life for living organisms. The gravitational pull causes heavier elements to settle in lower layers of the atmosphere. The Earth's atmosphere is therefore denser near the surface and becomes lighter as the altitude increases. This physical fact is important in the dynamics of the atmosphere and influences chemical reactions, circulations and other atmospheric events. Global climate change, ozone depletion et cetera are well explained through studying the atmospheric density.

The chemical composition of the Earth's atmosphere and the resulting phenomena does affect the atmospheric heat distribution. Measuring atmospheric temperature then improves one's appreciation of the dynamics taking place. It has been shown experimentally that the Earth's atmospheric temperature exhibits steady behaviour for specific height intervals. This behaviour led to the stratification of the Earth's atmosphere according to temperature variations. The temperature distribution in the Earth's atmosphere is demonstrated through vertical profiling of the atmosphere. Different layers are defined and they all depict a particular heat distribution due to either physical dynamics or the chemical composition. They are described in the vertical structure of the atmosphere (see section 1.1).

The three physical quantities discussed above (atmospheric pressure, density and temperature), impact on atmospheric circulations and often lead to the ascendance of forced waves from tropospheric heights into the mesosphere lower thermosphere (MLT) region where they trigger interesting physical phenomena.

The MLT region connects the middle atmosphere to the upper atmosphere. It covers the complete mesospheric layer at about 50 to 60 km above mean sea level and extends to the lower thermosphere at about 120 km. Its strategic position triggers interesting physical and chemical phenomena. It hosts a combination of physical dynamics due to forced waves from lower atmospheric layers and photochemical reactions enhanced by solar radiation. It proves rather complicated to trace the origins of mechanisms observable in the MLT region given the dynamic duo-influence (solar radiation and forced wave behaviour). Atmospheric waves playing major role in MLT dynamics include gravity waves, tides and planetary waves (Johnson and Killeen, 1995). The MLT region is deemed unique and significant in the Earth's atmosphere owing to complex mechanisms that it hosts. Researchers (for eg: Pancheva, 2000; Pancheva and Mitchel, 2004, Sridharan et al., 2009; Chang et al., 2009) have been simulating observations to better understand the dynamical behaviour in this region. Most of the MLT research has been carried out in the Northern Hemisphere. A lot still has to be done in the Southern Hemisphere. Fewer reseachers have published findings on the MLT dynamics looking from the south (see Riggin et al., 1999; Hibbins et al., 2007; Murphy et al., 2007 etc).

This work focuses on the influence that forced atmospheric waves (for eg. planetary waves and solar tides) from lower atmospheric layers have on MLT dynamics. Super Dual Auroral Radar Network (SuperDARN) High Frequency (HF) radar is used to study short term planetary wave activity in the MLT over Southern Hemisphere. In this work the 'short term planetary wave' terminology refers to planetary waves with a period range of 2-6 days. The emphasis on the short term behaviour is motivated by the substantial work conducted on the relatively large period planetary waves (for eg. 14, 16, 20, 23 and 27 day waves). Similar methods applied when studying long term atmospheric waves are used on short term waves so as to broaden the present understanding and appreciation of MLT dynamics. This work also studies interactions between tides and planetary waves in the MLT region. The planetary wave activity and planetary wave- semi diurnal tide (SDT) possible interaction is investigated during the occurrence of minor sudden stratospheric warming (SSW) events thus further addressing the proposition that planetary wave activity and its interaction with tides in the MLT region induce SSW events. The study contributes to ongoing efforts by the South African based researchers (Malinga et al., 1997; Mthembu, 2013; Mbatha, 2012; Mbatha et al., 2010) to use SuperDARN to investigate atmospheric dynamics at meteor heights. This follows a milestone discovery by Hall et al. (1997) that SuperDARN radars can be used for neutral atmospheric investigations at meteor heights.

1.1. Vertical Structure of the Earth's Atmosphere

The schematic diagram in Figure 1.2 shows temperature variations in the Earth's atmosphere. The middle atmospheric dynamics are a function of the heat variation in the atmosphere's thickness.

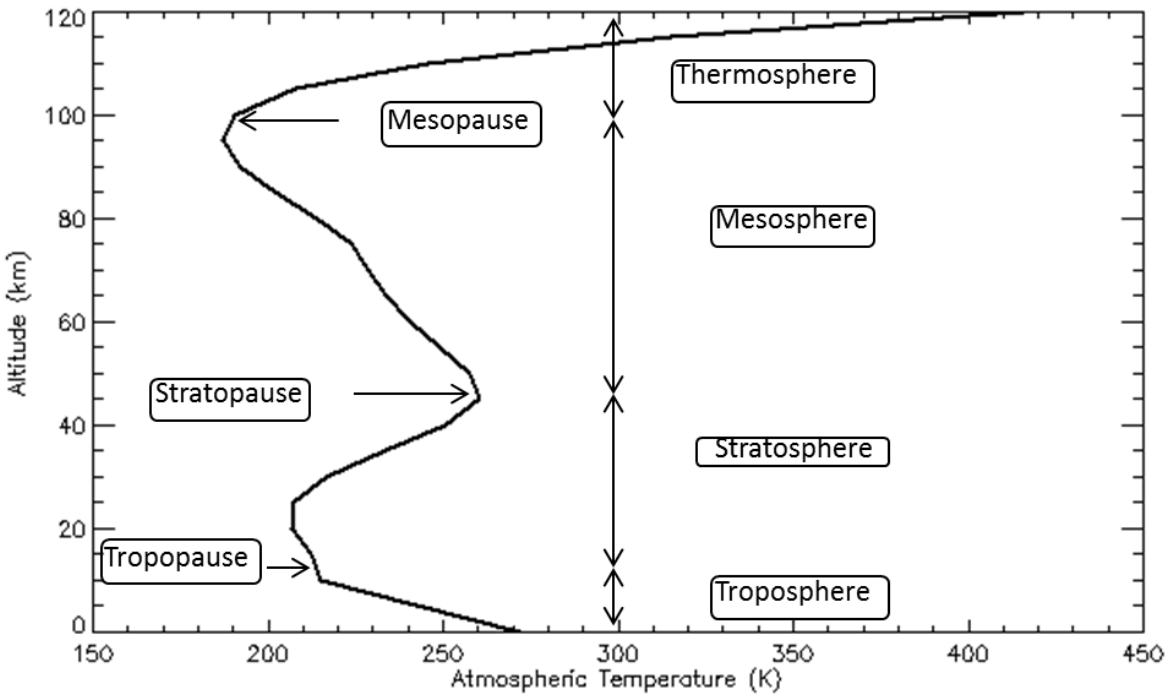

Figure 1.2: A plot showing different layers of the atmosphere classified according to varying temperature. The diagram is generated from the Mass Spectrometer- Incoherent Scatter Experiment (MSISE90) model for the upper atmosphere.

As it can be seen from Figure 1.2, the atmosphere is divided into four layers based on temperature variations namely: the troposphere, the stratosphere, the mesosphere and the thermosphere. The transition between the troposphere and the stratosphere is called the tropopause while the stratopause connects the stratosphere to the mesosphere. The mesopause links the mesosphere with the thermosphere. The heat variation in each layer is caused by the particles present, the physical process occurring and the chemistry involved. To see this in more light, a description of each layer's position, the composition and the phenomena that it hosts where applicable is given.

1.1.1. Troposphere

Troposphere is the lowest layer in the Earth's atmosphere. It extends from the surface of the Earth to an altitude of about 11 km in the polar regions and about 16 km near the equator. It houses about 80 percent of the atmosphere's total mass. Heavier elements in the atmosphere tend to settle in this layer due to the gravitational pull. It is therefore characterised by big clouds and accounts for most of the day to day weather observable near the surface of the Earth. Troposphere is vital for the survival of the living organisms on planet Earth. Amongst many gaseous molecules found in this layer is the oxygen molecule. Oxygen molecule is vital for the respiration process of many animals on Earth. Water vapour is mostly found in this layer and accounts for the rain that Earth sees. Beside the biological importance, this layer sees the formation of atmospheric waves through couplings with the oceanic Earth and also with the dry land portion of Earth. These couplings affect thermodynamics of the troposphere thereby inducing circulations in upper layers. The temperature in the troposphere decreases with increasing height. This is because temperature depends on the density and pressure of the atmosphere which decreases exponentially with height.

1.1.2. Stratosphere

Stratosphere also known as the ozonosphere is the layer above the troposphere. From the tropopause; the decreasing trend of the temperature starts to change and the increasing altitude sees an increasing temperature. This variation occurs until a stratopause is reached at an altitude of approximately 50 km above mean sea level. The temperature increase in this layer is due to the emission of energy during the formation of an ozone molecule. Ultra violet radiation from the Sun bombards oxygen molecules splitting them into monatomic oxygen. Atoms of oxygen then recombine with oxygen molecules to form ozone. Figure 1.3 shows these photochemical reactions taking place in the stratosphere.

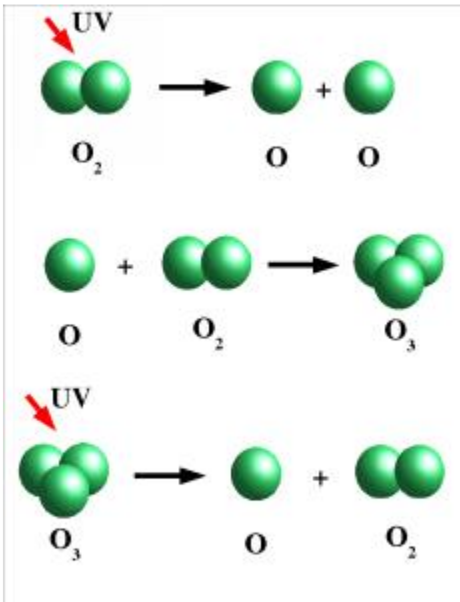

Figure 1.3: A schematic diagram representing photochemical reactions taking place in the stratosphere. Source: http://ozone.meteo.be/meteo/view/en/1547746-Formation+of+ozone.html .

Frequent recombination of monatomic oxygen with molecules of oxygen leads to the formation of ozone layer. Ozone layer intercepts Sun's direct radiation thereby protecting life on Earth. As per the schematic diagram in Figure 1.3, active UVC radiation can also disassociate ozone into atomic oxygen and a dioxygen molecule. This molecule breakdown and reactions with CFCs reduces the ozone concentration in the atmosphere hence the term "ozone depletion". A resulting ozone hole refers to a drastic decrease in the concentration of ozone. Stratosphere also hosts the Brewer – Dobson (BD) circulation. This is a global scale cell in which air rises in the tropics and then moves poleward and downwards in winter hemisphere (Butchart et al., 2005). The BD circulation accounts for denser concentrations of ozone in the poles in comparison to the concentrations in the tropics. Another important event taking place in this layer is the sudden stratospheric warming. Different studies addressing issues like ozone depletion and Global climate change are conducted on this layer.

1.1.3. Mesosphere

Mesosphere is the third layer of the atmosphere from the surface. It extends from the stratopause to an altitude of about 90 km in the mesopause. Mesosphere sees a decreasing temperature with increasing height. This inverse relationship between the temperature and the altitude is due to a thin layer of ozone in the mesosphere and the absence of the local source of heat. Mesopause marks the coldest spot in the atmosphere. The rarefied nature of the atmosphere in this region encourages lager wave amplitudes which ultimately result in wave breaking. This layer forms part of the MLT region which is the zone of interest in this study.

1.1.4. Thermosphere

Thermosphere also known as the upper atmosphere is a layer originating from the mesopause and stretching upwards. Thermosphere exhibits a direct proportionality relationship between the temperature and the atmospheric height. It is close to the interplanetary space. It is subjected to the solar wind and direct radiation from the sun's photosphere. Some particles exist in ionic state due to intense heat and low densities. It therefore forms part of the ionosphere. This layer sees the occurrence of northern lights known as the aurora and it is here that small meteorites burn up. The lower parts of this layer form part of the MLT region.

1.2. Atmospheric dynamics

Mankin Mak (2011) describes atmospheric dynamics as the subject concerned with "*how and why different classes of geophysical disturbances form, what dictates their structure and movement, how the Earth's uneven surface impacts with them, how they evolve to mature stage, how they interact with the background flow, how they decay and how they collectively constrain the general circulation of the atmosphere*". From this description, it is coherent to deduce that atmospheric dynamics are a function of the couplings between the Earth's surface and its immediate space. The Earth's surface introduces its level of complexity due to non-uniform topographical forms and also consists of the oceanic portion. Depending on where one is on the surface of the Earth, the temperature distribution is different and this has a direct influence on atmospheric circulations. For example the dynamics evident near the equator are different from those taking place at the poles. High evaporation levels in the oceanic Earth also contribute to day to day atmospheric dynamics. The Earth's motion about the sun and also the rotations about its own axis also induce changes in atmospheric mean flow.

Temperature distributions, topographical changes, ocean-atmosphere coupling and land-ocean couplings all act as forcing quantities leading up to wave formation. The resulting atmospheric waves then act as transportation modes moving energy, momentum and time varying particles from one region to another. Interesting phenomena that can result from wave activity in the atmosphere include sudden stratospheric warming, Brewer- Dobson circulation, wave breaking etc. Atmospheric waves are classified according to periods that they have. This work focuses on planetary waves and atmospheric tides only. Planetary waves have periods ranging from 2 to 35 days while tides range from half a day periods (semi-diurnal) to one day (diurnal) tides. The mathematics explaining some of the dynamics observable in the atmosphere will be outlined in the following sections.

1.2.1. Fundamental equations

An attempt to formulate a thorough mathematical representation of the dynamics taking place in the Earth's atmosphere is an involved exercise which for the purposes of this study may not be necessary. A rigorous treatment of the fundamental equations describing atmospheric dynamics is complicated (Andrews et al, 1987). As an effort to simplify the mathematics of atmospheric dynamics, certain approximations are made. These approximations include making use of the fact that the Earth's atmosphere is in a hydrostatic equilibrium and using the hydrostatic balance over the vertical momentum. The Coriolis force is neglected and an average radius a is used over the actual varying radius r. Spherical coordinates become the most effective coordinate system to use. The formulation introduced in equation 1.1 permits the use of log pressure coordinates. The resulting user friendly equations are called primitive equations. Primitive equations encompass equations of motion (momentum equations) for zonal and meridional wind components, mass continuity equation, thermodynamic energy equation and hydrostatic balance in the vertical.

If the time parameter can be represented by t, latitude by ϕ, longitude by λ, eastward, northward and upward velocities by u, v and w respectively, Coriolis force equalling $2\Omega\sin\phi$ by f, Earth's angular velocity by Ω, geopotential by $\left(\Phi = \int_0^h g\,dz\right)$ where h is a finite height along z, temperature by T, specific heat at constant pressure by c_p, gas constant equivalent to R/c_p by κ, heat rate per unit mass by J, and lastly the horizontal components of unspecified non-conservative forcing by X and Y; primitive equations can be respectively represented (Andrews et al, 1987) by

$$\frac{\partial u}{\partial t}+\frac{u}{a\cos\phi}\frac{\partial u}{\partial\lambda}+\frac{v}{a\cos\phi}\frac{\partial v}{\partial\phi}(a\cos\phi)+w\frac{\partial u}{\partial z}-fv+\frac{1}{a\cos\phi}\frac{\partial\Phi}{\partial\lambda}=X, \qquad (1.3)$$

$$\frac{\partial v}{\partial t}+\frac{u}{a\cos\phi}\frac{\partial u}{\partial\lambda}+\frac{v}{a}\frac{\partial v}{\partial\phi}+w\frac{\partial u}{\partial z}+\frac{u^2\tan\phi}{a}+fu+\frac{1}{a}\frac{\partial\Phi}{\partial\phi}=Y, \qquad (1.4)$$

$$\frac{1}{a\cos\phi}\frac{\partial u}{\partial\lambda}+\frac{1}{a\cos\phi}\frac{\partial}{\partial\phi}(v\cos\phi)+\frac{\partial w}{\partial z}-\frac{w}{H}=0, \qquad (1.5)$$

$$\frac{\partial T}{\partial t}+\frac{u}{a\cos\phi}\frac{\partial T}{\partial \lambda}+\frac{v}{a}\frac{\partial T}{\partial \phi}+w\left(\frac{\partial T}{\partial z}+\frac{\kappa T}{H}\right)=\frac{J}{c_p}, \text{ and} \tag{1.6}$$

$$\frac{\partial \Phi}{\partial z}=\frac{RT}{H}. \tag{1.7}$$

If one moves from spherical coordinates (ϕ,λ) to Cartesian coordinates (x,y); the increment distances in eastward and northward directions become $dx=a\cos\phi d\lambda$ and $dy=ad\phi$. The momentum, continuity and the thermodynamic energy equations become:

$$\frac{Du}{Dt}-\left(2\Omega+\frac{u}{a\cos\phi}\right)(v\sin\phi-w\cos\phi)+\frac{1}{\rho}\frac{\partial p}{\partial x}=X, \tag{1.8}$$

$$\frac{Dv}{Dt}+\frac{wv}{a}+\left(2\Omega+\frac{u}{a\cos\phi}\right)uv\sin\phi+\frac{1}{\rho}\frac{\partial p}{\partial y}=Y, \tag{1.9}$$

$$\frac{Dw}{Dt}-\frac{u^2+v^2}{a}-2\Omega u\cos\phi+\frac{1}{\rho}\frac{\partial p}{\partial z}+g=Z, \tag{1.10}$$

$$\frac{1}{p}\frac{D\rho}{Dt}+\frac{\partial u}{\partial x}+\frac{\partial v}{\partial y}+\frac{\partial w}{\partial z}=0, \text{ and} \tag{1.11}$$

$$\frac{D\theta}{Dz}=-g\rho. \tag{1.12}$$

$\frac{D}{Dt}$ in the above equations is a material derivative equalling $\frac{\partial}{\partial t}+u\frac{\partial}{\partial x}+v\frac{\partial}{\partial y}+w\frac{\partial}{\partial z}$, Z stands for the vertical component of unspecified non-conservative forcing, ρ is density and $\theta=T(p_0/p)^\kappa$ is the potential temperature. Equations 1.8 to 1.12 are still not convenient to work with; further approximations are applied to achieve a simpler and usable form of primitive equations. These approximations are:

$$\frac{|u|}{a\cos\phi}<<2\Omega,$$

$$|w\cos\phi|<<|u\sin\phi|,$$

and

$$|wv|/r=|u\sin\phi|.$$

The resulting equations are

$$\frac{Du}{Dt} - fv + \frac{1}{\rho}\frac{\partial p}{\partial x} = X, \tag{1.13}$$

$$\frac{Dv}{Dt} + fu + \frac{1}{\rho}\frac{\partial p}{\partial y} = Y, \text{ and} \tag{1.14}$$

$$\frac{Dw}{Dt} + \frac{1}{\rho}\frac{\partial p}{\partial z} + g = 0. \tag{1.15}$$

Primitive equations with time independent wind speeds are referred to as diagnostic an antonym for prognostic. Under this condition (time independency) equations 1.13 to 1.15 become

$$fv = \frac{1}{\rho}\frac{\partial p}{\partial x}, \tag{1.16}$$

$$-fu = \frac{1}{\rho}\frac{\partial p}{\partial y}, \tag{1.17}$$

$$\frac{\partial p}{\partial z} = -g\rho. \tag{1.18}$$

Equations 1.16 and 1.17 represent the geostrophic flow while equation 1.18 is hydrostatic. Applying the ideal gas assumption made earlier on and substituting $p = RT\rho$ leads to the formation of thermal wind-shear equations given as

$$f\frac{\partial v}{\partial z} = \frac{g}{T}\frac{\partial T}{\partial x}, \tag{1.19}$$

$$f\frac{\partial u}{\partial z} = \frac{g}{T}\frac{\partial T}{\partial y}. \tag{1.20}$$

1.2.2. Planetary Waves

Planetary waves are large scale forced waves which dissipate energy in the upper atmosphere. They are generated in the troposphere and propagate upwards to the middle atmosphere where they induce interesting atmospheric dynamics (eg Brewer Dobson circulation, sudden stratospheric warming and wave breaking). They give rise to large scale meteorological processes and can be used to explain the climatic behaviour (Saha, 2008). The formation of atmospheric planetary waves is a complex phenomenon involving the motion of the earth and the weather conditions near the earth's surface. They can be caused by wind-flow over continental scale topography, by earth ocean couplings and by disturbances in the atmosphere (Mbatha, 2012).Their periods range from 2 to 35 days with commonly observed periods of 2, 5, 10 and 16 days (Beard et al 2001, Mthembu 2013, Mbatha 2012). Planetary waves drive circulations in the middle atmosphere and dissipate momentum in the MLT region (Day et al, 2012). They also increase their intensity by interacting with other atmospheric waves (eg tides).

The generic way in which planetary waves form involves dynamics that take place when Earth orbits the Sun and when it rotates about its own axis. The phenomenon responsible for the planetary wave formation due to Earth's motion is known as the vorticity. It is the small scale circulation resembling large scale atmospheric circulations (Saha, 2008).

The theoretical layout to be presented here is based on the previous work by Holton (1975) and Volland (1988). Equations 1.16 and 1.17 restrict the flow to a quasi-geostrophic flow thus permitting the use of Boussinesq equations. The approximated Boussinesq equations lead to a quasi-geostrophic vorticity equation given by

$$D_g q = 0, \tag{1.21}$$

where $D_g \left(= \frac{\partial}{\partial t} + u_g \frac{\partial}{\partial x} + v_g \frac{\partial}{\partial y} \right)$ is the time derivative applied during the geostrophic flow. The geostrophic flow v_g is given as

$$v_g = \frac{1}{\rho 2\Omega Sin\phi} \frac{\Delta P}{d}. \tag{1.22}$$

The conserved parameter q represents the quasi-geostrophic potential and is expressed as

$$q = f_0 + \beta y + \frac{\partial^2 \psi}{\partial x^2} + \frac{\partial^2 \psi}{\partial y^2} + \frac{\partial}{\partial z}\left(\frac{f_0^2}{N^2} \frac{\partial \psi}{\partial z} \right). \tag{1.23}$$

ψ stands for the geostrophic stream function equivalent to $p/f_0\rho_0$, N is the buoyancy frequency and f_0 represents the Coriolis factor. The first two terms of equation 1.23 represent the beta plane approximation. The geostrophic stream function can be expressed as

$$\psi = -Uy + \psi', \tag{1.24}$$

to account for the disturbances incurred, assuming uniform zonal background flow with small amplitude. U in equation 1.24 stands for the zonal background flow and ψ' is the perturbation stream function. Substituting 1.24 into 1.23 leads to a differential equation given as

$$\left(\frac{\partial}{\partial t}+U\frac{\partial}{\partial x}\right)\left(\frac{\partial^2\psi}{\partial x^2}+\frac{\partial^2\psi}{\partial y^2}+\frac{f_0^2}{N^2}\frac{\partial^2\psi}{\partial z^2}\right)+\beta\frac{\partial\psi}{\partial x}=0. \tag{1.25}$$

A differential form in equation 1.25 can be evaluated by assuming that the geostrophic stream function behaves as a simple harmonic oscillator and expressing it as

$$\psi=\mathrm{Re}\left(\psi_0\exp\left[i\left(\omega t+kx+ly+mz\right)\right]\right). \tag{1.26}$$

Equation 1.26 takes only the real portion (cosine) of the solution. Parameters k, l and z represent the zonal, meridional and vertical wavenumbers respectively. ψ_0 and ω represent the amplitude and the angular frequency respectively. Planetary waves are dispersive waves and their dispersion relation is given by

$$m^2=\frac{N^2}{f_0^2}\left(\frac{\beta}{U-\left(\omega/k\right)}-\left(k^2+l^2\right)\right). \tag{1.27}$$

If β is always positive; solving for the phase velocity $c\left(=\omega/k\right)$ gives

$$c=U-\frac{\beta}{k^2+l^2+f_n^2m^2/N^2}$$

Implying that

$$U-c=\frac{\beta}{k^2+l^2+f_n^2m^2/N^2}$$

which shows that planetary waves always propagate westward with respect to the background mean flow since $U-c>0$.

1.2.3. Atmospheric Tides

Atmospheric tides are global scale oscillations whose periods are integral fractions of a lunar or a solar day (Lindzen, 1979). There are diurnal tide and semidiurnal tides (Lindzen, 1979). The former registers a single cycle per day while semidiurnal tides are a 12-hour Fourier component thus registering two cycles per day. This work focuses on thermally excited atmospheric tides. These are generally known as solar atmospheric tides. They are formed by the absorption of solar radiation throughout the earth's atmosphere. In the troposphere, water vapour absorbs infrared radiation; in the stratosphere and the mesosphere ozone absorbs ultraviolet radiation while the molecular oxygen does the absorption of the ultraviolet radiation in the thermosphere (Mthembu, 2013). There are also 8 hour and 6 hour tides respectively known as terdiurnal and quadiurnal tides, but these are less effective. Atmospheric tides can be migrating or non-migrating. Tides with Sun synchronous horizontal phase velocities are migrating and all other phase velocities are non-migrating (Chang et al., 2009). The interest has always been on the migrating tides since they are an important mechanism for transporting input energy from lower atmospheric layers to the upper atmosphere (Chapman and Lindzen, 1970; Chang et al., 2009). Atmospheric tides originate from the troposphere and the stratosphere and ascend to the upper most layers. In the troposphere; atmospheric tides manifest themselves as small oscillations with less significant amplitudes. This is caused by the high density levels near the earth's surface. Due to decreasing air density as the altitude increases, tides become more and more effective. The more rarefied atmosphere sees increasing tidal amplitudes. The amplitude increase in a tidal wave is a means of conserving kinetic energy in response to a decreased air density. Tides at mesospheric heights influence MLT dynamics. This includes nonlinear interactions with gravity waves (eg Fritts and Vincent, 1987; Ortland and Alexander, 2006) and also with planetary waves (eg Beard et al., 1999; Jacobi, 1999; Pancheva, 2001; Mthembu et al., 2013). Their influence carries on until dissipation by gravity wave breaking and increasing molecular diffusion in the lower thermosphere takes place (Chang et al., 2009; Hagan et al., 1995). Atmospheric tides are in many ways analogous to ocean tides. Laplace extended his study from uniform depth seas to an atmosphere. His formulas describing tidal wave behaviour were more close to reality in the atmospheric case than they were in the ocean due to varying depth in the sea (Chapman and Lindzen, 1970). For a more detailed presentation of the mathematics of atmospheric tides one may refer to Chapman and Lindzen (1970). Mthembu (2013) also provides a brief mathematical background on the subject. To be presented here are the final forms of the Laplace's Tidal equations. We first present Laplace's Tidal wave equation describing the horizontal structure of the tide. This equation is given as

$$F'\left(\Theta_n^{\sigma,s}\right) = -\frac{4a^2\Omega^2}{gh_n^{\sigma,s}}\Theta_n^{\sigma,s} , \qquad (1.28)$$

Hough (1897) re-expressed equation 1.28 as

$$\frac{d}{d\mu}\left(\frac{1-\mu^2}{f^2-\mu^2}\frac{d\Theta_n}{\mu}\right) - \frac{1}{f^2-\mu^2}\left[\frac{s}{f}\frac{f^2+\mu^2}{f^2-\mu^2} + \frac{s^2}{1-\mu^2}\right]\Theta_n + \frac{4a^2\Omega^2}{gh_n}\Theta_n = 0 , \qquad (1.29)$$

The inhomogeneous vertical structure equation can be represented as

$$H\frac{d^2L^{\sigma,s}}{dz^2}+\left(\frac{dH}{dz}-1\right)\frac{dL_n^{\sigma,s}}{dz}=+\frac{1}{h_n^{\sigma,s}}\left(\frac{dH}{dz}+\kappa\right)L_n^{\sigma,s}=\frac{\kappa J^{\sigma,s}}{\gamma gHh_n^{\sigma,s}}, \quad (1.30)$$

Considering $z=-\log\left(\frac{p_0}{p_0(0)}\right)$ and $L_n^{\sigma,s}=e^{\frac{z}{2}}W_n^{\sigma,s}$ Equation 1.30 becomes

$$\frac{d^2W_n^{\sigma,s}}{dz^2}-\frac{1}{4}\left[1-\frac{4}{h_n^{\sigma,s}}\left(\kappa H+\frac{dH}{dz}\right)\right]W_n^{\sigma,s}=\frac{\kappa J_n^{'\sigma,s}}{\gamma gh_n}e^{\frac{-z}{2}}, \quad (1.31)$$

where the variables from equation 1.28 to 1.31 can be described as follows:

$F^{'}$	Laplace's tidal wave
$\Theta_n^{\sigma,s}$	Tidal wave's eigenfunction
$\frac{\sigma}{2\pi}$	Solar day
s	Number of waves along the latitudinal cycle
n	Number of possible solutions
$h_n^{\sigma,s}$	Constant of separation
$\frac{4a^2\Omega^2}{g}$	Tidal wave's eigenvalues
μ	Latitude variable equivalent to $\sin\phi$
f	The equivalence of $\frac{\sigma}{2\Omega}$
$L_n^{\sigma,s}$	The atmospheric height component of tidal wave
γ	The ratio of the specific heat at constant pressure and volume (c_p/c_v)
W	Perturbation in the vertical velocity

Other variables are as described earlier.

1.2. Thesis Outline

This work investigates middle atmospheric dynamics germinating from the planetary wave activity and its interaction with atmospheric tides in the MLT region. Chapter 1 provides the necessary background theory thus enhancing one's view of the Earth's atmosphere both according to chemical composition and multilayer stratification. The literature on the subjects under investigation is presented as introductory information on each chapter (chapters 3 to 5).

Chapter 2 covers the instrumentation and analysis techniques employed. It gives a brief description how instruments operate and the data they provide. The Super Dual Auroral Radar Network (SuperDARN) and the National Centre for Environmental Prediction (NCEP) is used to measure mesospheric and stratospheric parameters respectively. This chapter further describes the mathematical tools used to unpack atmospheric dynamics. This is done under the analysis techniques section. It starts with simple statistical measures and develops into explaining Fourier transform based signal processing techniques. These include short time Fourier transform (STFT), wavelet and bispectral analysis.

Succeeding Chapter 2 is Chapter 3; in this chapter we begin the analysis and investigation of stratospheric and MLT dynamics. Chapter 3 provides an introductory set of results that serve as a basis for all the analysis to be carried out in this work. These sets of results include the presentation of daily temperature variability plots in the stratosphere as a means to identify years with significant temperature enhancements. Mesospheric winds at MLT heights are also investigated during significant warming days so as to establish the correlation between mean wind behaviour in the MLT and SSW formation at stratospheric heights.

Chapter 4 delves in and investigates the tidal and planetary wave activity at day intervals established in Chapter 3. The tidal wave behaviour is revealed through short time Fourier transform (STFT) while the wavelet analysis helps unpack the planetary wave activity during warming days. Chapter 4 also presents the first phase in investigating the possible non-linear interaction between planetary waves and atmospheric tides. It does this through investigating the possible modulation of tides by planetary wave activity.

Chapter 5 presents two more methods that help validate the assertion that a possibility exists that there is a non-linear interaction between the primary waves (planetary waves and atmospheric tides) being investigated. Bispectrum analysis investigates the possible inter-mixing between planetary waves and atmospheric tides while the amplitude-period spectrum reveals the secondary waves that may be formed through the addition or subtraction of primary wave frequencies.

Chapter 6 provides a summary of the entire work. It states the primary goal and reflects and concludes on the results presented. There is also a section that highlights areas of interest in relation to this work that could not be covered in full. These are suggested as possible topics of research in future.

Chapter 2

Instrumentation and Analysis Techniques

2.1. Instruments and Data Sets

There are two methods primarily used for obtaining experimental data. There is an observational method whereby an instrument records and presents raw data which can then be processed for further analysis. The instrument can be ground based or it can be positioned in a region of interest in space. The other method is somewhat linked to the observational method but differs in that it employs theoretical means to assimilate data and draws up models that predict the most likely behaviour. In this thesis both methods are used to facilitate the investigation. Ground based Super Dual Auroral Radar Network (SuperDARN) is used to observe the dynamical behaviour in the MLT region. NCEP temperature data is used as the latter method and helps identify the periods with significant warmings. This section provides a brief description of the instrumentation used.

2.1.1. SuperDARN HF Radar

SuperDARN is a network of High Frequency (HF) radars located in the auroral positions of the Northern and Southern hemisphere. They are coherent scatter radars which receive scatter from magnetic aligned irregularities in E and F regions (Lester, 2013). This technology exploits radio wave ability to traverse altitudes that span hundreds of kilometres. The radio wave suitability is also amplified by their refractive properties making them ideal for revealing plasma range dynamics. Radio waves are transmitted from HF radar sites and are sent to high altitudes where upon refraction and reflection, convection patterns are studied (Malinga, 1997). However; the significant feature of the SuperDARN radars and the advantage they possess over other instruments is that the beam lobe is wide in elevation angle (5 – 55 degrees) (Greenwald et al, 1995). This permits observation over large land coverage.

This radar network was originally designed to conduct large scale measurements of world-wide ionospheric convections driven by the solar wind interaction with the magnetosphere and establish the existing link between plasma activity in the Northern and Southern hemisphere (Lester, 2013). The process involves the phasing of signals from the 16 beam antenna array. The emitted beam is therefore piloted to 16 different directions (Mthembu, 2013). The directions differ by increments of 3.25° covering a segment with the nominal azimuth of 52° (Mbatha, 2012). Each beam can accommodate up to 75 range gates with each range gate having resolution range of about 45 km. This means that on a day where all antennas are operational, observations can cover up to 3000 km^2 of land area.

The SuperDARN operational frequency ranges from 8 MHz to 20 MHz. Radio wave frequency dictates the azimuthal resolution. Within the frequency range, the maximum land coverage is obtained at 8 MHz with an azimuthal resolution of 6° while at 20 MHz the resolution is 2.25°. The antennas can transmit as many as 7 pulses over a 100 m.s time interval (Malinga et al., 1997). After encountering a medium in the ionosphere, the signal is either transmitted or backscattered. Backscatter can also be produced when a signal experiences ground scatter. The motion of the magnetic aligned irregularities in E and F regions creates a Doppler shift in the frequency of the backscattered signal. By comparing the phase of the backscattered pulses to the transmitted signal one is able to work out the plasma velocity. This is achieved by sampling and processing the backscattered signal upon arrival at ground level to produce multilag auto correlation functions (ACFs) (Malinga et al., 2007). These parameters can be seen from the example of SuperDARN results calculated using ACFs. Resulting parameters include backscattered power, the mean Doppler velocity and the width of the Doppler power spectrum for each range with appreciable returns. From these, convection patterns can be derived. The said measurements can be seen from the example of SuperDARN results on Figure 2.1 below.

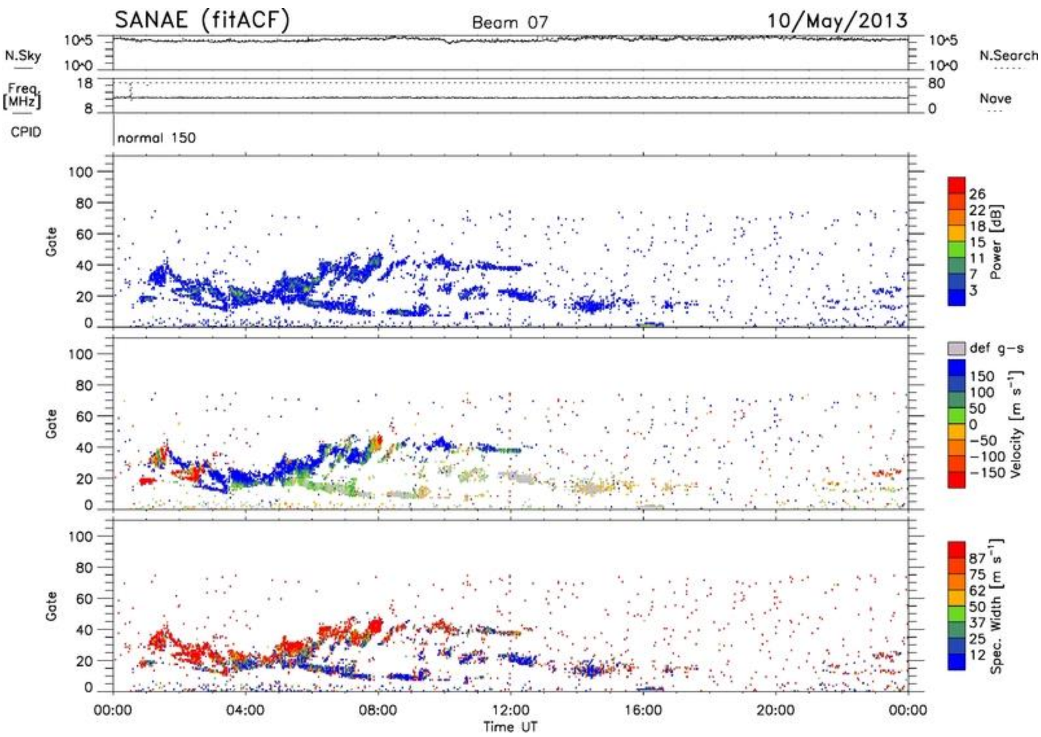

Figure 2.1: The plots showing data of 1 minute resolution averaged outputs of auto correlated functions in the SANAE HF radar operations. The top subplot shows the backscattered power, followed by the line of sight velocity in the middle and the spectral width in the bottom. The data covers all the range gates from 0 to 110.

SuperDARN radars were later found useful in detecting near range echoes in the absence of geomagnetic disturbances. Hall et al. (1997) showed that SuperDARN HF radars can be used to track meteor trails at altitudes of about 94 km. This means that grainy echoes are observable from range gates as low as 0 to 5. To demonstrate these, 0 to 5 range gates from Figure 2.1 are magnified resulting in a zoomed in version observable in Figure 2.2. However, this study only uses data from range gate 0 to 4. The alternating reddish and greenish bands in the velocity plot imply positive and negative velocity fluctuations respectively. This supports Hall et al. (1997) findings. SuperDARN HF radars have since been used to study mesospheric winds (eg Mbatha, 2012; Jenkins et al., 1998; Jenkins et al., 1999; Tsutsunami et al., 2009), quasi two day waves (eg Malinga et al., 1997; Bristow et al., 1999) and interactions between planetary waves and atmospheric tides (eg Mthembu, 2013). This study follows on the path of these investigations and makes use of the Hall et al. (1997) findings to get a comprehensive account of the planetary wave activity in the southern hemisphere.

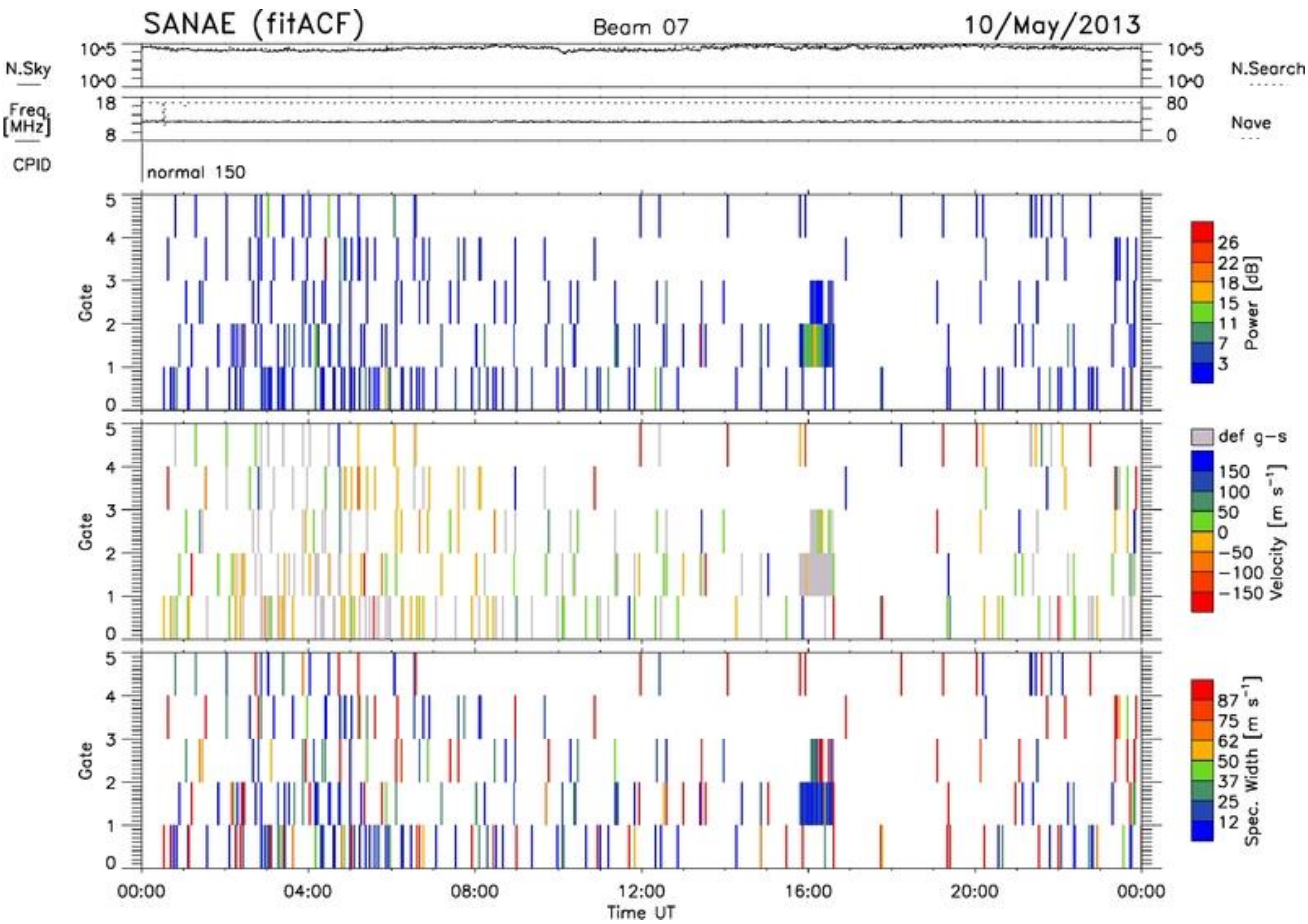

Figure 2.2: Same as Figure 2.1 but for range gates from 0 to 5. Alternating green and reddish bands in the middle plot demonstrate negative and positive velocity fluctuations. Red and blue

alternating colours mean Doppler velocity that is away and towards the radar along the beam's look direction.

The zonal and meridional components of the MLT winds are calculated from the line of sight Doppler velocity. The derivation of zonal component wind speeds involves applying the beam-swinging algorithm to the horizontal component of the mesospheric winds while meridional winds are deduced from the weighted average velocity from the beams that point towards the geographic pole (Matthews et al., 2006). SANAE HF radar is used as a primary source of experimental data. Figure 2.3 shows the geographical position of the SANAE HF radar and its field of view.

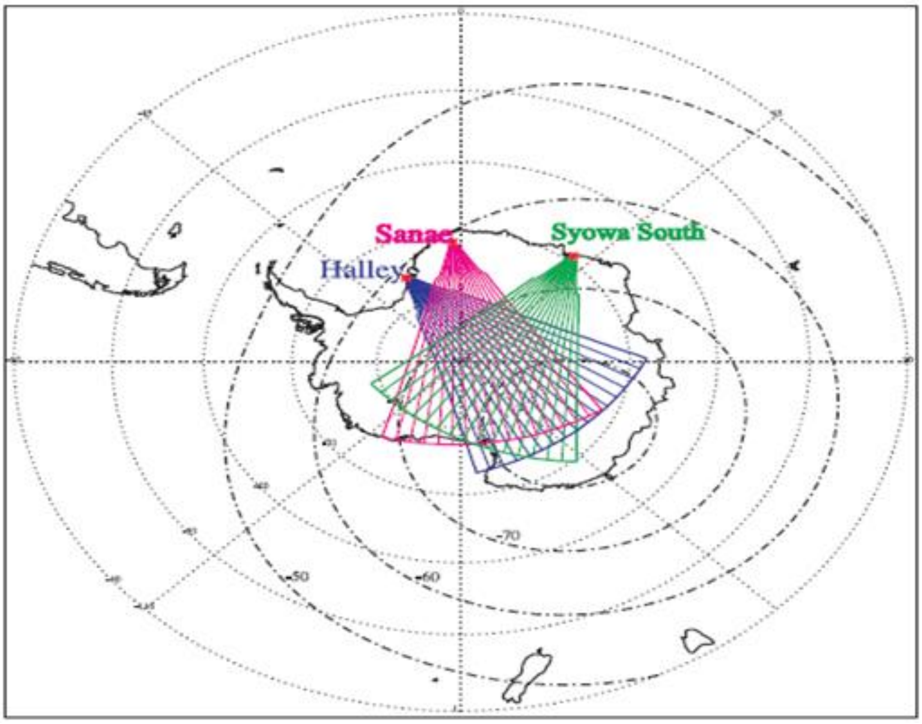

Figure 2.3: A plot showing the field of view of the SANAE HF radar in Antarctica with a twin station Halley and a nearby Syowa South

The antennas in this station (SANAE) were taken down by the powerful storm in 1997. The newly designed antennas were inserted in year 2009 and are structurally capable of withstanding powerful storms (see Figure 2.4).

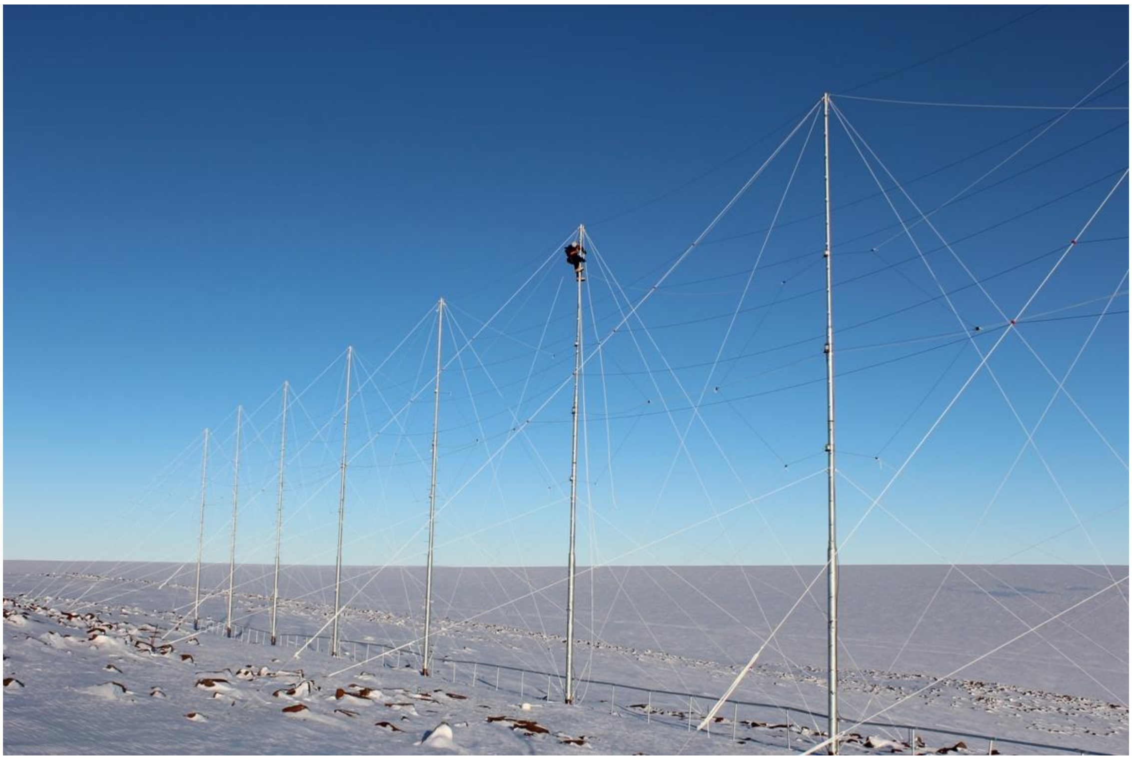

Figure 2.4: Newly erected folded dipole antenna at the SANAE HF radar station in Antarctica. Photo Credit: Jon Ward.

2.1.2. NCEP Data

The temperature data used in this work is sourced from the National Centre for Environmental Prediction and National Centre for Atmospheric Research (NCEP/NCAR) reanalysis project. Atmospheric temperature is one of many meteorological parameters that this project measures and calculates. The measurements are made at 17 pressure levels. The pressure levels include 1000, 925, 850, 700, 600, 500, 400, 300, 250, 200, 150, 100, 70, 50, 30, and 10 hPa. The temperature readings used here correspond to a 10 hPa pressure level. The 10 hPa pressure level marks an atmospheric height from which planetary waves and atmospheric tides originate.

The use of the NCEP temperature data is advantageous in many ways. It is a good representation of the global temperature data as it is a combination of many meteorological instruments around the world. The instruments make measurements on land surface, in the seas and in upper air. The assimilated data is then re-analysed and packaged for many research goals such as this work. By employing simple statistical quantities like the mean and standard deviation it was possible to envisage the heat behaviour in stratospheric heights and track any likely SSW events.

2.2. Data Analysis Techniques

This section presents mathematical methods employed when unravelling complicated real life mean wind dynamics. Measurements provided by the in-situ equipment often require refining and proper analysis in order to pave way for sound scientific interpretation and conclusions. In this study a three phased approach was taken to facilitate the process of arriving at meaningful conclusions. The first phase involves identifying years with significant warmings and the classification of warmings as to whether they are minor or major. This phase makes use of simple statistical measures like the mean, standard deviation and error of the mean. The second phase involves spectral representation of the mean wind frequencies in the zonal and meridional components. This phase makes use of the short time Fourier transform (STFT) technique. The third phase constitutes the investigation of a time active wave using wavelet analysis. Here an hourly sampled zonal and meridional data produces plots that are compared with the SDT amplitude behaviour sifted from STFT plots. Still under the third phase, bispectrum analysis is used to verify planetary and tidal wave interaction. We then check for secondary waves to ascertain the non-linearity of interactions. We describe all the mathematical tools used.

2.2.1. Statistical Methods

2.2.1.1. Mean

A mean represents an overall or average outcome of an experiment after a series of events taking place under the same conditions. The outcome may be a physical parameter, a phenomenon or any variable that can be tested over a number of times. The mean value is then assumed to be the most accurate reflection of the variable being measured. Consider an experiment with N measurements and N discrete outcomes. The mean value of this experiment can be calculated by summing up all the outcomes and dividing by the number of attempts. The mean $\bar{x}$ can be expressed as:

$$\bar{x} = \frac{1}{N}\sum_{i=1}^{N} x_i \quad . \tag{2.1}$$

2.2.1.2. Standard Deviation

This is a statistical quantity that provides an allowable straying or off path from the assumed perfect value. It defines the maximum positive and negative deviations. To understand standard deviation one needs to appreciate variance. For the same data described in 2.2.1.1 the variance V would be given as:

$$V = \frac{1}{N-1}\sum_{i=1}^{N-1}\left(x_i - \bar{x}\right)^2 \quad . \tag{2.2}$$

The standard deviation σ would then be the positive and negative roots of the square root of the variance. The expression is:

$$\sigma = \sqrt{V} \quad . \tag{2.3}$$

2.2.2. Fourier Transform

Fourier transform (FT) is an effective mathematical tool that translates information presented in a time domain into a frequency space. This technique makes use of the finding that all signals in our existence are combinations of cosine and sinusoidal profiles. The Fourier transform effectively decomposes mixed signals in a time domain into fundamental signals. This improves the visibility of variables like amplitude and phase of a signal at any given frequency. Brook and Wayn (1998) present the Fourier transform of a time varying signal $x(t)$ as

$$X(f) = \int_{-\infty}^{\infty} x(t)e^{i2\pi ft}\,dt \quad , \tag{2.4}$$

and the inverse as

$$x(t) = \frac{1}{2\pi}\int_{-\infty}^{\infty} X(f)e^{i2\pi ft}\,d\omega \quad . \tag{2.5}$$

The FT of *x(t)* is a time independent and frequency dependent $X(f)$ function. Squaring $X(f)$ gives the power spectrum P_f expressed as

$$P_f = \left|X(f)\right|^2 \quad . \tag{2.6}$$

The FT technique gets rid of a time variable altogether making it difficult to tell the time of occurrence of an event depicted in a frequency space. To circumvent this limitation, improved techniques like STFT and wavelet analysis are developed and they entertain a degree of compromise depending on the dimension being sought after at that particular moment.

2.2.3. Short Time Fourier Transform (STFT)

The short time Fourier transform technique is a one-step progression from the traditional FT method. It incorporates the lost time parameter by applying Fourier transform on a defined time interval and multiplying the entire signal by the averaged window. This gives a spectral representation that constitutes time, amplitude and frequency of the signal. The mathematical definition of the STFT method is

$$STFT\left(t^{'}, f\right) = \int_{t} \left[x(t) \bullet W^{*}\left(t - t^{'}\right)\right] e^{-j2\pi ft} dt \quad , \qquad (2.7)$$

where $x(t)$ is a time varying parameter being studied, $W(t)$ represents a window function and * is a complex conjugate. The window shifting operation employed here compromises frequency resolution. Real signal information is averaged and compressed to a given window reducing precision. To the contrary this technique excellently reveals active wave amplitudes in a given dynamical behaviour. For better frequency-time resolution we turn to wavelet analysis.

2.2.4. Wavelet Analysis

Wavelet analysis is a technique designed to solve challenges presented by the STFT method. In order to appreciate the superiority of this technique, a background theory on wavelet analysis is provided. The study provides the definition of a wavelet, describe a continuous wavelet transform and close by uncovering time-frequency localisation.

2.2.4.1. Wavelet

Misiti et al. (1996) defines wavelet as a finite waveform whose average value is zero. The wavelet is a significant improvement from the traditional Fourier transform in that it better approximates real life signals. The arbitrariness associated with the wavelet allows for the capturing of finer details. This will be better demonstrated when time-frequency localisation is explained in section 2.2.4.3. There is a mother wavelet which is the fundamental version of the wavelet and from which all other wavelets effectively known as daughter wavelets are derived. There are different types of mother wavelets but the ones which are frequently used for atmospheric wave periods extraction include Morlet, Paul and Dog wavelets (Torrence and Compo, 1998). In this work a Morlet mother wavelet is used.

2.2.4.2. Continuous Wavelet Transform

Wavelet analysis involves applying a scaled wavelet that can dilate or compress on a time varying signal from the beginning to the end. This process transforms a signal into a frequency revealing space while retaining the time parameter. The operation is known as the continuous wavelet transform and is defined as the sum over a signal multiplied by a scaled and shifted wavelet. The mathematical representation of the continuous wavelet transform is

$$WT(\tau, s) = \frac{1}{\sqrt{|s|}} \int x(t) \psi^* \left(\frac{t-\tau}{s} \right) dt , \qquad (2.8)$$

where the wavelet basis function $\psi\left(\frac{t-\tau}{s}\right)$ depends on the ratio of the difference between time t and the translation τ to the scaling parameter s. The symbol * represents the convolution. WT refers to wavelet coefficients and these indicate a degree of alignment between the wavelet and the actual signal. Higher wavelet coefficients mean better correlation (Malinga, 2001). The parameters τ and s speak of the time information and frequency of the signal respectively. The scaling parameter is set such that there is an inverse relation with the frequency. The constant of proportionality between frequency and the scaling parameter differs from one mother wavelet to another (Mthembu, 2006). To work out the proportionality constant, a power spectrum of a cosine function with predetermined frequency is calculated and the scale of the largest power is determined (Malinga, 2001). Taking the modulus of the wavelet transform coefficients gives the wavelet amplitude spectrum (Torrence and Compo, 1998). This can be represented as

$$A(s, \tau) = |WT(s, \tau)| , \qquad (2.9)$$

where $A(s, \tau)$ is the amplitude spectrum. Torrence and Comp (1998) also define the phase of a wavelet spectrum $\phi(s, \tau)$ as

$$\phi(s, \tau) = \arctan\left[\frac{\mathrm{Im}(WT(s, \tau))}{\mathrm{Re}(WT(s, \tau))} \right] . \qquad (2.10)$$

2.4.2.3. Time-Frequency Localisation

The time frequency localisation is the process through which a wavelet scans a signal. The operation reveals either a time or a frequency of the signal depending on the level of resolution. Higher frequencies lead to a more accurate time resolution while broader time intervals ensure high frequency resolution.

2.2.5. High Order Spectra (HOS)

The miscellaneous and simultaneous existence of a variety of wave types in the same or different media speaks of an unescapable possibility of their interaction. It is of utmost importance that we understand the dynamic behaviour that gets manifested as soon as interaction or wave-wave mixing takes place. A tool that is able to disintegrate or decompose complex waves into primary and secondary waves becomes useful. The function of the mathematical or statistical tool ideally is to detect present non-linearities and segregate primary from secondary waves. High order spectrum also known as polyspectra performs this task with satisfying degree of accuracy. HOS is an advanced spectral analysis technique in that it retains the phase information hence facilitating the detection of non-linearities (Clark and Bergin, 1997).

2.2.5.1. Bispectrum

Bispectrum is a special case of the high order spectrum. It is characterised by being a two dimensional Fourier transform of a third order cumulant (Mthembu, 2013). This technique identifies the quadratic phase coupling. To appreciate how the bispectrum works, take an arbitrary signal $x(t)$ expressed as $A_1 \cos(\omega_1 t + \phi_1) + A_2 \cos(\omega_2 t + \phi_2)$. The random signal $x(t)$ is passed through a second order non-linear polynomial function $Q(t) = ax^2(t)$ where a is a non-zero constant. The multiplication of $Q(t)$ by $x(t)$ will yield roots which represent fundamental, sums and differences of phase and frequencies given by $(2\omega_1, 2\phi_1)$, $(2\omega_2, 2\phi_2)$, $(\omega_1 + \omega_2, \phi_1 + \phi_2)$ and $(\omega_1 - \omega_2, \phi_1 - \phi_2)$.

To calculate a bispectrum, a time series is divided into K equidistant intervals. Beard et al. (1999) gives the kth segment bispectrum as

$$B_k(\omega_1, \omega_2) = \lim_{T \to \infty} \frac{1}{T} E\{X_k(\omega_1) X_k(\omega_2) X_k{}^*(\omega_1 + \omega_2)\} \tag{2.11}$$

and in turn

$$X_k(\omega_1) X_k(\omega_2) X_k{}^*(\omega_1 + \omega_2) = |X_k(\omega_1)| |X_k(\omega_2)| |X_k{}^*(\omega_1 + \omega_2)| e^{j\phi(\omega_1, \omega_2)} \quad . \tag{2.12}$$

In equation 2.8 and 2.9 $E\{\}$ represents the expectation, T refers to the entire time domain of the series, $X(\omega)$ is the fast Fourier Transform (FFT) of the time dependent signal $x(t)$, * is the complex conjugate and $\phi(\omega_1, \omega_2)$ is the byphase and is expressed as $\phi(\omega_1, \omega_2) = \phi(\omega_1) + \phi(\omega_2) + \phi(\omega_1 + \omega_2)$. Equation 2.9 demonstrates that the bispectrum is an outcome of averaging a product of three spectral components. This action exposes the phase coherence that takes place among the three components (Clark and Bergin, 1997). Beard et al. (1999) stipulates that the bispectrum is only non-zero if spectral components with frequencies ω_1, ω_2 and $\omega_1 + \omega_2$ have phases that are coherent. This implies that bispectrum verifies the existence of a quadratic phase coupling.

Chapter 3

Sudden Stratospheric Warming

3.1. Introduction

The sudden stratospheric warming (SSW) is an unforeseeable significant rise of the temperature in the high latitude middle atmosphere (~ 10 to 100 km). The newly acquired heat is often accompanied by the disturbance of routine mean wind behaviour. It leads to increased energy dissipation in the MLT region. SSW event takes place poleward from 60° latitude and at a pressure level of 10 hPa or below. It precedes the slowing down of winds or total change in direction from westerly to easterly winds (Schoeberl, 1978). Mbatha (2012) rules out radiative heating as a primary cause of the rise in temperature during the SSW event. His account is that temperature amplitudes during an SSW event are higher than radiation induced amplitudes. The first SSW event to be recorded occurred in the Northern Hemisphere in the 1950s. A comprehensive coverage of this incident can be found in a publication by Labitzke and Van Loon (1999).

There are four types of SSW events, such as minor SSW, major SSW, Canadian SSW and the final warming. Minor warming is classified as an event where the temperature increase per week at 10 hPa or below is greater than 25 Kelvins (K) with no wind reversal (Schoeberl, 1978). If the rise in temperature under the same conditions causes a zonal wind reversal from eastward to westward direction then the warming is classified as a major SSW (Schoeberl, 1978; Andrews et al., 1987; Labitzke and Naujokat, 2000). Wind reversal may influence splitting of the polar vortex. Canadian warmings are unique to the Northern Hemisphere and only result in the distortion and displacement of the polar vortex without the pure split (Mbatha, 2012). Final warming is usually an outcome of a series of successive minor warmings. It occurs during spring time when the latitude temperature gradient changes the sign and westward winds remain in the middle atmosphere and at high latitudes (Mbatha, 2012).

SSW is the thermo-dynamical event which is reported to be an outcome of various atmospheric dynamic processes including planetary wave activity. Matsuno (1971) pioneered the modern day understanding of the SSW event by showing that planetary waves induce wave-mean-flow interaction. In the investigation of the SSW dynamical model, Matsuno (1971) illustrated that there is an ascendance of global scale fluctuations formed at tropospheric heights to the stratosphere. He demonstrated that planetary wave activity tends to slow down the polar night jet thus distorting and possibly causing the breakdown of a polar vortex. The persistence of the formed disturbances may lead to a total wind reversal from westerly to easterly winds.

Other authors who reported about SSW dynamics include Dowdy et al., 2004; Hoffmann, 2007; Mbatha et al., 2010 and others. Dowdy et al, (2004) observed an increased planetary wave activity in the winter of 2002 where major SSW event had occurred. This was later supported by Hoffmann (2007) who observed that major SSW activity coincided with increased planetary wave 1 activity in the MLT at high latitudes. Dowdy et al, (2004) also reported weaker zonal winds during the 2002 warming event. Another finding that Dowdy et al, (2004) made which was later reinforced by Mbatha et al, (2010) is that the mesospheric zonal winds in 2002 reversed about a week prior the stratospheric reversal linked with the SSW event.

The Southern Hemisphere region is known for its quiet or less robust stratospheric warming activity. Unlike Northern Hemisphere, it rarely sees major significant warming events. This is caused by often smaller amplitudes that Southern Hemisphere planetary waves have compared to the larger planetary wave amplitudes in the Northern Hemisphere (Espy et al., 2005). The variation in planetary wave amplitude size is associated with the impact that orographic and thermal forcing have. The Northern Hemisphere has a stronger orographic and thermal forcing compared to the Southern Hemisphere hence the often larger planetary wave amplitudes (Andrews et al., 1987). It then follows that any occurrence of a major warming event in the Southern Hemisphere is an outcome of atypical dynamic conditions. The unique and extensively studied recent stratospheric warming is the above mentioned major SSW event of 2002. Publications by Baldwin et al, (2003), Mbatha (2012) and Mthembu (2013) and others reported on and investigated the year 2002 major SSW event. Mbatha (2012) looked at the MLT wind and temperature structure in the middle atmosphere during the 2002 major SSW. Mthembu (2013) looked at the planetary waves and atmospheric tides in the MLT region during the same event. Mthembu (2013) had his interest on relatively long term periods such as 10 and 16 day planetary waves. His results revealed that the non-linear interaction between an SDT and a 10 day planetary wave possibly influenced the SDT behaviour during and in the vicinity of an SSW event. He has also studied how the middle atmosphere couples with the ionosphere and proposed that the ionospheric dynamo effect is an outcome of an upward propagating SDT wave modulated at 16 day planetary wave amplitudes.

This study focuses on the atmospheric wave dynamics during minor SSW events. The study aims to investigate the short term planetary wave activity (p-waves with 2 to 6 day period) and its possible non-linear interaction with atmospheric tides in the mesosphere lower thermosphere (MLT) region during minor warming events in the Southern Hemisphere.

In order to achieve the above mentioned goal, stratospheric temperature and stratospheric wind data together with mesospheric wind data is used. The NCEP data accessible at http://acdb-ext.gsfc.nasa.gov/Data_services/met/ann_data.html is used. The NCEP website only provides the variability of zonal winds hence the absence of meridional winds in the presentation of wind speeds at stratospheric heights (see Figure 3.3). Temperature measurements are taken at an altitude corresponding to 10 hPa pressure level.

The mesospheric wind used in this study was extracted from the South African National Antarctic Expedition (SANAE) HF radar which is part of the SuperDARN network. To see how SuperDARN antennas record data, the reader is referred to section 2.1.1. The raw mesospheric wind data consist of invisible data gaps which were identified and filled up with NaNs (Not a Number). A NaN is a variable that fills up an entry originally made for a reading in an instance where a measurement could not be taken. Data gaps occur when the equipment used to obtain measurements is not operational or when the parameter being sought after is not observable. For example, mesospheric zonal and meridional wind speeds can only be measured using SuperDARN HF radars in the absence of geomagnetic storms.

The mesospheric wind data presented in this study is hourly averaged. Velocities exceeding the magnitude of 100 m/s have been filtered out since significant meteors travel within the range [-100, +100] m/s (Mthembu, 2013). The filtering is employed in all velocity variations and along both zonal and meridional components. The investigation of the planetary wave behaviour implied the use of the wavelet function. Since this function (wavelet function) does not accommodate NaNs, data were linearly interpolated so as to eliminate data gaps. Linear interpolation was only carried when 60 % or more data in the window being examined were available.

This chapter seeks to identify and classify SSW events using a criterion outlined in section 3.1. The analysis commences by presenting the stratospheric temperature distribution in the years where significant warmings were identified. This is done in section 3.1.1. After identifying days with significant warmings, the study proceeds to investigate mesospheric zonal wind behaviour in the MLT region and compares it with the zonal wind behaviour at stratospheric heights thus arriving at a conclusion whether the MLT wind reversal predates stratospheric warming by a week or not. The analysis further suggests through interpretation of stratospheric parameters (wind velocity and temperature enhancements) whether the event is a minor or major warming.

It should be noted that this work uses the Julian calendar to mark time intervals and days of the year. The Julian calendar characterises a year as a period of time made up of 365 days and 366 days in every fourth year (leap year). A day is a unit of time equivalent to 24 hours.

3.1.1. The Stratospheric Temperature Distribution

Diagnosing the dynamics manifested in the MLT region as wave induced and borne in the lower atmospheric layers involves identifying time corresponding to the occurrence of such waves. The identification of significant stratospheric warmings then leads to the time of the year during which planetary waves and atmospheric tides are mostly active. The presentation of the stratospheric temperature variability exposes significant warmings which can be investigated further to see if they can be classified as SSW events.

To locate days where there are significant warmings, temperature data from year 1998 to year 2008 was considered. The availability of mesospheric wind data from year 1998 to year 2008 dictated that stratospheric temperature variability is investigated within this interval. The temperature data used in this work was sourced from the NCEP/NCAR reanalysis project. Daily temperature variability for the years of interest is shown in Figure 3.1. Years studied in Figure 3.1 were considered for investigation because of temperature perturbations that exceeded standard deviation. These years include year 2002, year 2003, year 2004, year 2005 and year 2007 shown in Figure 3.1 (a), (b), (c), (d) and (e) respectively. Other years (1998, 1999, 2000, 2001, 2006 and 2008) did not show any significant temperature enhancements. A mean temperature profile calculated from an 11 year temperature data spanning from year 1998 to year 2008 was produced and each year could then be superimposed to clearly see temperature enhancements. Temperature measurements are taken at a latitudinal range 50-90^{o} S and are averaged over all longitudes.

It is noticeable in all the plots in Figure 3.1 that the temperature variation displays an annual cycle with maximum temperatures during summer months and minimum temperatures in winter. The first 100 days in all the plots display close alignment between the mean profile and the year being investigated. In all the years, temperature enhancements begin to occur just after 200 days, mostly from day 250 to just before day 300. The enhancements are deemed significant when they exceed error bars and are indicated by arrows labelled ‘significant warming’.

The year 2002 in Figure 3.1 (a) consists of 4 peaks signifying well defined temperature enhancements. The said peaks occur near days 235, 243, 255 and day 268. Year 2003 in Figure 3.1 (b) registers a significant warming near day 287 around the period of maximum heat in the year. The significant warming in year 2004 is observable near day 220 (see Figure 3.1 (c)). Year 2005 in Figure 3.1 (d) sees weak but significant warmings near days 250, 260 and day 270. Year 2007 in Figure 3.1 (e) displays sudden temperature enhancement in day 263. This is a significant warming as indicated in Figure 3.1 (e).

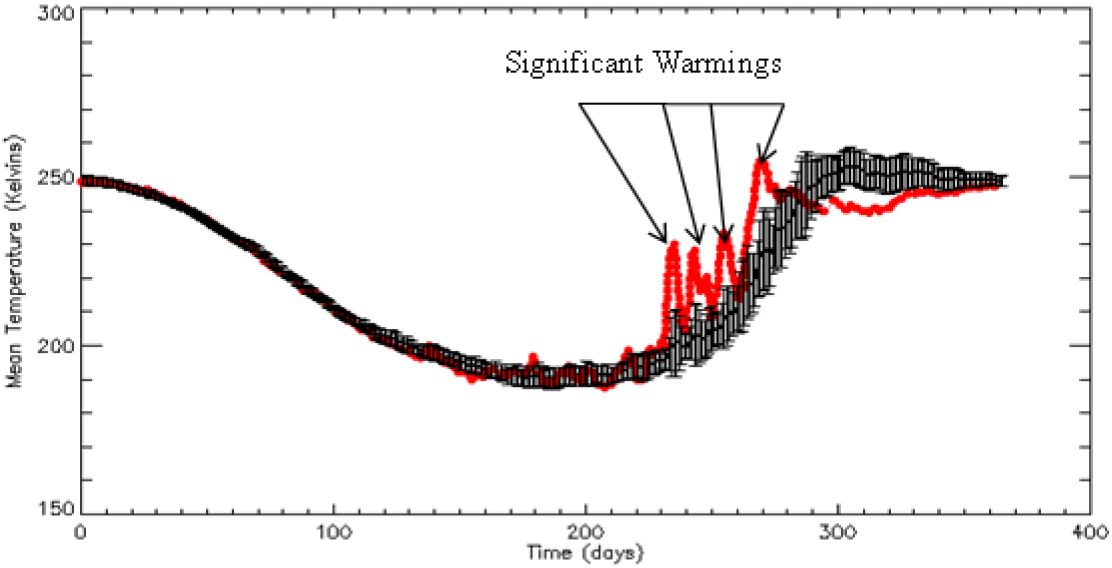

Figure 3.1 (a): Year 2002 stratospheric temperature variation (red variation) plotted over a mean temperature profile with error bars. Measurements are taken at a latitudinal range 50-90º S and are averaged over all longitudes. Error bars indicate standard deviation in the calculation of the mean temperature on a given day. The mean profile is black and within error bars for the entire 365 day duration.

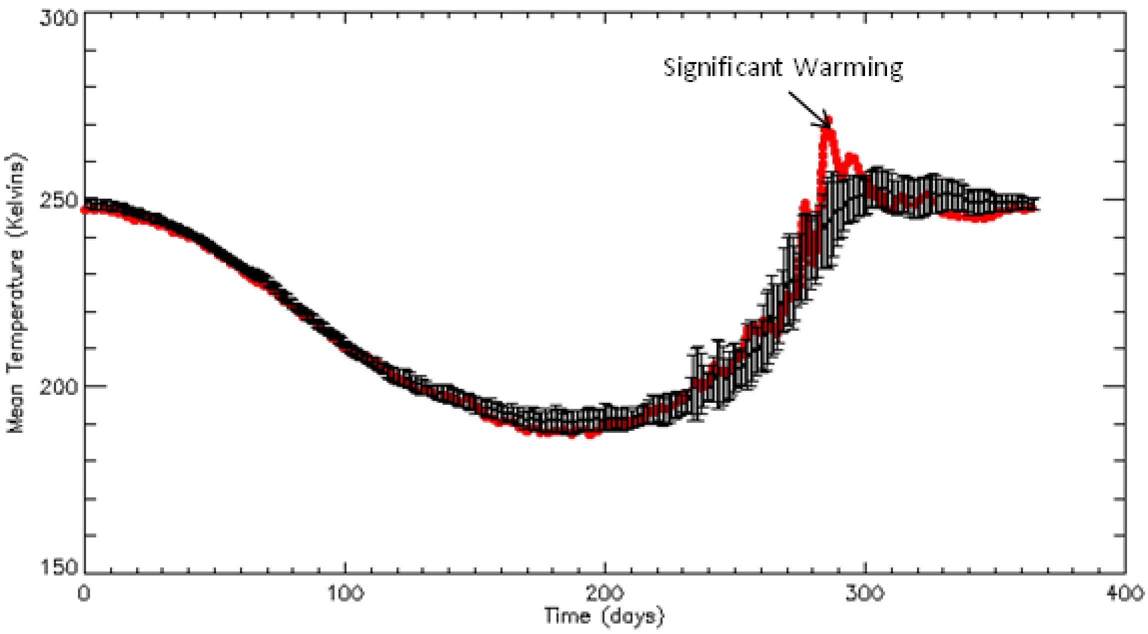

Figure 3.1 (b): Same as Figure 3.1 (a) but for year 2003.

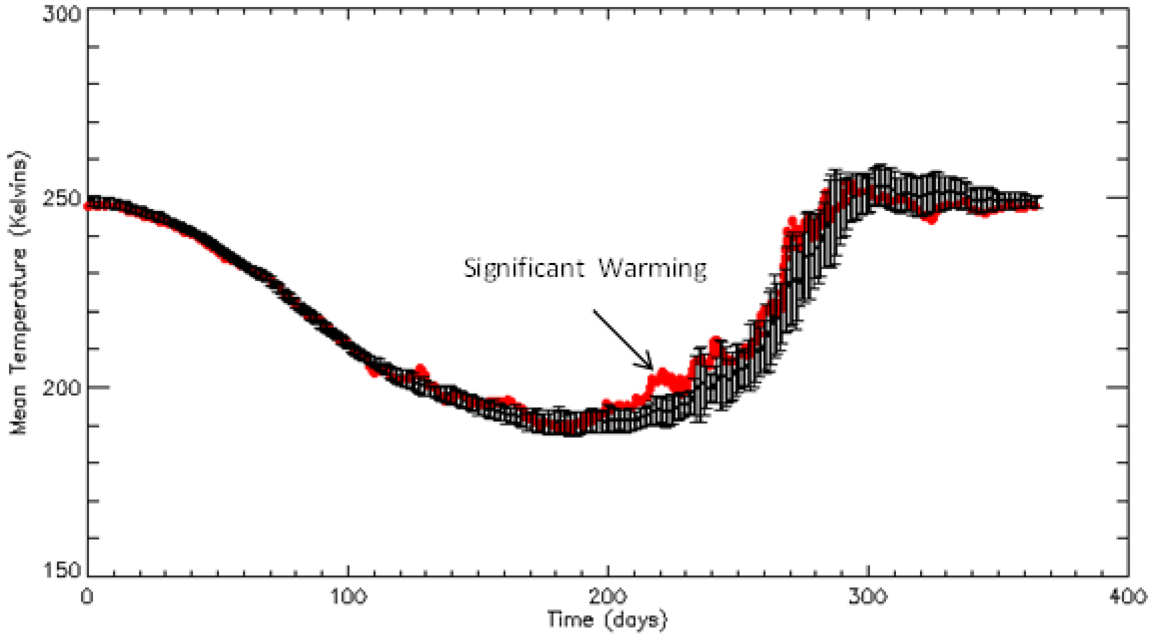

Figure 3.1 (c): Same as Figure 3.1 (a) but for year 2004.

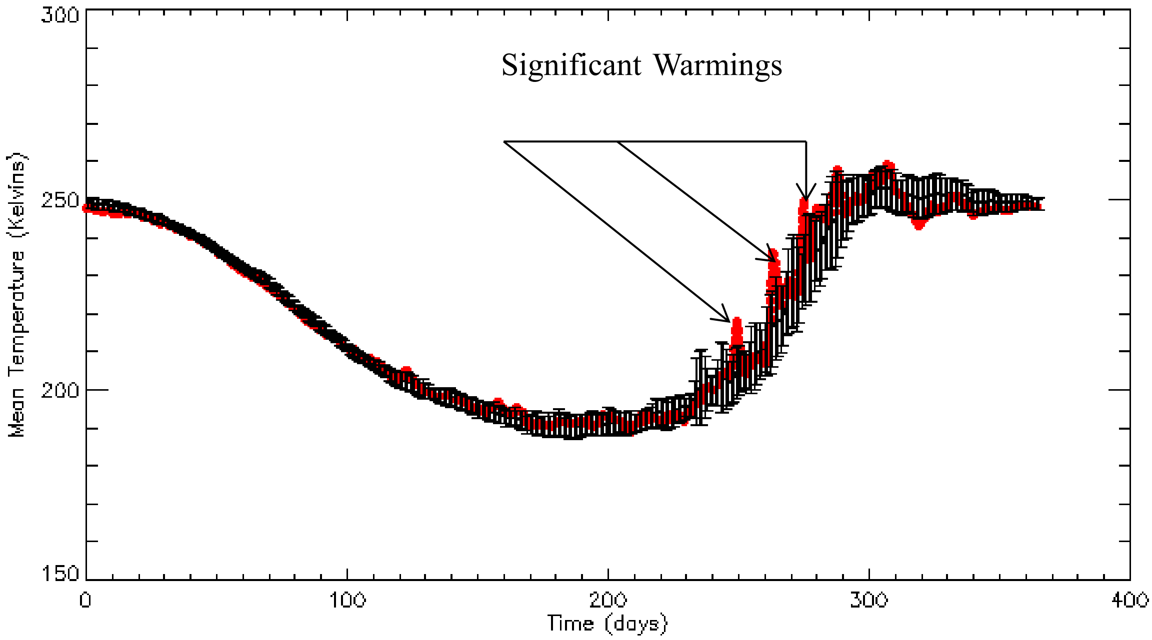

Figure 3.1 (d): Same as Figure 3.1 (a) but for year 2005.

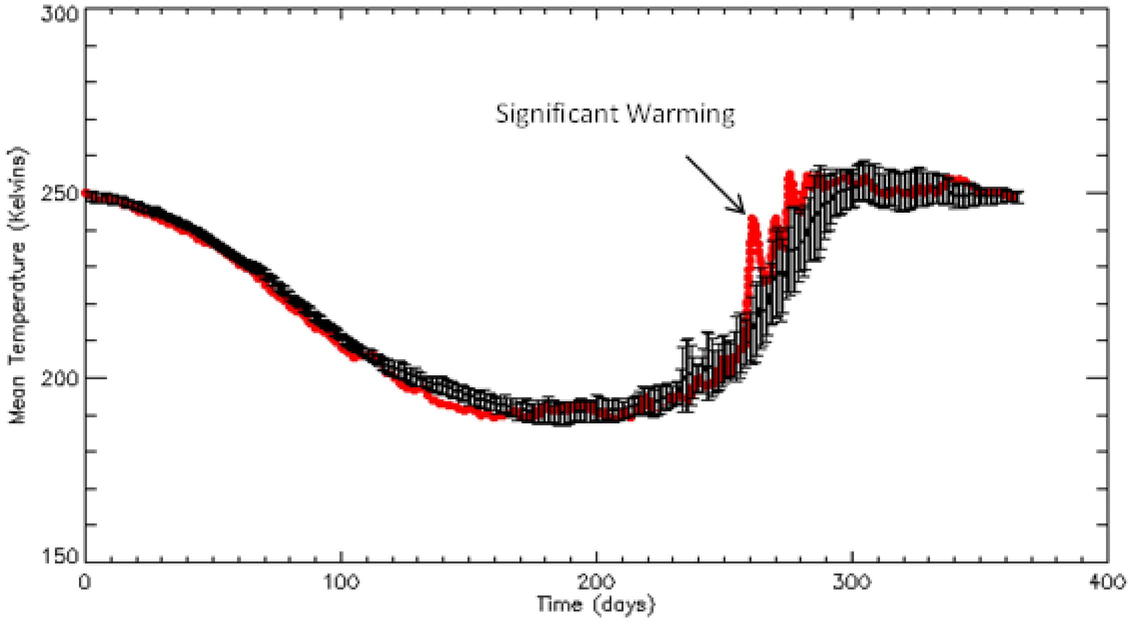

Figure 3.1 (e): Same as Figure 3.1 (a) but for year 2007.

Having presented the stratospheric temperature distribution for years 2002, 2003, 2004, 2005 and 2007 and noted days with significant temperature enhancements, the following step is to identify and classify SSW events. This is done in section 3.1.2.

3.1.2. Identification of SSW Events

As a means to adequately identify and classify SSW events, temperature enhancements in section 3.1.1 are investigated further. The investigation focuses on an interval from day 200 to day 300 for all years. This time interval encompasses all the significant warming days in Figure 3.1. Selecting the same interval for all the years is done deliberately so as to form basis for comparisons in mean wind behaviour among the years.

Figure 3.2 up to Figure 3.9 presents mesospheric zonal mean wind variations for years 2002, 2003, 2004, and year 2007. The analysis during year 2005 has been omitted due to a lack of significant temperature enhancements upon close examination. Each plot from the MLT region is paired up with the corresponding zonal mean wind and temperature plots from the stratospheric heights. Plots from the stratospheric region serve to indicate minor and major warmings. Mesospheric plots reveal MLT dynamical action prior the occurrence of stratospheric warmings. The analysis commences with the mean wind behaviour during year 2002. Year 2002 mesospheric zonal wind, stratospheric zonal wind and stratospheric temperature variability are presented in Figures 3.2, 3.3 A and 3.3 B respectively. The positive fluctuations of the zonal wind velocities imply eastward propagation while negative variations depict westward movement.

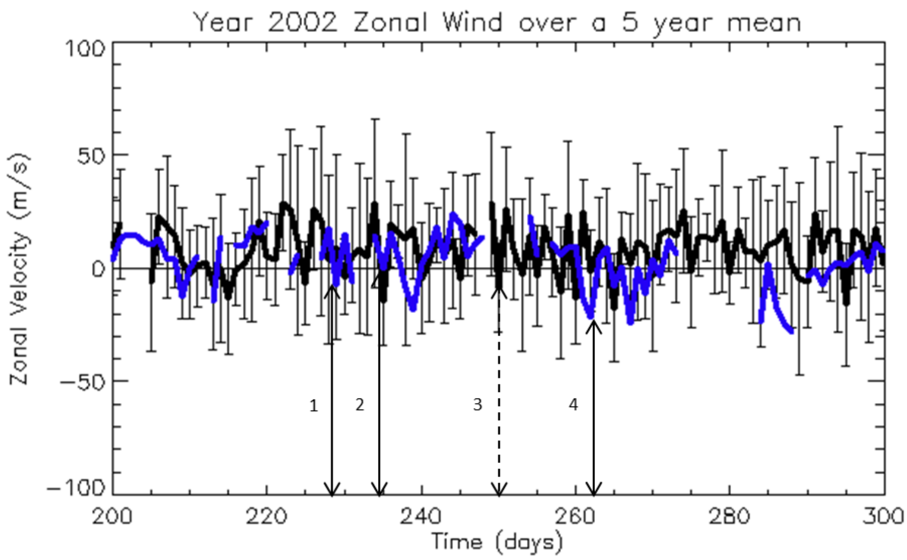

Figure 3.2: Year 2002 mesospheric zonal wind (blue variation) plotted with the five year mean (black variation) between day 200 and day 300, an interval corresponding to 2002 temperature perturbations in Figure 3.1 (a). Mesospheric winds depicted here were measured at SANAE HF radar station (72^{O} S, 3^{O} W). The arrows labelled 1, 2, 3 and 4 show mesospheric wind reversal that occurred a week before the significant warmings.

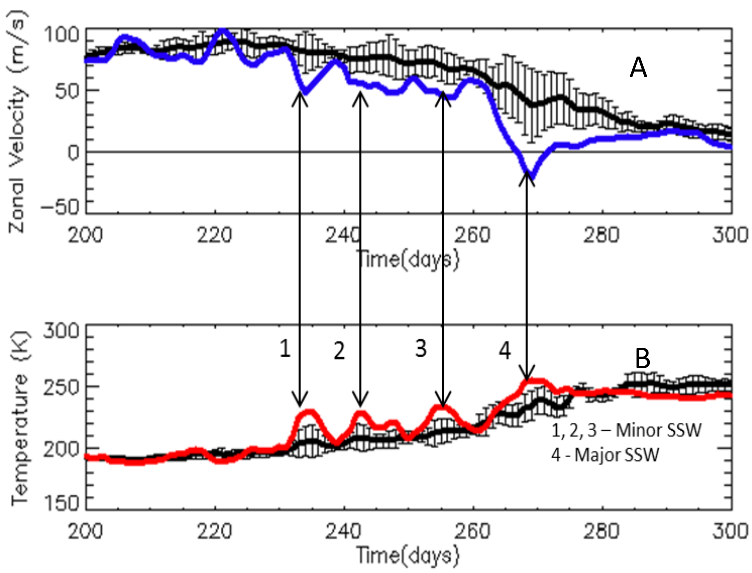

Figure 3.3: The top subplot depicts the 2002 stratospheric zonal wind (blue variation) plotted with a 5 year zonal mean (black variation) with error bars. The bottom subplot features the stratospheric temperature in year 2002 plotted with a five year temperature mean with error bars. The arrows 1, 2, 3 and 4 show minor and major SSW events.

Figure 3.2 shows the zonal mean wind behaviour in the MLT region for year 2002 while Figures 3.3 A and 3.3 B respectively show stratospheric zonal mean wind and temperature enhancements during year 2002. The arrow labelled ‘1’ in Figure 3.2 shows the MLT wind reversal that occurred in day 228, 7 days before the observed stratospheric significant warming in day 235. Arrows 2, 3 and 4 in Figure 3.2 show in the same way as arrow 1, MLT wind reversals that took place in days 235, 248 and 262 preceding stratospheric significant warming events a week later in days 243, 255 and 268 respectively. In Figure 3.3, the arrow labelled ‘1’ shows the coincidence occurring in day 235 between the stratospheric temperature increase in Figure 3.3 B and the stratospheric zonal wind reduction in Figure 3.3 A indicating signs of the stratospheric warming. The zonal wind reduction in day 235 as seen from Figure 3.3 A does not indicate a complete directional overturn. The temperature amplitude in day 235 is measured through subtracting minimum temperature (T_{min}) at the beginning of the warming near day 231 from the maximum temperature (T_{max}) in day 235. Day 231 corresponds to the temperature of 195 K while day 235 corresponds to 230 K making the temperature increase (ΔT) equate to 35 K an amplitude temperature well above 25 K. Combined, the stratospheric zonal wind partial decrease and the stratospheric temperature perturbation suggest that the enhancement in day 235 is a minor SSW event.

Similarly, the arrows 2 and 3 in Figure 3.3 illustrate symptoms of a minor warming in days 243 and 255 respectively while arrow 4 shows signs of a major warming near day 268. Arrow 4 in Figure 3.3 illustrates a major warming event since wind speeds cross to the negative territory indicating a total directional change.

The same criterion was also applied to the zonal mean wind data for years 2003, 2004 and 2007. The zonal mean wind in the MLT region for year 2003 is shown in Figure 3.4 while the stratospheric zonal mean wind and temperature data in the same year are plotted in Figures 3.5 A and 3.5 B respectively. For year 2003, a sign of a minor SSW event is shown to exist in day 287 (see arrow 1 in Figure 3.5 A and 3.5 B). A plot depicting zonal mean wind behaviour in the MLT region for year 2004 is presented in Figure 3.6 while zonal mean wind and temperature data in the stratosphere for the same year are presented in Figures 3.7 A and 3.7 B respectively. There are no signs of an SSW event in year 2004. For year 2007, MLT zonal mean wind is shown in Figure 3.8 while stratospheric zonal mean wind and stratospheric temperature plots are presented in Figures 3.9 A and 3.9 B respectively. According to these plots (see Figures 3.8, 3.9 A and B), symptoms of a minor SSW event in year 2007 are observable in day 263.

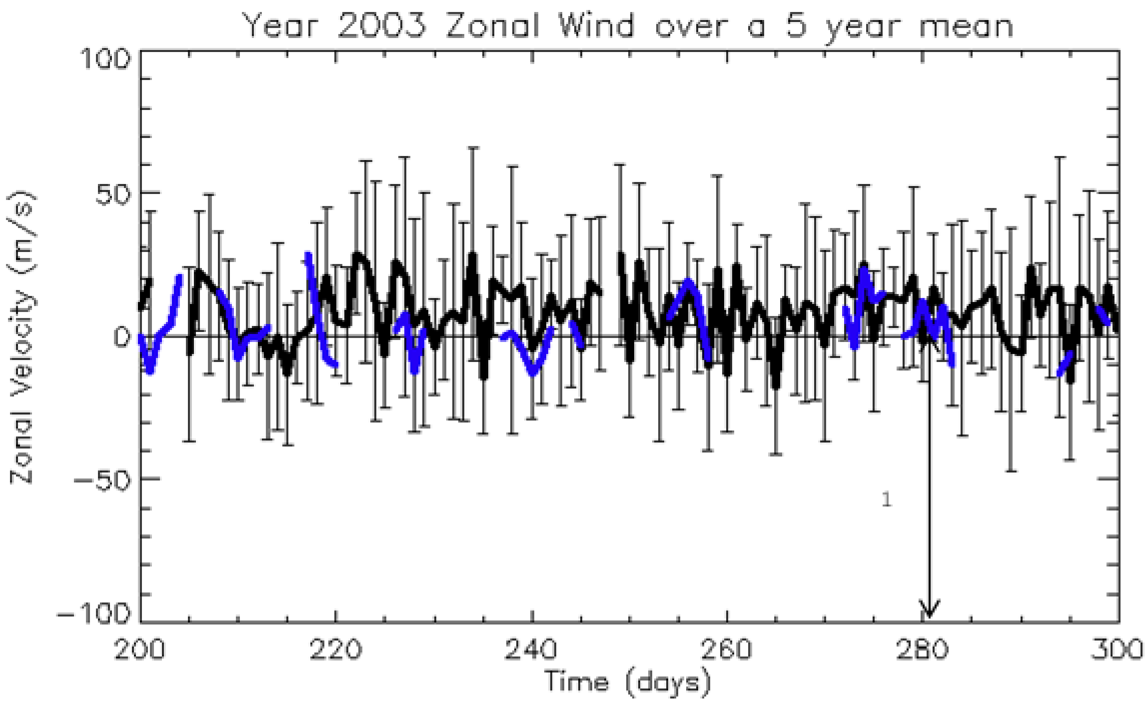

Figure 3.4: Same as Figure 3.2 but for year 2003.

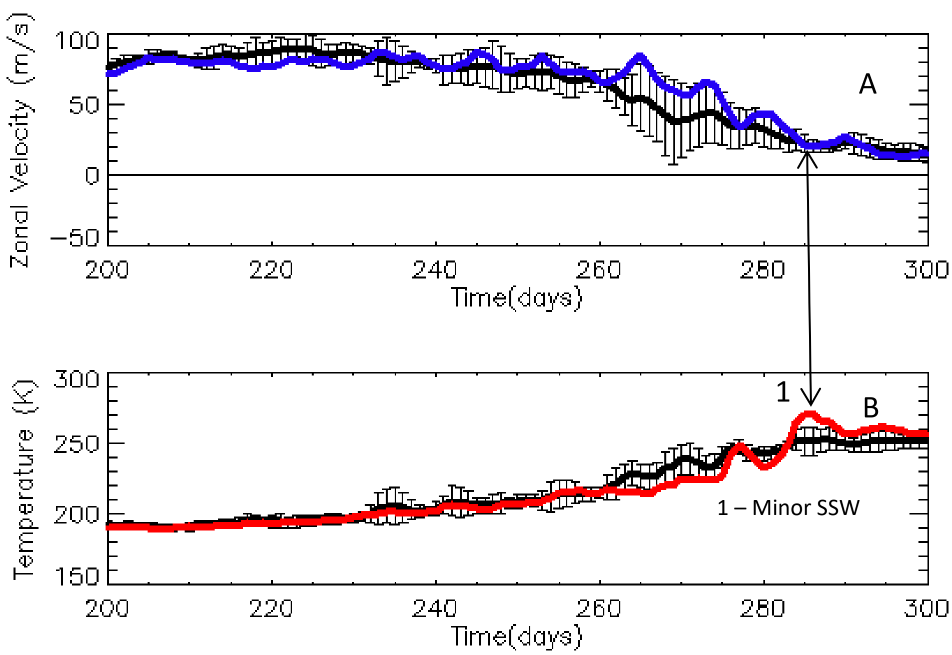

Figure 3.5: Same as Figure 3.3 but for year 2003.

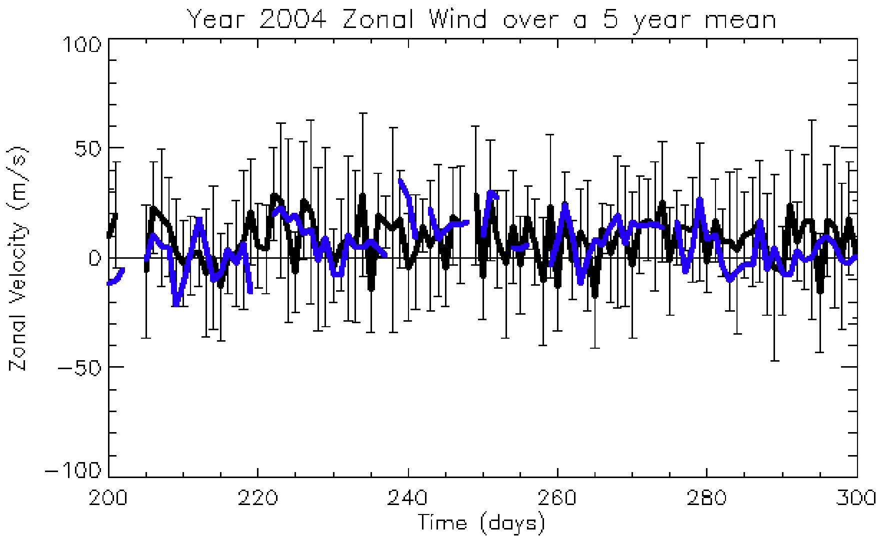

Figure 3.6: Same as Figure 3.2 but for year 2004.

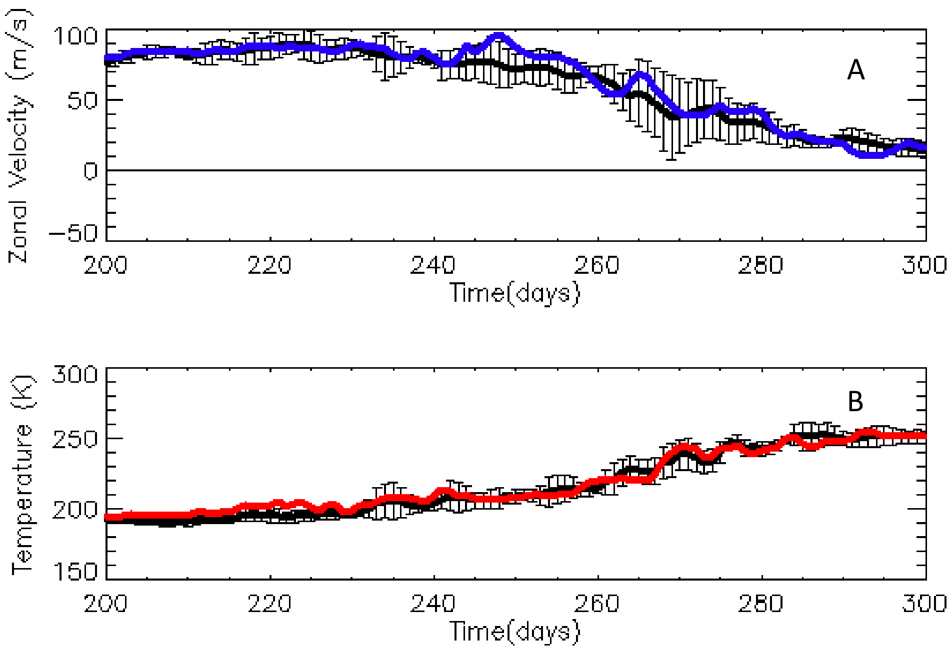

Figure 3.7: Same as Figure 3.3 but for year 2004.

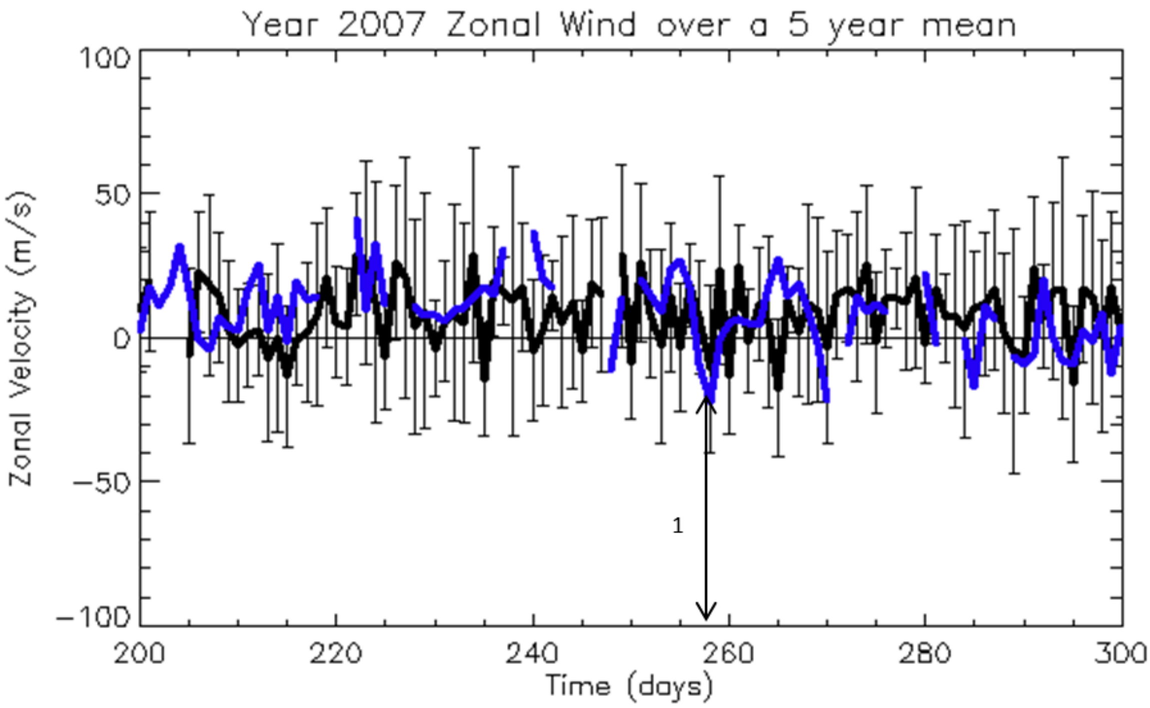

Figure 3.8: Same as Figure 3.2 but for year 2007.

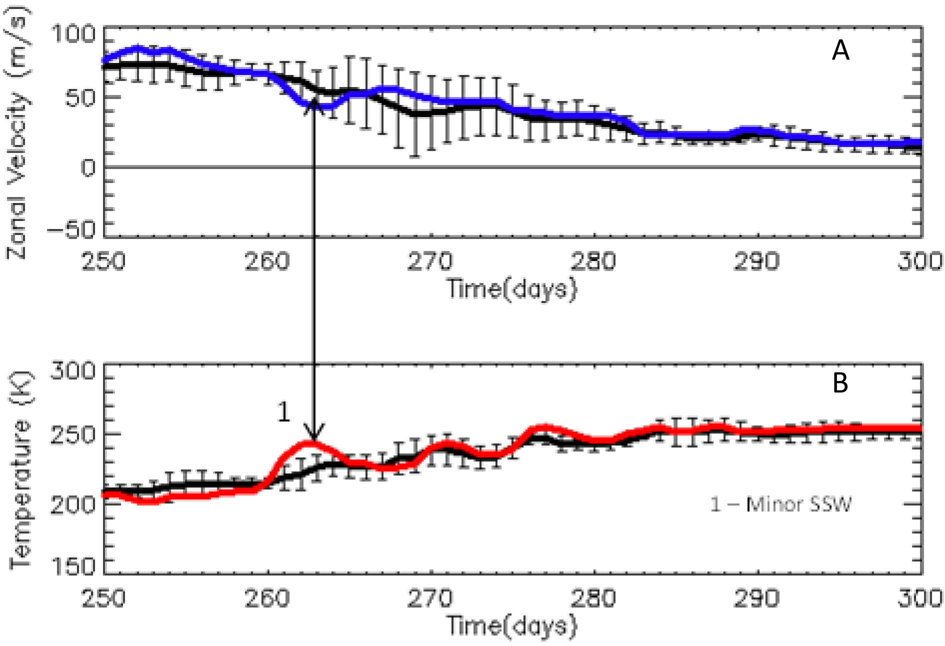

Figure 3.9: Same as Figure 3.3 but for 2007.

A summary of all stratospheric warming events that occurred from year 2002 to year 2007 is given in Table 3.1. The subscript ‘m’ in Table 3.1 refers to the mean value. The symbols T and U respectively represent temperature and zonal wind velocity. The temperature difference ΔT is an equivalent of the expression '$T_{max} - T_{min}$' as explained when diagnosing the SSW events. T_{max} is the temperature on the day of a significant warming while T_{min} refers to the minimum temperature measured during the week of the occurrence of a warming event. Other symbols and abbreviations carry usual meanings. The panel titled 'stratospheric parameters' gives values describing stratospheric temperature and zonal wind variability. Mesospheric parameters give the mesospheric zonal wind velocities observed a week prior the occurrence of the SSW.

Table 3.1: The classification of minor and major stratospheric warmings with the aid of the plots from Figure 3.2 to Figure 3.9 produced using NCEP and SANAE HF radar data.

STRATOSPHERIC PARAMETERS							**MESOSPHERIC PARAMETERS**			**WARMING TYPE**	
Year	**Day**	**$T_m \pm \sigma$ (K)**	**T_{min} (K)**	**T_{max} (K)**	**ΔT (K)**	**U_{ssw} (m/s)**	**Day**	**$U_m \pm \sigma$ (m/s)**	**U_{mlt} (m/s)**	**Minor SSW**	**Major SSW**
2002	235	205±12	195	230	35	48	228	5 ± 39	-8	✓	
	243	208±9	200	230	30	55	235	20±20	-28	✓	
	255	210±11	205	235	30	40	248	-12±20	-	✓	
	268	230±12	210	240	30	-22	261	2 ± 16	-22		✓
2003	287	250±10	230	270	40	23	281	0 ± 15	15	✓	
2004	220	190±4	196	205	9	84	214	2±20	20	-	-
2007	263	220±13	210	245	35	42	256	0 ± 22	24	✓	

The criterion for classifying major and minor warmings is described in section 3.1 and informs the interpretation of the results in Table 3.1. Under the panel titled stratospheric parameters, it is intended to establish the significance of temperature perturbations at stratospheric heights. Column 3 in Table 3.1 gives the day of the temperature enhancement and a mean temperature with a standard deviation corresponding to it ($T_m \pm \sigma$). If the sum of the positive standard deviation $+\sigma$ and the mean value (T_m) is less than the recorded temperature for the day, the enhancement is deemed significant. Mathematically, an inequality '$(T_m + \sigma) < T_{max}$' implies a significant warming. If the difference between the minimum temperature during the week of the warming and the maximum temperature during the same week is greater or equal to 25 K with no wind reversal then the phenomenon is defined as minor warming. Where there is total change of direction in zonal mean wind propagation the phenomenon is defined as major warming. This means that the condition '$\Delta T \geq 25$ K' is a prerequisite for any SSW event to occur.

The panel titled 'mesospheric parameters' depicts the zonal mean wind behaviour in the MLT that took place a week prior the occurrence of a significant warming. Column 8 depicts the day of a mesospheric wind reversal while Column 9 shows the average zonal wind velocity and its standard deviation ($U_{mlt} \pm \sigma$) a week before the occurrence of the SSW. Column 10 reveals the velocity (U_{mlt}) signifying the actual wind reversal. To illustrate how the measurements in Table 3.1 were interpreted in order to arrive at a conclusion whether the SSW event was minor or major, the results of day 235 in year 2002 (first row) are explained.

Consider data corresponding to day 235 for year 2002; the recorded mean temperature in column 3, 205 K, has an uncertainty ±12 K and the maximum allowable mean temperature is obtained by adding +12 K to 205 K giving the sum total of 217 K. The recorded stratospheric temperature on day 235 in column 5 is 230 K demonstrating a 13 K warming significance (obtained by subtracting 217 K from 230 K). The temperature increase in day 235 shown in column 6 is 35 K. The stratospheric zonal mean wind velocity in day 235 observable in column 7 is positive implying a partial reduction that does not lead to a total directional overturn. The negative mesospheric velocity corresponding to day 235 indicates the wind reversal that took place a week prior the event. All these observations show that the warming in day 235 of year 2002 is a minor SSW event. Had the stratospheric zonal wind velocity in column 7 been negative, the warming in day 235 would have been classified as a major SSW event. This is the case in day 268. The columns under the panel 'warming type' give the final conclusion on the type of a significant warming based on the outlined procedure.

After employing the above described criterion, the results shown in Table 3.1 suggest that years with minor SSW events are years 2002, 2003 and 2007. In keeping with the main objective of this work which is to study short period planetary wave activity during minor warming events, the planetary wave variability at mesospheric heights and the possible interaction with tides is investigated in the said years only. Only zonal and meridional mesospheric wind observations of the years 2002, 2003 and year 2007 are presented in Chapter 4. Years 2004 and 2005 are excluded since they show no evidence of a minor SSW event occurring.

It is now established that the dynamic state of the Southern Hemisphere stratosphere during the winter of 2002 is atypical (see Baldwin et al., 2003; Dowdy et al., 2004; Esp et al., 2005; Siskind et al., 2005). Researchers also understand that these unprecedented stratospheric dynamic conditions influenced the mesospheric wind and temperature distribution (eg Espy et al., 2003; Hernandez, 2003; French et al., 2005). The results shown from Figure 3.1 to Figure 3.9 are in agreement with existing literature in this regard. The temperature plots shown in Figure 3.1 (a) to (e) illustrate that the arbitrary increase in stratospheric temperature due to planetary wave activity in all the years studied (2002, 2003, 2004, 2005, 2007), occurs during winter months between August and October thus agreeing with existing literature (see Matsuno (1971), Labitzke and Vanloon (1999) and others). The stratospheric temperature behaviour in year 2002 shown in Figure 3.1 (a), is characterised by many stratospheric significant warmings compared to years 2003, 2004, 2005 and year 2007 demonstrating the uniqueness of the 2002 stratospheric wind behaviour as previously reported by other researchers (eg Mbatha et al., 2010; Yamashita et al., 2010; Mthembu (2013) and others). It is apparent from all presented MLT zonal mean winds that an MLT wind reversal often precedes a stratospheric warming by about a week (see Figure 3.2 to Figure 3.9) and this is consistent with the results presented by Dowdy et al, 2004; Espy et al, 2005; Mbatha et al, 2010 and others. According to Baldwin et al., 2003; minor SSW events in year 2002 occurred near days 236, 244 and 256 while a major SSW was reported to have occurred near day 269 essentially agreeing with days shown in Figure 3.3 and presented in Table 3.1. The occurrence of a 2002 major SSW event can be attributed to large planetary wave amplitudes that were present during this year (2002) as reported by Espy et al, 2005; Baldwin et al, 2003 etc and this is investigated further in Chapter 4.

Having investigated the possible link between the wind behaviour in the MLT region and the behaviour in the stratosphere; the planetary and tidal wave behaviour at mesospheric heights is examined thus unpacking waves that possibly led to stratospheric temperature enhancements.

Chapter 4

Tides and Planetary Waves during SSW

4.1. Introduction

Understanding wind propagation and the activity of different kinds of waves in the MLT region proves resourceful when investigating the dynamical link between the middle and upper atmosphere. Planetary waves, tides and gravity waves play a significant and an influential role in the manifestation of processes in the middle atmosphere. The focus of this study is on the tidal and planetary wave activity in the MLT region during SSW events.

There is a significant number of publications on the meteorological processes that are caused by, result in or affected by the planetary and tidal wave ability to induce SSW events. Randel (1993) suggested that during SSW events ozone concentration increases at lower latitudes while it decreases at higher latitudes. This then implied that during SSW events, the SDT amplitude variation depended on ozone variability. Chau et al. (2009) studied the quiet variability of equatorial electric field cross magnetic field ($E \times B$) drifts during SSW events. In their findings, they made an assertion that there is a possible link driven by the global planetary wave activity between $E \times B$ drifts and SSW events. Sridharan et al. (2009) and Chang et al. (2009) attributed the tidal wave variability during SSW events to non-linear interactions between SDT and planetary waves. Goncharenko et al. (2010) employed a general circulation model to establish that non-linear interaction between tides and planetary waves during SSW events could be a possible cause of persistent variations in the low latitude ionosphere occurring several days after the SSW. Lim et al. (2012) in their investigation of tidal behaviour during SSW events demonstrated that tidal amplitude decreased during the course of SSW events and increased right after the occurrence of this event. Due to this, they ruled out ozone and water vapour as inducers of tidal amplitude variation. Their conclusion was that latent heat from tropospheric heights and extreme SSW events might be the possible cause. Other researchers who have described the activity and interaction of tides and planetary waves include Pancheva and Mitchell, 2004; Hibbins et al., 2007, Mthembu et al., 2013 and others. Though much has been done in understanding and unpacking planetary and tidal wave activity and possibly their interaction in the MLT region during SSW events, very little attention has been paid to planetary waves with a 2 to 6 day period range occurring during minor warmings in the Southern Hemisphere region. This is the space or a gap that this work attempts to fill.

This section seeks to draw a tidal and planetary wave picture in a manner that reveals prominent wave periods in the MLT region. The period interval being investigated (day 200 to day 300) coincides with the occurrence of minor warmings established in Chapter 3. This is done so as to track any likely influence that planetary and tidal waves might have in the stratospheric heat distribution. The investigation first looks at the atmospheric tidal behaviour taking place at meteor heights. This is done in section 4.2. The study then through the application of a wavelet transform presents the planetary wave activity in section 4.3. Planetary waves, to be referred to as p-waves, are presented after the tidal wave activity so as to enable the investigation of the possible modulation between these primary waves. The investigation of a possible Semi-diurnal tide (SDT) modulation in section 4.3 is the first step towards supporting a proposition that there is a possible non-linear interaction between p-waves and tides.

4.2. Tidal Wave Activity in the MLT Region

In an effort to visualise dominant atmospheric tides, the study first presents the hourly zonal/meridional wind variation for the year of investigation. This plot is generated using mesospheric wind data processed as outlined in section 3.1. The zonal or meridional velocity is then entered into the short time Fourier transform (STFT) so as to reveal the dominant wave periods and their time of occurrence. The output of the STFT technique is a two dimensional dynamic spectra whose components include frequency, time and amplitude. This is achieved through employing a travelling window over the entire signal. In this work, the window length of the data considered for the FT calculation was 24 hours and the said window was incremented by 24 hours at a time. This means that the FT technique was conducted on a window that stretched 24 hours in the time series and the results were attributed to one day. The window was then shifted to the next 24 hours and same calculations were made. This activity was conducted over the entire series giving daily frequency and amplitude variations and the corresponding time of occurrence of any frequency-amplitude event. The established interval or time of the year corresponding to the minor warming event is extracted thus increasing the visibility of the tidal wave activity during minor warming events. This is done for all the years under examination (years 2002, 2003 and 2007).

4.2.1. Year 2002 Tidal Wave Activity

The tidal wave analysis commences with year 2002. The analysis has been performed from the year 2002, 2003 and 2007 HF radar wind data. Figure 4.1 (a) displays a column of plots along the zonal component for year 2002. Figure 4.1 (a) (i) shows the mean zonal wind fluctuation in meters per second (m/s) while Figure 4.1 (a) (ii) is the wind dynamic spectra obtained after applying STFT into the zonal mean wind. The dynamic spectra in Figure 4.1 (a) (ii) covers the entire year of 2002. The frequency is measured in cycles per day (CPD) and different spectral colours mark varying amplitude as per the wave activity. It is apparent from the annual dynamic spectra that a 2 CPD frequency wave known as the semi-diurnal tide (SDT) is highly active throughout the year. This is consistent with previous literature which suggests that SDT waves are the most active tides at high latitude (eg. Pancheva (2001), Srindharal (2009), Chang et al. (2009), Mthembu (2013) etc). This work is interested in the wave activity during minor warming days hence the results are narrowed down in Figure 4.1 (a) (iii). Figure 4.1 (a) (iii) is a segment of the year round dynamic spectra starting from day 200 to day 300, a region coinciding with the presence of significant temperature enhancements. The dynamic spectrum displayed in Figure 4.1 (a) (ii) ranging from 0 to 4 CPD is marked by many data gaps represented as white bands. Data-gaps may be a result of equipment not operational or the presence of geomagnetic storms among other reasons.

Diurnal tides have a frequency of 1 CPD and their activity is observed in Figure 4.1 (a) (iii) at around day 205, 248, 264 and 287. These are localised in time with amplitudes averaging at 25 m/s. Observable also in Figure 4.1 (a) (iii) are signatures of wave activity with a frequency of 3 CPD near day 218, having amplitude speed of about 35 m/s. Localised patches of SDTs are observable in days 203, 217, 220, 228, 229, 235, 239, 247, 261, 263, 265, 267, 285, 294 and 297. These non-continuous waves have amplitude peaks ranging from 20 to 40 m/s.

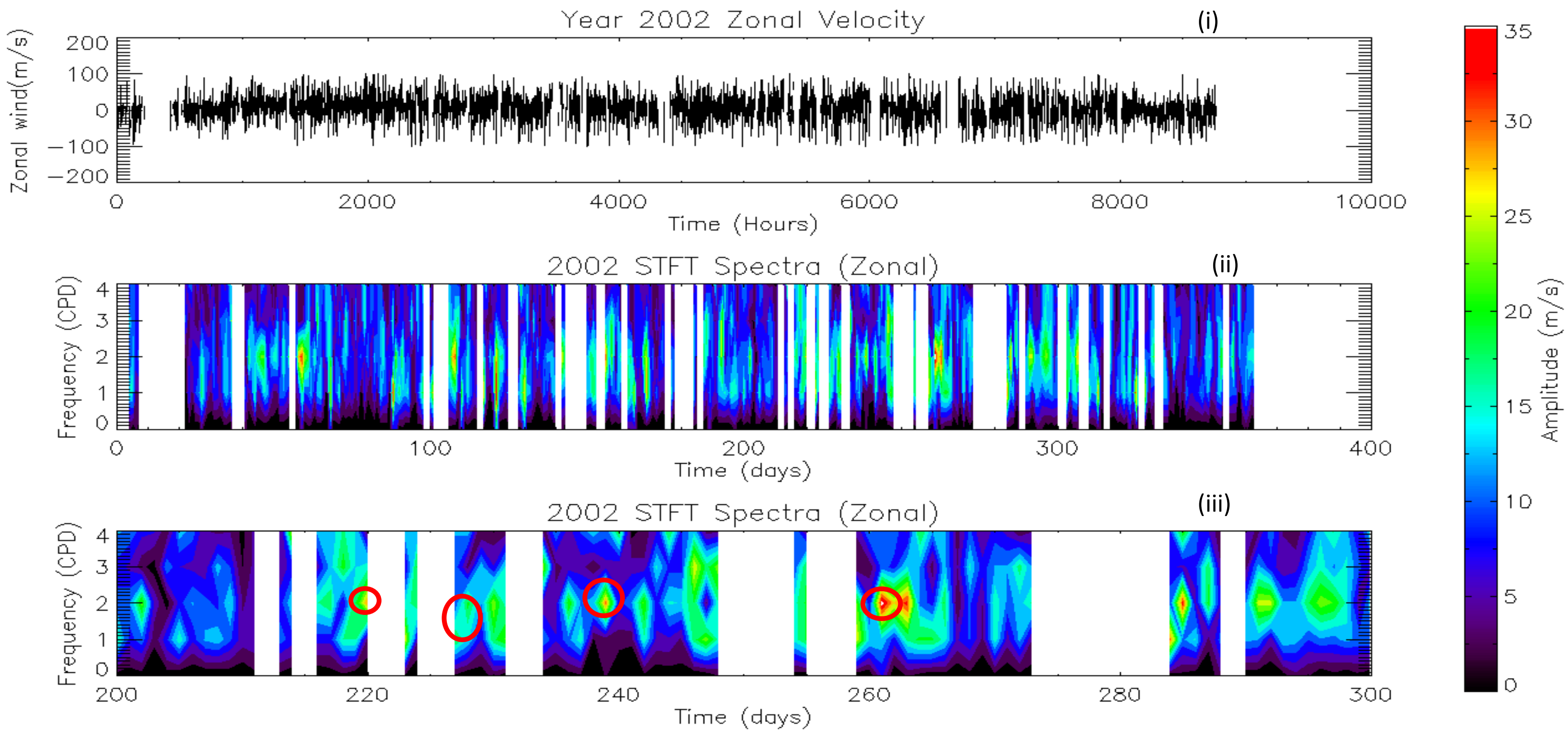

Figure 4.1 (a): Year 2002 mesospheric wind behaviour along the zonal component. The top panel (i) shows the zonal velocity fluctuation, the second plot (ii) shows the STFT dynamic spectra for the entire year of 2002 while the third subplot (iii) reveals tidal wave activity in an interval concurring with SSW events. The red circled tidal activity occurred about a week prior the SSW events.

Though tidal wave activity is spread throughout the selected day interval (ie. from day 200 to day 300), extra attention is given to the activity that took place in days 228, 235, 250 and 262. The SDT activity in days 228, 235, 250 and 262 displays amplitudes of 25, 25, 45 and 45 m/s respectively. The above mentioned SDT wave manifestation occurred 7 days before minor SSW events were recorded. This work will investigate a possible relationship between the SDT activity in day 228 and the minor warming in day 235, between the localised tide in day 235 and the warming event in day 243 and between the SDT in day 262 and the SSW event in day 268. The proposal of a 7 day relationship between mesospheric winds and stratospheric warmings was reported by Mbatha et al. (2010). They observed that a directional detour in the MLT always occurred about a week prior the occurrence of significant temperature enhancements in the stratospheric region.

Figure 4.1 (b) presents a column of plots similar to Figure 4.1 (a) but for the meridional component. It is apparent that the meridional wind displays reduced wave activity compared to its zonal counterpart. There is minor diurnal tide activity in days 202, 205, 213 and 296 reaching amplitudes of about 18 m/s. SDT waves continued to display their dominance. The localised SDT patches reveal reduced intensity compared to the ones along the zonal component. Localised SDT activity is observed near days 204, 208, 218, 228, 238, 246, 248, 260, 264 and day 286. Out of these days, our coordinates of interest are days 228, 238 and 260. According to Table 3.1, significant warmings in year 2002 occurred in days 235, 243, 247 and day 268. In a way similar to findings by Mbatha et al. (2010), localised activity in days 228, 238, 240 and 261 can be thought to have possibly influenced the manifestation of significant warmings. It is important however, to note that Mbatha et al. (2010) studied planetary waves not tides.

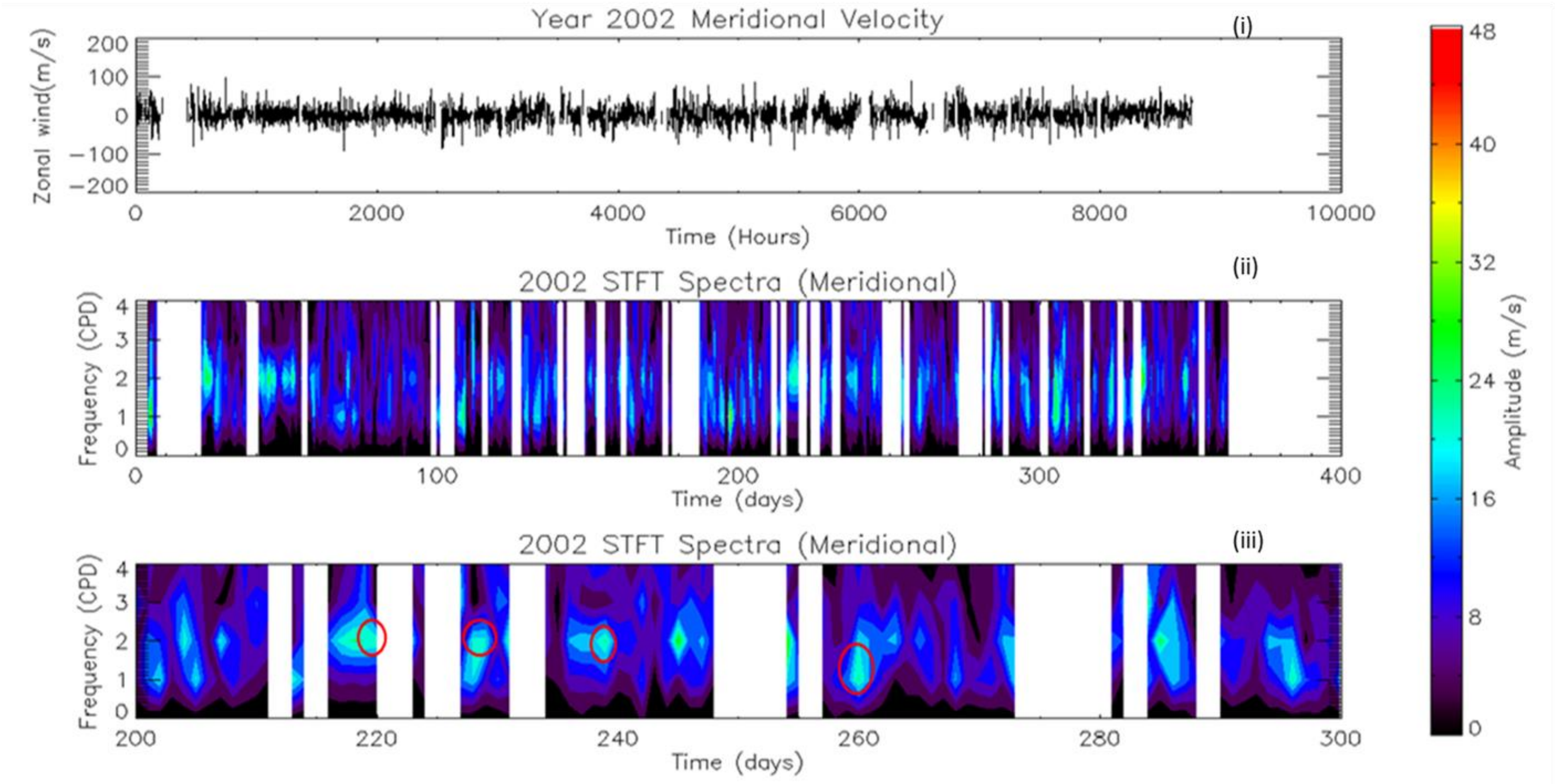

Figure 4.1 (b): Same as Figure 4.1 (a) but along the meridional component.

4.2.2. Year 2003 Tidal Wave Activity

Continuing with the investigation of the tidal wave activity at mesospheric heights, year 2003 findings are presented in Figure 4.2 (a). This figure shows a panel of plots presented in the same format as for year 2002 along the zonal component. Year 2003 suffers many data gaps making it difficult to conduct conclusive analysis. Analysis was only carried out where available data exceeded 60 % of a day. The diurnal tide observable in day 283 is the only activity that may be associated with a significant temperature rise in the stratosphere near day 287. SDT activity is observed in days 202, 213 and 256. There is a high chance that these were not the only days where SDT wave displayed prominence but the invisibility can be attributed to limited experimental data.

Figure 4.2 (b) follows the same format as Figure 4.2 (a) but is for the meridional component. Mean wind fluctuation along the meridional component still exhibits low activity compared to the zonal component. There is tidal wave activity by both diurnal and SDT waves. Diurnal tides are active in days 200, 212, 238, 240, 245 and day 285. The diurnal tide in day 285 is particularly interesting because it registers maximum amplitude (48 m/s). This activity took place only two days before the SSW event in day 287. SDT active days include day 227, day 241, day 275 and day 279. The activity in day 279 is near day 280, seven days before the significant warming. This suggests a possible tidal influence on the observed significant rise in stratospheric temperature.

When comparing the meridional wind behaviour in year 2003 to that of year 2002, one can see that the latter year saw increased SDT variability. This is apparent when comparing Figure 4.1 (b) (ii) (year 2002 meridional tides) to Figure 4.2 (b) (ii) (year 2003 meridional tides). This remark holds despite hindrances in the interpretation of results due to data gaps in year 2003. It is however the diurnal tides in year 2003 that had well defined peaks compared to the diurnal tides in 2002.

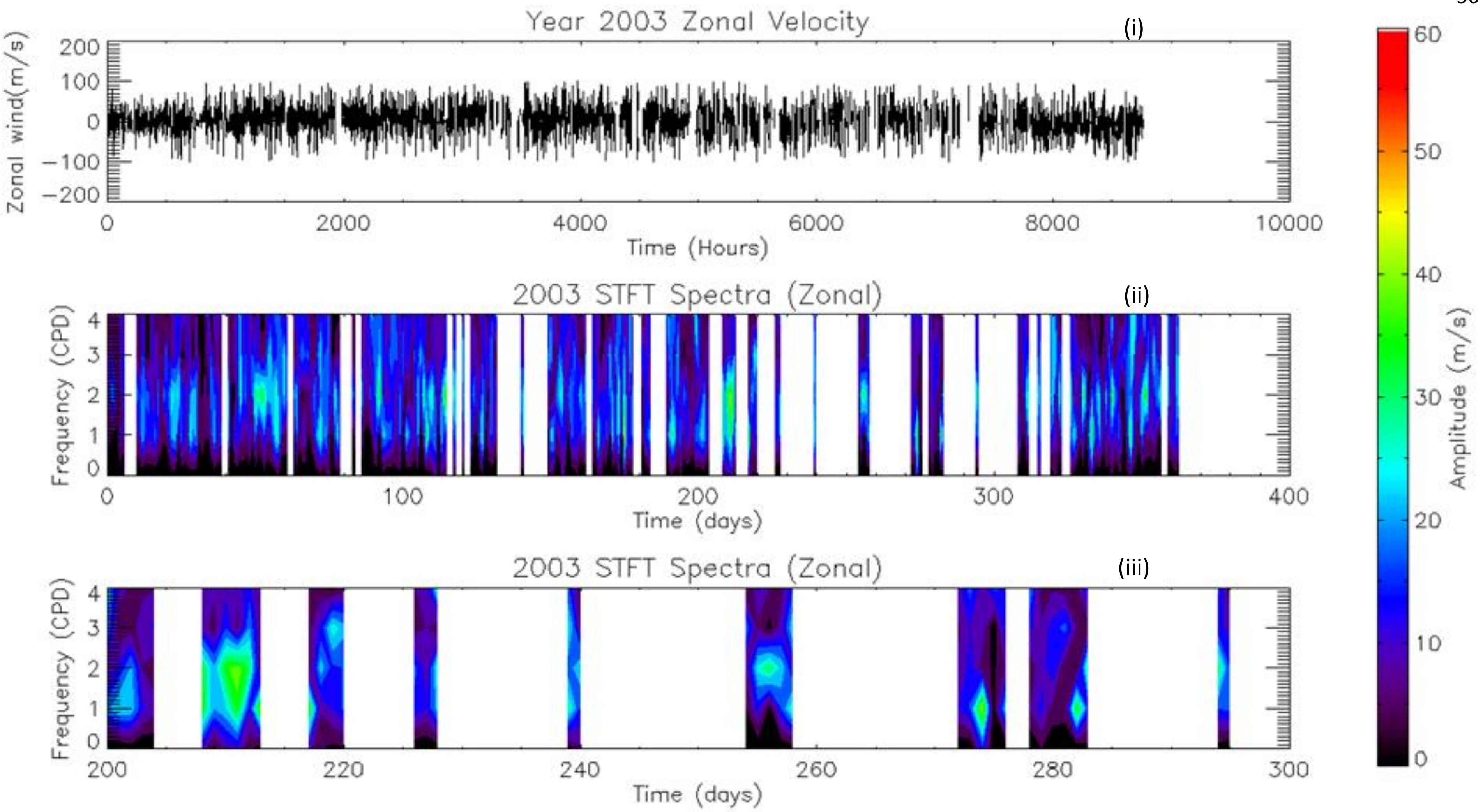

Figure 4.2 (a): Same as Figure 4.1 (a) but for year 2003 along the zonal component.

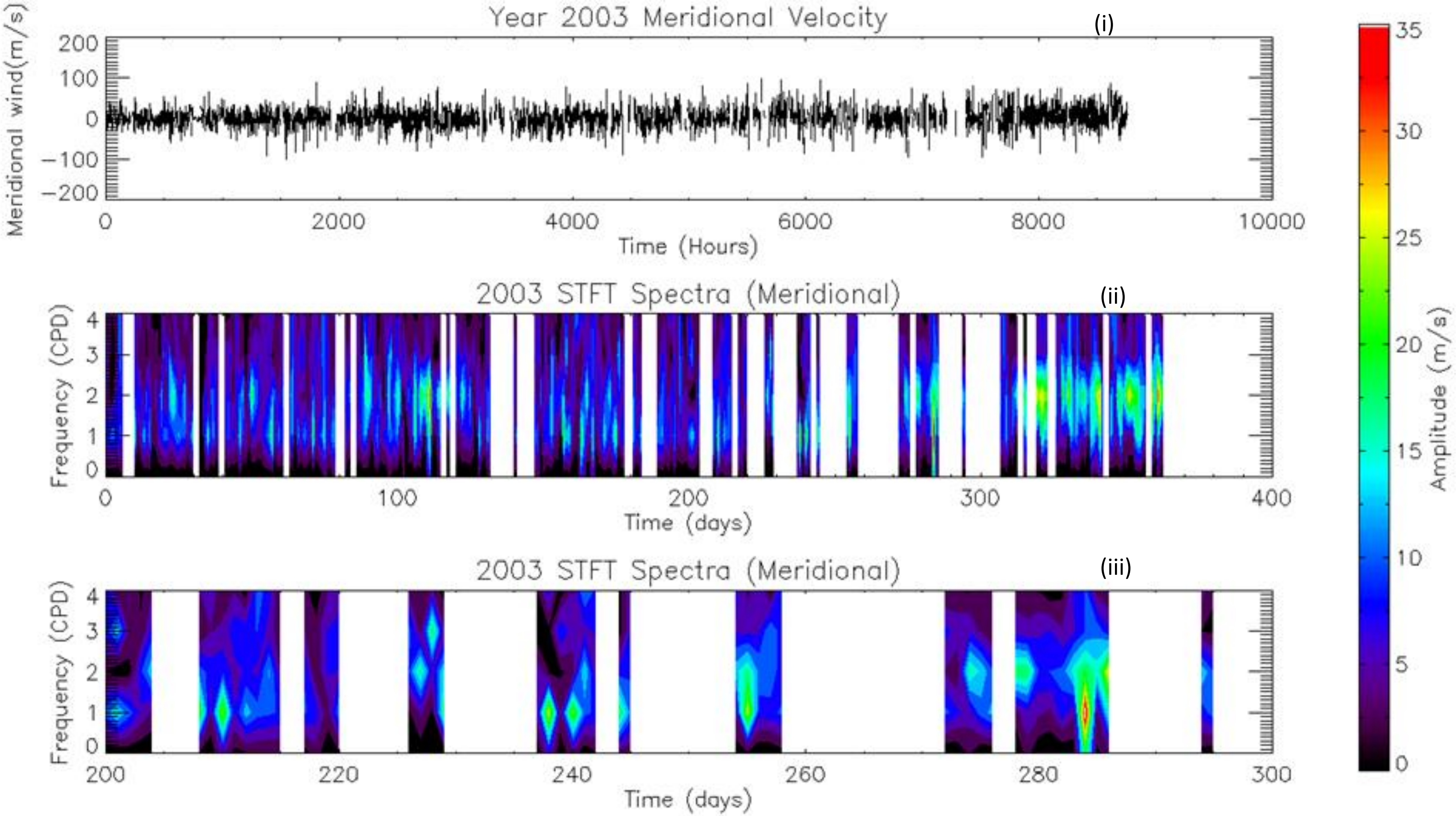

Figure 4.2 (b): Same as Figure 4.1 (b) but for 2003.

4.2.3. Year 2007 Tidal Wave Activity

The tidal wave behaviour at mesospheric heights for year 2007 is shown in Figures 4.3 (a) and (b). The first column of graphs (Figure 4.3 (a)) demonstrates activity along the zonal component and is presented in the same format as for year 2002. Figure 4.3 (b) presents findings along the meridional component. Zonal component still sees more robust activity compared to the meridional direction. In Figure 4.3 (a) diurnal tidal activity is observable near days 200, 210, 212, 214, 230, 254, 291 and day 299. These diurnal tides have amplitudes ranging from 20 to 25 m/s. SDT activity is observed near days 230, 252, 256, 262, 263, 275, 286, 288 and day 295. Days 256, 275 and 286 displayed activity with amplitudes ranging from 40 to 45 m/s. Day 295 registered maximum activity compared to other days and even to the other two years (2002 and 2003) with amplitudes reaching close to 60 m/s. However, this study will focus in the SDT activity in day 256 since it took place about a week prior the occurrence of a significant temperature enhancement in the stratosphere hinting a possible influence. The significant warming in year 2007 was recorded to have taken place near day 262 (see Table 3.1).

Figure 4.3 (b) displays tidal wave activity for the meridional component. Diurnal tides can be seen in days 205, 211, 215, 224 and 236. These diurnal tides are localised in time and have amplitudes close to 25 m/s. High SDT activity is mostly observed towards the end of the selected interval from day 250 to day 300. This is not surprising since this time coincides with winter months in the Southern hemisphere. Days that see localised SDT activity include day 216, 225, 234, 241, 254, 256, 258, 265, 269, 275, 286, 290, 292 and day 292. These are clearly defined SDT wave signatures with amplitudes ranging from 24 to 32 m/s. This work will however investigate activity in days 254 and 256 near a week before the occurrence of a minor SSW event in day 262. When examining the SDT activity along the meridional component in year 2007 against the same activity in years 2002 and 2003, one notices that the 2007 propagation is consistent, well defined and though localised, it is spread throughout the selected interval.

Having identified stratospheric warmings and the presence of tidal wave activity prior the SSW events, the study now investigates a possible interaction between planetary waves and tides. This is going to be done in three steps, namely:

1. Investigation of a possible modulation of tides at planetary wave periods.
2. An investigation of a possible interaction between p-waves and tides using bispectral analysis.
3. An examination of a possible formation of secondary waves due to a possible interaction between the primary waves (planetary waves and tides).

The above three steps address the proposition that there exists a non-linear interaction between p-waves and tides. Chapter 4 only covers the first step which is modulation. Bispectral analysis and secondary wave formation are investigated in Chapter 5.

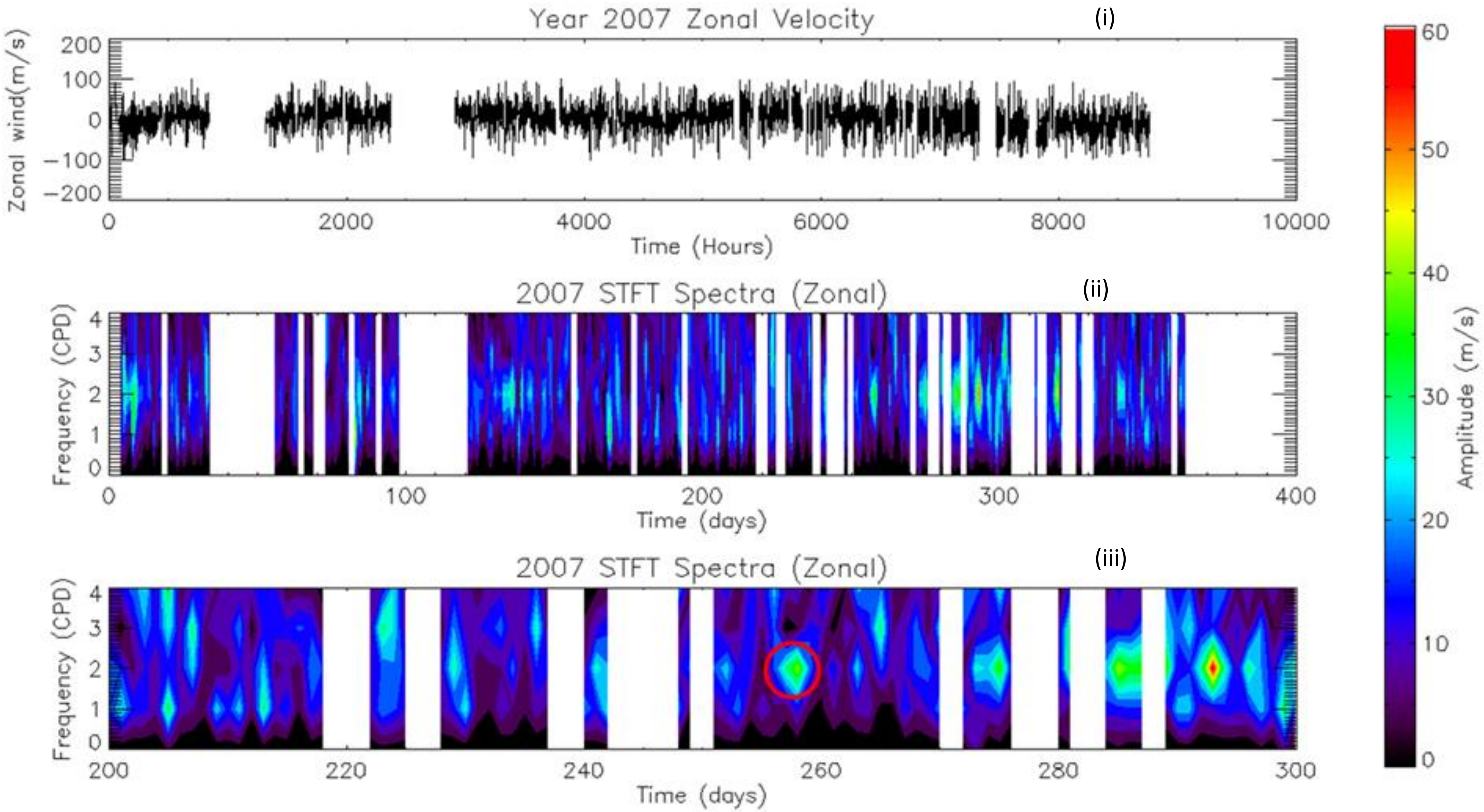

Figure 4.3 (a): Same as Figure 4.1 (a) but for year 2007.

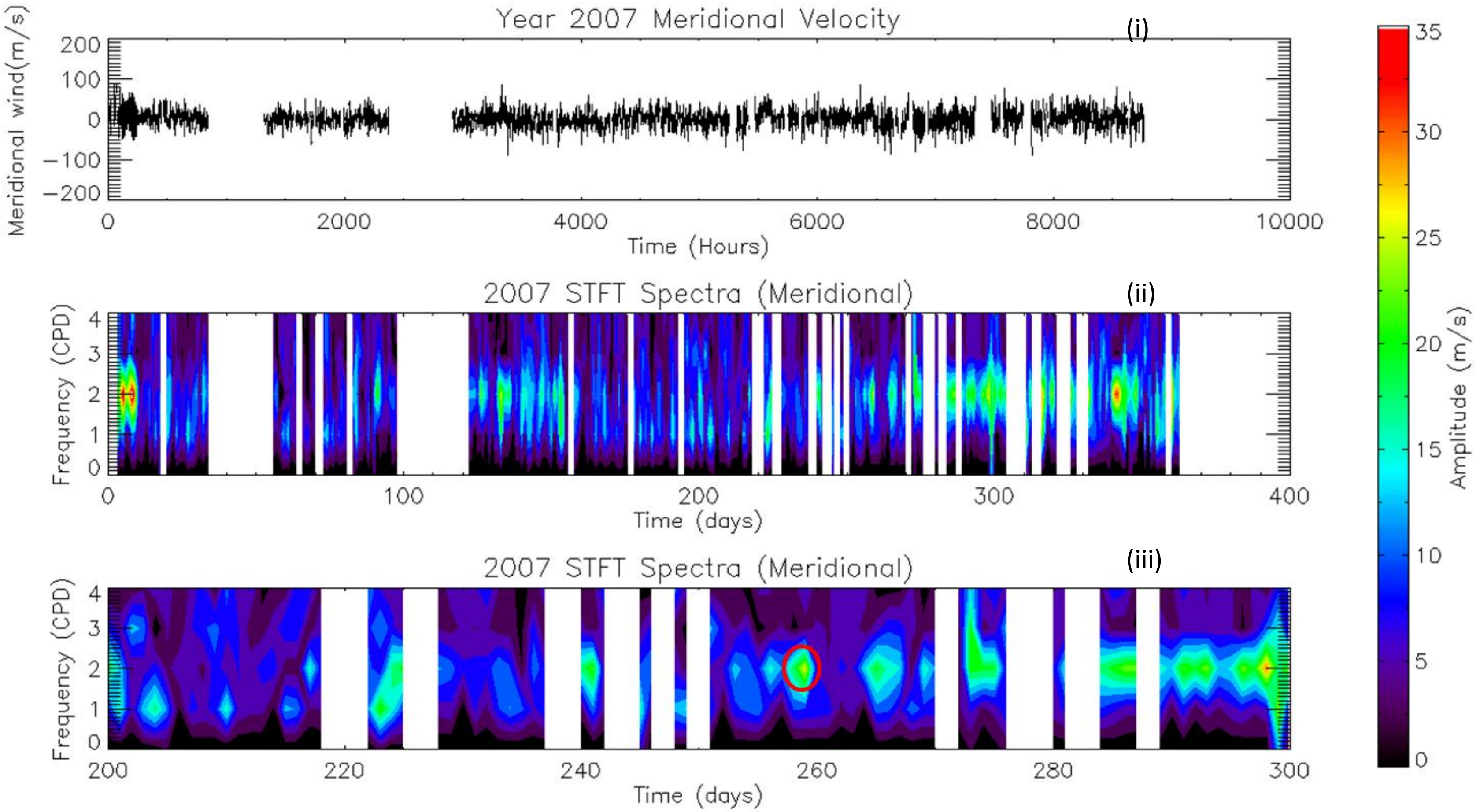

Figure 4.3 (b): Same as Figure 4.1 (b) but for year 2007.

4.3. Planetary Wave Activity and SDT Modulation

To obtain a comprehensive picture of the p-wave activity and how these modulate tidal wave behaviour in the MLT region, wavelet analysis is conducted. As indicated in the analysis techniques, this procedure retains the time parameter thus improving visualisation of the dynamic wave behaviour. Wave periods considered in this study are only limited to periods between 2 and 6 days. Constraining the range to a maximum of 6 day periodicity provides clear visualisation of short term p-waves and eliminates any possible over shadowing by larger period waves.

The planetary wave activity and SDT modulation for year 2002 is presented first in Figure 4.4 followed by the same behaviour but for year 2003 in Figure 4.5 and lastly for year 2007 in Figure 4.6. In each case the study presents activity along zonal and meridional components. Each figure consists of a panel of plots arranged in the hierarchal format starting with the p-wave activity (the top panel) followed by the zonal or meridional SDT amplitude variation (middle panel) and lastly the SDT wave modulation (bottom panel). Plots are presented in this format so as to investigate the modulation that exists between p-waves and atmospheric tides. The second panel depicts the SDT amplitude variation extracted from STFT dynamic spectra in section 4.1.1. This amplitude is the input for the wavelet transform so as to yield the third panel (SDT modulation). The study therefore trace any likely indicators of an interaction between p-waves and atmospheric tides around days of significant stratospheric warming. The minimum period in the SDT wavelet spectrum is 2 days (see bottom panel of Figure 4.4 (a)). This is because for SDT amplitudes, the sampling period is one day making the Nyquist frequency to be 0.5 CPD. This translates to a minimum observable period of 2 days. There are no data gaps in the p-wave and SDT wave variability as per the wavelet analysis. This is because data was linearly interpolated to eliminate NaNs thus facilitating the application of the wavelet function. Linear interpolation was only carried out if available data in the window being studied exceeded 60 percent.

4.3.1. Year 2002 P-Wave Activity and Tidal Wave Modulation

As a means to study p-wave variability during the winter months of year 2002 in the MLT region, the study first presents in Figure 4.4 (a), MLT wave activity along the zonal component. Distinct and localised p-wave activity is observed throughout the first panel of Figure 4.4 (a). The p-waves found to be active along the zonal component include 2, 3 and 4 day p-waves. P-waves with 2 day periodicity are observable in days 230, 250, 284 and day 300. All these days display localised 2 day p-wave activity averaging at about 45 % of the maximum power. The 3 day period p-wave is observable on day 250. This activity is localised in time and displays maximum power (100 %) (See the white dot in day 250 of Figure 4.4 (a)). The near 4 day period p-waves are seen in days 210, 275 and day 360. These days have power spectra reaching approximately 20 %, 60 % and 25 % of the normalised power spectrum respectively. It is noticeable that most of the p-wave activity takes place between day 200 and day 300, an interval concurring with the presence of SSW events. This is consistent with existing literature that p-wave activity causes and affects SSW manifestation.

The second panel in Figure 4.4 (a) shows the zonal wind amplitude extracted from the third panel of Figure 4.1 (a). This is the daily variation of the zonal wind amplitude as per the year 2002 STFT. The chosen amplitudes correspond to SDT frequency (2 CPD) and are entered into a wavelet transform constrained to 2 to 6 day period range. This action reveals the modulation of SDT at p-wave periods and results in an activity shown in the third panel of Figure 4.4 (a).

The third panel in Figure 4.4 (a) reveals SDT wavelet spectra. The third panel of Figure 4.4 (a) indicates some modulation of SDT wave at p-wave periods. The period at which SDT amplitude varies include 2 days, 4 days and 5 days. The SDT activity in the 2 day periodicity is evident in days 230, 240, 260 and day 284. The corresponding normalised power spectra for the said days reach about 20 %, 85 %, 60 % and 75 % respectively. In the 4 day periodicity, SDT waves are active around days 200, 220 and day 265. The normalised wave power for the said days is about 45 %. The SDT variation at 5 day periods is observable in day 300. The normalised power spectrum characterising this variation reaches about 80 %.

When examining the correlation between the activity in the top panel and the bottom panel in Figure 4.4 (a), it is observable that the coincidence between p-wave activity and SDT variation at p-wave periods took place in days 220, 230, 250 and day 284. This suggests that during the said days p-wave activity possibly modulated SDT waves. In day 220, a near 3 day p-wave seen in the top panel, possibly modulated an SDT wave active at 4 day periodicity in the bottom panel. In day 230, five days before a minor SSW event, a 2 day p-wave active in the top panel of Figure 4.4 (a) possibly modulated an SDT wave at 2 day periodicity. This activity is red circled and will be carried over to Chapter 5 for further investigation. Day 250 hosts a 3 day p-wave with maximum power and a localised 2 day p-wave possibly modulating an SDT wave with about 20 % normalised wave power. The peak in day 250 and the corresponding SDT peak are red circled for further investigation in Chapter 5. Day 284 presents a possible SDT modulation at 2 day periodicity in the bottom panel by a 2 day p-wave. The rest of p-wave-SDT wave modulation activity is encircled with white circles and there are arrows connecting the activity in the top panel with the activity in the bottom panel.

Figure 4.4 (b) shows activity along the meridional component. The p-waves active along the meridional component have the period range stretching from 2 to 6 days. These are localised 2, 3, 4, 5 and 6 day p-waves active throughout the first panel of Figure 4.4 (b). P-waves with a period of 2 days are observed in days 300 and 350. These p-waves have the normalised power spectrum reaching about 25 % and 40 % respectively. 3 day period p-waves are seen active in days 205, 230 and day 340. They are characterised by normalised power spectra reaching 25 %, 25 % and 70 % respectively. P-wave activity with 4 day periodicity in the top panel of Figure 4.4 (b) is witnessed in days 210 and 350. There is a 75 % normalised power spectrum in day 210 and a localised activity with a normalised power spectrum of about 40 % in day 350. The only p-wave activity with a period of 5 days occurs in day 300. This is the localised activity with a normalised power spectrum reaching about 45 %. P-waves with a period of 6 days are observable in days 210, 250 and day 270. These have normalised power spectra reaching 75 %, 20 % and 25 % respectively.

Similar to the second panel of Figure 4.4 (a), the second panel of Figure 4.4 (b) shows the meridional wind amplitude extracted from the STFT contour plots in Figure 4.1 (b). The truncations in the zonal amplitude variation signal data gaps. The meridional amplitude shown was entered into the wavelet transform to produce wave variation in the third panel.

SDT activity at p-wave periods along the meridional component can be seen in the third panel of Figure 4.4 (b). The p-wave periods hosting the SDT wave variability include 2, 3, 4 and 5 day periodicity. The SDT variability corresponding to 2 day periodicity is witnessed in days 230, 246, 286, 305 and day 335. The normalised SDT wave power in the said days reaches 45 %, 35 %, 25 %, 60 % and 35 % respectively. SDT waves exhibiting variability at 3 day periods occur in days 205, 256 and day 303. The respective normalised wave power for the said activity is 85 %, 40 % and 60 % respectively. 4 day periodicity in the bottom panel of Figure 4.4 (b) hosts SDT variation in days 322 and 348 having 60 % and 45 % power spectra respectively. SDT waves active in 5 day periods are observable in days 230, 250 and 290 with normalised power spectra of 45 %, 15 % and 60 % respectively.

The evidence of a possible SDT modulation is found in days 205, 230, 250 and day 350. In day 205, a near 3 day period p-wave in the top panel of Figure 4.4 (b) seems to have modulated the SDT active at 3 day periodicity in the bottom panel of the same figure. In day 230, a red circled 4 day p-wave peak in the top panel of Figure 4.4 (b) coincides with another SDT activity observable at 4 day periodicity in the bottom panel (see red circled peaks in the figure). Day 250 hosts a 6 day p-wave (see red circled) possibly modulating a red circled SDT peak active at 4 day periodicity. Peaks in days 230 and 250 will be studied further in Chapter 5. Some SDT modulation is observable in day 350 between a 3 day p-wave in the top panel and an SDT active at 3 day periodicity in the bottom panel.

The results presented above show p-waves in the MLT region with periods ranging between 2 and 6 days manifesting themselves before, during and after the occurrence of SSW events, a behaviour consistent with existing literature (eg Dowdy et al., 2004, Mthembu, 2013 and others). Dowdy et al., 2004 reported a similar behaviour with a 14 day p-wave. When comparing activity along the meridional component with the wave variability in the zonal direction, it is evident that for 2 to 6 day periods the latter component sees a more robust and energetic wave variation. The maximum power in the zonal component reaches 100 % while the meridional component sees its maximum variability at 75 % power spectrum. Dowdy et al. (2004) found that p-waves were more apparent in the meridional component compared to zonal direction. The difference in observation can be attributed to the fact that Dowdy et al. (2004) looked at relatively larger periods (eg 14 day p-waves). It is worth noting that there is usually a distinct p-wave activity before every SSW event. This can be seen with the reported 2 day p-wave in day 230 and also with a 3 day p-wave in day 250 which all occurred approximately a week before minor SSW events. Espy et al. (2005) reported a similar behaviour with p-waves with a period range 10 – 16 days. They found that periods in the 10–16 day band grow and become the dominant modes before the peak of the first minor warming. Mbatha et al. (2010) also observed using normalised power spectrum that a 14 day wave signature is registered before the occurrence of the SSW event. The amplified p-wave activity a few days prior the occurrence of an SSW event was first reported by Labitzke and Van Loon (1999) after studying p-wave's phase structure and amplitude in the vicinity of the SSW event. They reported that p-waves often experiences resonant amplification just before the minor warming.

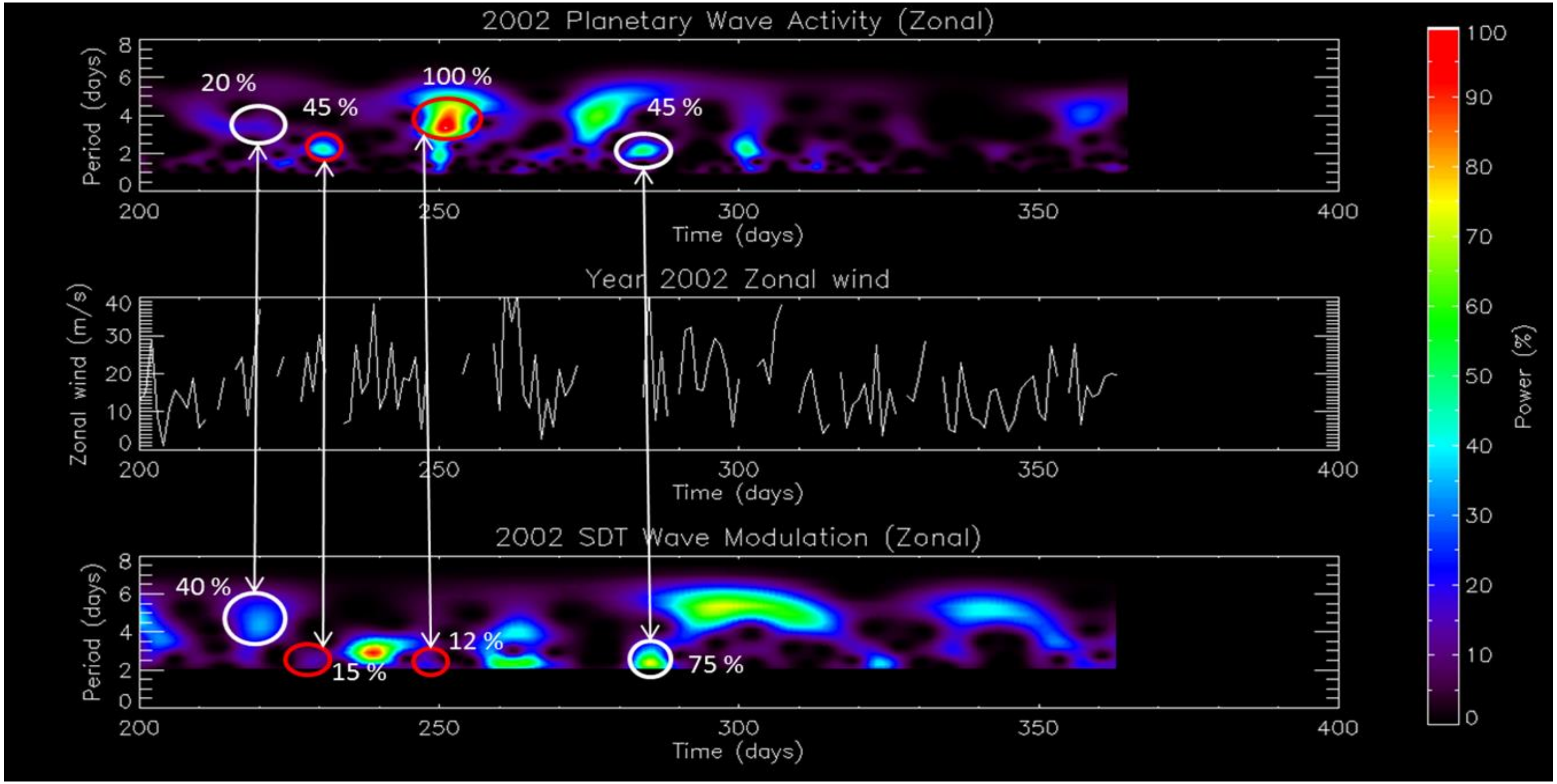

Figure 4.4 (a): The top panel depicts planetary wave activity along the zonal component in the day interval concurring with stratospheric warming events. The middle panel is the SDT amplitude variation sifted from the 2002 STFT spectra plot. The bottom panel shows SDT modulation. The white circled activity shows modulation not related to SSW events while red circled patches are thought to have influenced the reported warmings.

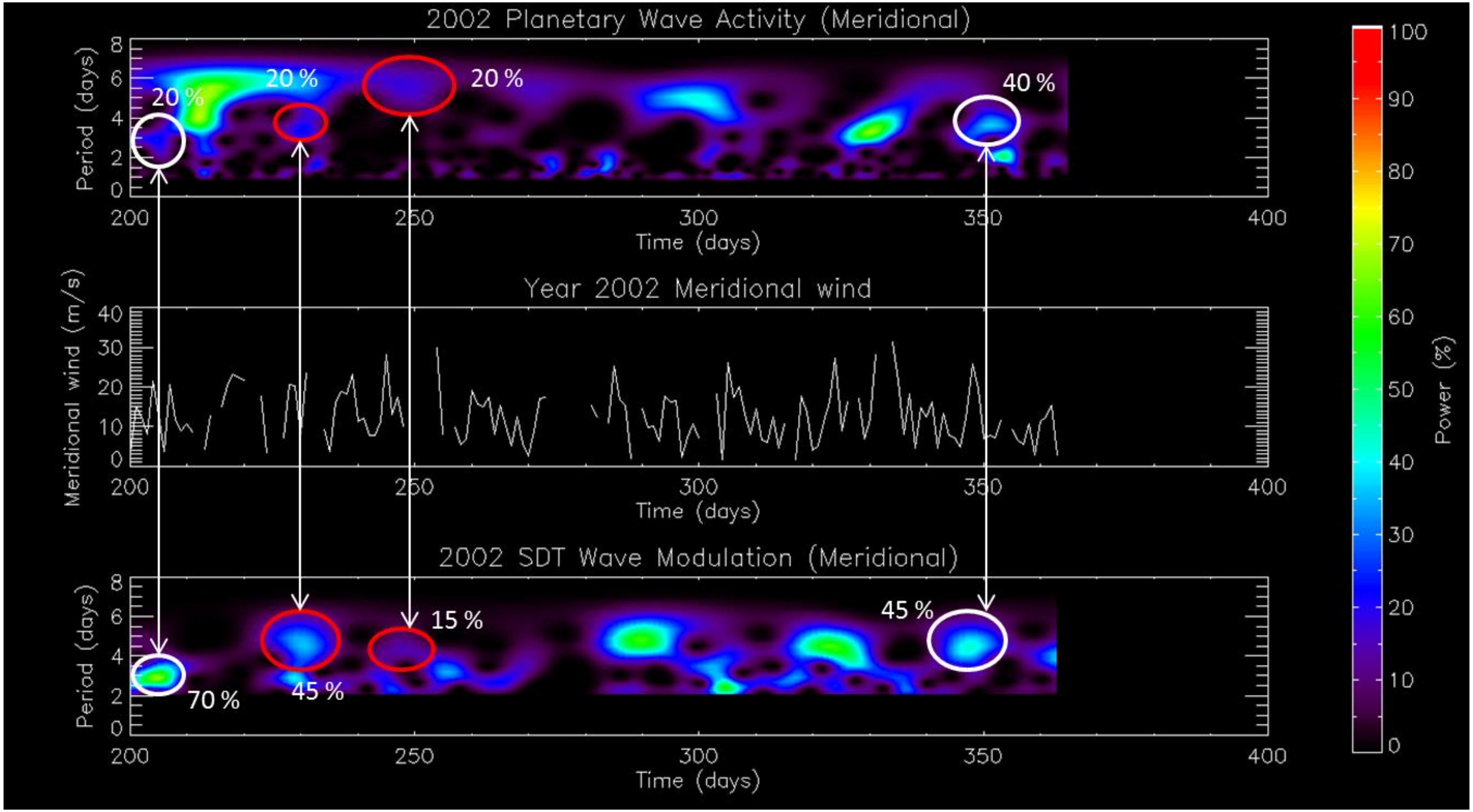

Figure 4.4 (b): Plots depicting the same wave behaviour shown in Figure 4.4 (a) with activity occurring along the meridional component.

4.3.2. Year 2003 P-Wave Activity and Modulation

The wave activity during year 2003 is presented in Figures 4.5 (a) and (b). Zonal activity is shown in Figure 4.5 (a) while Figure 4.5 (b) reveals activity along the meridional component. The analysis for year 2003 p-wave activity resembles that of year 2002. It should be noted that the depiction of results for year 2003 suffers reduced quality due to large data gaps. Where analysis has been conducted, data availability exceeded 60 %. P-wave activity along the zonal component can be seen in the first panel of Figure 4.5 (a). The wave variability in the said panel shows observable p-waves to be 2-day, 3-day and 4-day waves. P-waves with 2 day periodicity are observable in days 222 and 319. These are characterised by power spectra reaching 60 % and 90 % of the normalised power spectrum respectively. 3 day period p-waves show their activity in days 205, 215, 250, 260, 270, 318, 350 and day 355. These have power spectra reaching 60 %, 50 %, 45 %, 25 %, 25 %, 45 %, 20 % and 30 % of the normalised power spectrum respectively. 4 day p-waves show localised activity in days 292 and 360. These have activity with normalised power spectra reaching 60 % and 45 % respectively.

The second panel of Figure 4.5 (a) shows daily zonal amplitude variation extracted from the STFT contour plot in the third panel of Figure 4.2 (a). The zonal amplitude corresponds to SDT variability at mesospheric heights in year 2003. The truncations in the zonal amplitude fluctuations are attributed to the reported data gaps. This SDT variation is pushed into the wavelet function to produce SDT activity at p-wave periods. The outcome is displayed in the third panel of Figure 4.5 (a) and facilitates the investigation of the possible modulation of SDT waves by p-waves.

The third panel of Figure 4.5 (a) shows possible SDT modulation in year 2003. The localised SDT wave activity can be seen in 2-day and 4-day periodicities. The activity corresponding to a 2-day periodicity is observable in days 320 and 330. Both localised wave signatures have power spectra reaching about 45 % of the normalised power spectrum. The SDT waves active at 4 day periodicity are present in days 210, 255, 280 and day 340. This activity has power spectra reaching 45 %, 30 %, 45 % and 20 % of the normalised power spectrum respectively.

Signs of SDT modulation by p-wave variability are observable near days 210, 230, 250, 280 and day 320. In day 210, a near 3 day wave with an activity reaching about 50 % of the normalised power spectrum possibly modulated an SDT wave active at 4 day periodicity. Day 250 sees a localised 4 day p-wave in the top panel possibly modulating the SDT active in the 4 day periodicity in the bottom panel. The activity in the vicinity of day 280 is indicated with a red circle since it may have an influence in the minor SSW event in day 287. The rest of the modulation incidences are indicated with white circles. The last activity to hint a possible modulation occurred in day 320. A 2 day p-wave activity shown in the top panel of Figure 4.5 (a) may have modulated an SDT wave active in the 2 day periodicity in the bottom panel of the same figure.

The p-wave activity at mesospheric heights in year 2003 is also investigated along the meridional component. This behaviour is displayed through the wavelet transform in Figure 4.5 (b). The data along the meridional component also suffered large data gaps thus impacting negatively on the quality of observations. However, data has been linearly interpolated. Wavelet spectrum was calculated only when available data exceeded 60 %. The top panel in Figure 4.5 (b) shows p-wave activity in the MLT region along the meridional component. P-waves that showed prominence in the meridional component include 2, 3, 4 and 5 day period waves. P-wave activity with a 2 day periodicity can be seen in days 285 and 325. The said activity is characterised by power spectra of about 100 % and 45 % of the normalised power spectrum respectively. The 3 day period p-wave is observable in days 235 and 300. The power spectra for said days reach about 45 % of the normalised power spectrum. The 5 day p-wave is seen in days 203 and 284 respectively. These have power spectra reaching 90 % and 65 % of the normalised power spectrum respectively. The wave activity in day 284 stretches from day 280.

The second panel in Figure 4.5 (b) shows daily amplitude variation similar to the one in the second panel of Figure 4.5 (a) but along the meridional component. The meridional amplitude variation is extracted from the meridional SDT variability indicated by the STFT contour plots in the third panel of Figure 4.2 (b). The amplitude variation is pushed to the wavelet transform to give rise to the SDT modulation in year 2003. The SDT modulation in the meridional component of year 2003 is shown in the third panel of Figure 4.5 (b).

The third panel in Figure 4.5 (b) shows some SDT modulation. The localised SDT activity in this panel is observed in 2 day, 4 day and 5 day periodicities. The SDT activity corresponding to the 2 day periodicity is witnessed in days 215 and 230. The said activity has the power spectrum reaching about 20% of the normalised power spectrum. The SDT active at 4 day periodicity is observed near day 280. This has the power spectrum nearing 40 % of the normalised power spectrum. This SDT signature may have been modulated by a 5 day p-wave visible in the top panel of Figure 4.5 (b). Both the SDT activity in the third panel in day 280 and the 5 day wave signature in the top panel are red circled and their possible interaction will be studied further in Chapter 5. There is also an SDT activity at 5 day periodicity in day 340 with a power spectrum reaching about 50 % of the normalised power spectrum.

Year 2003 MLT p-wave variability displayed above shows some similarities with the p-wave behaviour reported for year 2002. There is more p-wave activity in the zonal component than there is in the meridional. P-wave signatures were observed at mesospheric heights just before the occurrence of a minor warming at stratospheric heights agreeing with existing literature (see Labitzke and Van Loon (1999), Espy et al. (2005), Mbatha (2010) and others). A reported 5 day p-wave signature stretching from day 280 to day 284 indicates this wave activity occurring before a minor SSW occurrence in day 287. There is also a 2 day p-wave that displayed maximum power spectra in day 285, 2 days before the reported minor SSW. Both these incidents took place in the meridional component. In the zonal component, a 4 day p-wave signature emerged in day 292, 5 days after the occurrence of a minor SSW event in day 287. All of these results are in agreement with previous literature as pointed out in the earlier discussion of 2002 p-wave behaviour in this section.

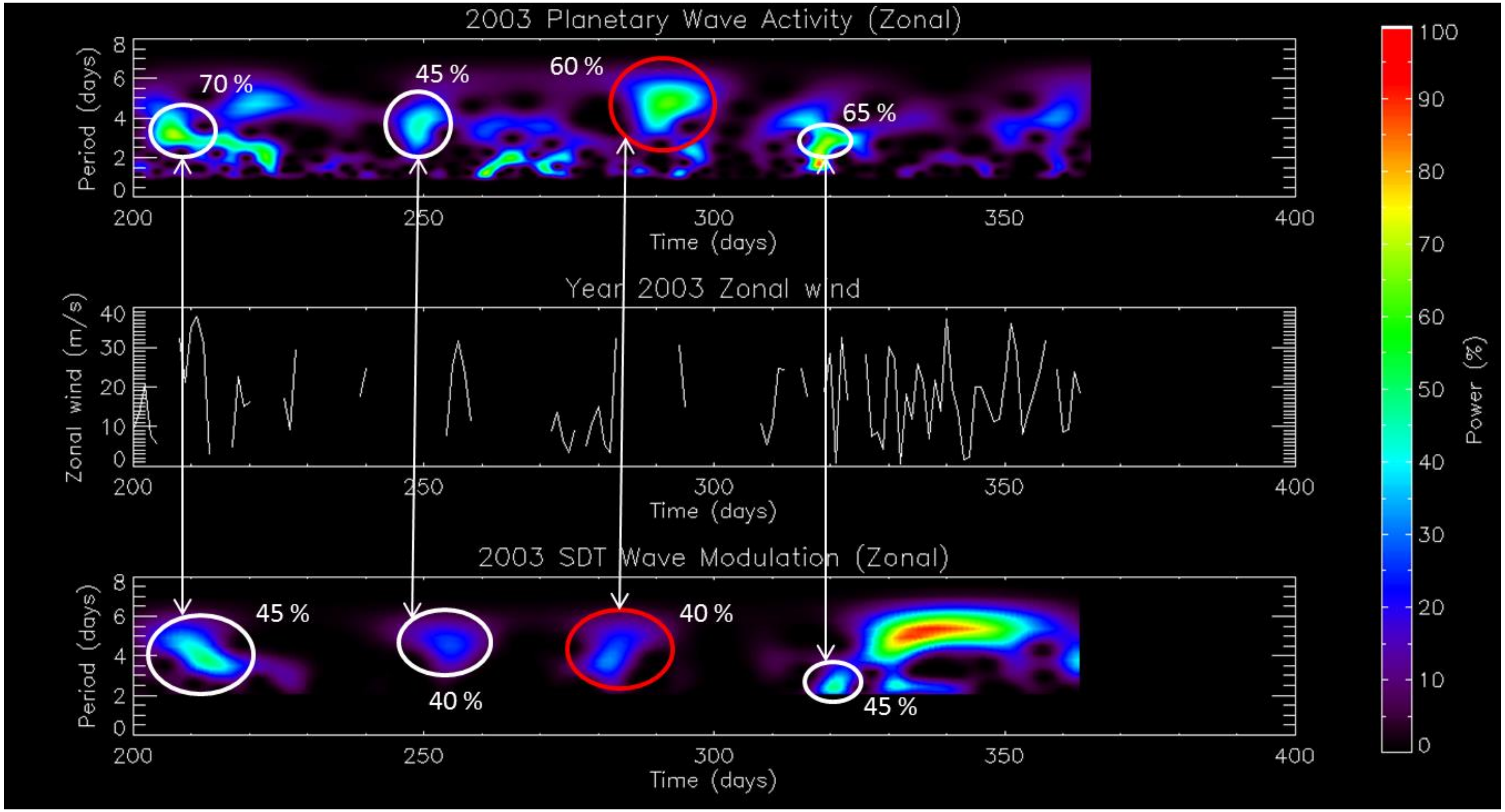

Figure 4.5 (a): Same as Figure 4.4 (a) but for year 2003.

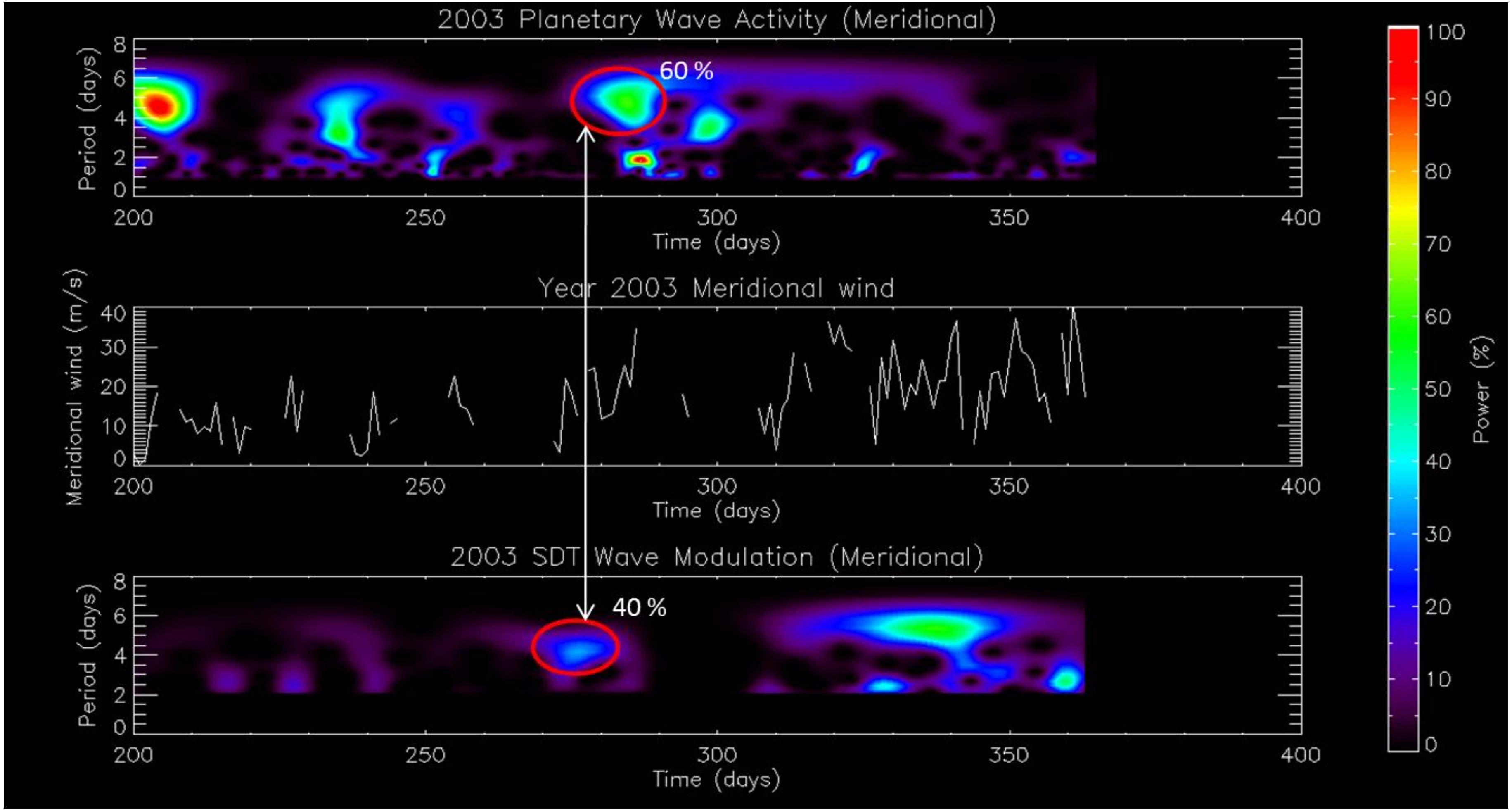

Figure 4.5 (b): Same as Figure 4.4 (b) but for year 2003.

4.3.3. Year 2007 P-Wave Activity and Tidal Wave Modulation

Following the investigation of the p-wave activity and tidal modulation in years 2002 and 2003, we present Figures 4.6 (a) and (b) depicting the same behaviour for year 2007. Zonal activity is shown in Figure 4.6 (a) while Figure 4.6 (b) shows activity along the meridional component. The presentation of results in year 2007 follows the same pattern and structure as year 2002. In Figure 4.6 (a), the top panel reveals the p-wave activity that took place throughout the selected interval along the zonal component. P-waves showing localised activity include 2 day, 3 day, and 5 day period waves. The p-wave activity corresponding to a 2 day periodicity is observable in day 223. The power spectrum due to this 2 day wave is about 40 %. P-wave activity with a period of 3 days displays its variability in day 330. This wave activity is characterised by a power spectra reaching about 45 %. The 4 day period p-waves are observable in days 210, 311 and 365. The corresponding power spectra is close to 20 %, 80 % and 45 % respectively. The near 5 day period p-wave is observed in days 235 and 255. These localised wave signatures have their power spectra reaching about 60 % of the normalised power spectrum.

The middle panel in Figure 4.6 (a) shows zonal amplitude variation in a way similar to the variation in the middle panel of Figure 4.4 (a) in year 2002. For year 2007, SDT amplitude is extracted in the third panel of Figure 4.3 (a). The zonal amplitude variation is then pushed to the 2007 wavelet transform in order to visualise SDT modulation.

The third panel in Figure 4.6 (a) displays SDT variability at p-wave periods for year 2007 along the zonal component. The SDT variability in this panel corresponds to a 2 day, 3 day, 4 day and 5 day periodicity. The activity corresponding to the 2 day periodicity is observable in days 260, 338 and 350. These have power spectra reaching about 20 %, 20 % and 45 % of the normalised power spectrum respectively. The SDT waves active at 3 day periodicity are observed in days 295 and 348. The respective power spectra for these signatures reach about 85 % and 20 % of the normalised power spectrum respectively. The activity occurring at 4 day periodicity in the third panel of Figure 4.6 (a) is observable in days 230 and 320. These have power spectra reaching about 20 % and 60 % of the normalised power spectrum respectively. There is some localised activity in the 5 day periodicity in day 256. The activity in this day registers the power spectrum of about 45 % of the normalised power spectrum.

When studying simultaneously the wave variability in the top panel and the bottom panel of Figure 4.6 (a), a broad near 6 day p-wave activity with a power spectrum nearing 60 % of the normalised power spectrum is observed. This activity stretches from day 230 to just before day 260. Close examination shows that it has local maxima near day 230 and in the vicinity of day 255. SDT signatures in the bottom panel coinciding with this activity are observable near days 230 and 255. The possible modulation in day 230 is shown with white circles while a more interesting activity in day 255 is shown with a red circle. The possible modulation in day 255 took place about a week prior the minor SSW event. The event will be studied further in Chapter 5. Another possible SDT modulation took place in day 295. A 4 day period p-wave with normalised wave power reaching about 45 % may have modulated an SDT signature with 85 % of the normalised power spectrum.

The p-wave activity and tidal modulation in the meridional component is shown in Figure 4.6 (b). In this figure, the top panel reveals p-wave activity that took place throughout the selected interval. P-waves showing localised activity include 2 day, 3 day, and 5 day period waves. The p-wave activity corresponding to a 2 day periodicity is observable in days 282, 290, 312 and day 340. The normalised power spectra due to a 2 day wave is 20 % for days 282, 290 and day 340 while it is 75 % of the normalised power spectrum for day 312. P-waves with a period of 3 days display their variability in days 210, 222 and day 330. These have normalised power spectra reaching about 20 %, 45 % and 45 % of respectively. The 4 day period p-waves are observable in days 245, 263 and 313. The corresponding normalised power spectra is close to 20, 45 and 80 % of the normalised power spectrum respectively. The near 5 day period p-wave is seen in day 292. This localised wave signature has its power spectrum reaching about 45 % of the normalised power spectrum.

The middle panel in Figure 4.6 (b) shows the meridional amplitude variation corresponding to an SDT frequency. Similar to the the middle panel in Figure 4.4 (b), the variation is extracted from the STFT contour plot for year 2007 in the third panel of Figure 4.3 (b). The amplitude variation is pushed to the wavelet transform and the resulting activity is shown in the third panel of Figure 4.6 (b).

The third panel in Figure 4.6 (b) shows the possible SDT modulation by p-waves. The localised wave activity in this panel corresponds with the 2 day, 3 day, 4 day and 5 day periodicity. Wave signatures corresponding to 2 day periodicity can be observed in days 235, 241, 297, 339 and day 351. These are characterised by normalised wave power spectra reaching about 15 %, 15 %, 45 %, 35 % and 45 % respectively. The activity corresponding to 3 day periodicity is seen in days 200, 260 and 320. These have normalised power spectra reaching 20 %, 20 % and 65 % respectively. Wave activity corresponding to 4 day periodicity is seen in days 216, 240, 270 and day 365. These days are observed to have the normalised power spectra reaching the values of 20 %, 20 %, 85 % and 45 % respectively. Activity in the 5 day periodicity is evident in days 295 and 335. They have normalised power spectra reaching 20 % and 45 % respectively.

The possible SDT modulation in the meridional component of year 2007 occurred in days 218, 260, 290 and day 318. In day 218, a near 3 day p-wave with about 20 % normalised power spectrum in the top panel modulated an SDT wave active in the 3 periodicity in the bottom panel. In day 260, a 4 day p-wave with 20 % normalised power spectra possibly modulated an SDT variation with 45 % normalised wave power. This activity is displayed with a red circle and will be studied further in Chapter

5 given the minor SSW event that occurred in day 263. Day 290 sees a 4 day p-wave with 45 % normalised wave power in the top panel of Figure 4.6 (b) possibly modulating an SDT wave with 20 % wave power. Near day 318, a 4 day p-wave with 85 % normalised power spectra may have modulated an SDT activity with 70 % normalised power spectra.

The strength of the p-wave activity in year 2007 follows that of year 2002. In the zonal component, year 2002 saw normalised wave power reaching 100 % near day 250 whereas in year 2007 during the same time period, the wave acitivity has been reduced to 60 %. The maximum p-wave activity in year 2007 was 85 % of the normalised power spectrum and this occurred near day 310. Along the meridional component, year 2007 is more robust compared to the same activity in year 2002. The activity in year 2007 reaches maximum normalised power spectra near day 250 whereas maximum variability in the meridional component of year 2002 is 75 % of the normalised power spectrum. Year 2007 short period p-wave activity is in agreement with the observation by Dowdy et al. (2004) for year 2002 that p-waves are more apparent in the meridional component compared to the zonal component. In the zonal component, a near 5 day p-wave signature was recorded in day 255 close to a week before the minor SSW, a behaviour consistent with previous literature (see Labitzke and Van Loon (1999), Dowdy et al., 2004; Espy et al., 2005; Mbatha et al., 2010 and others).

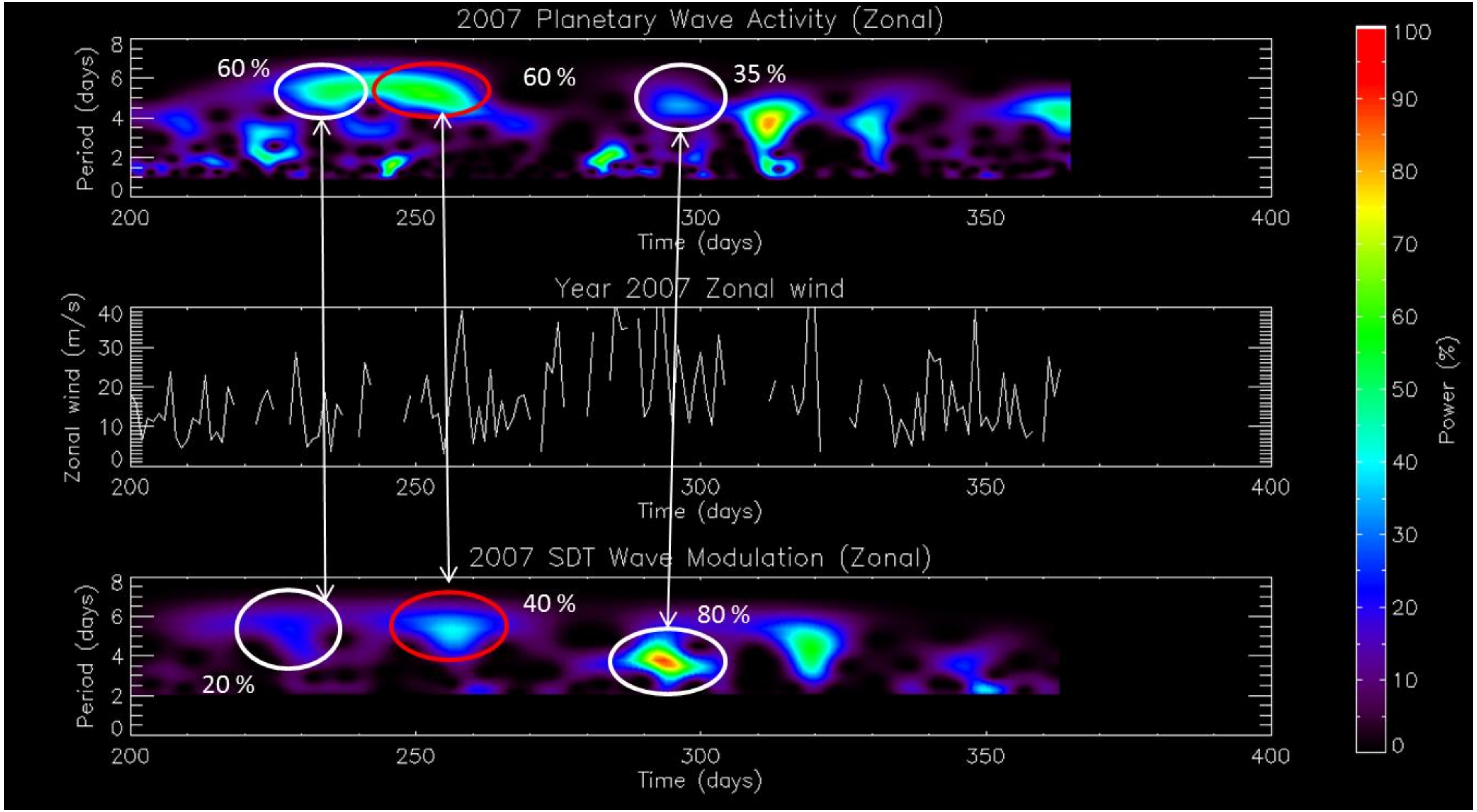

Figure 4.6 (a): Same as Figure 4.4 (a) but for year 2007.

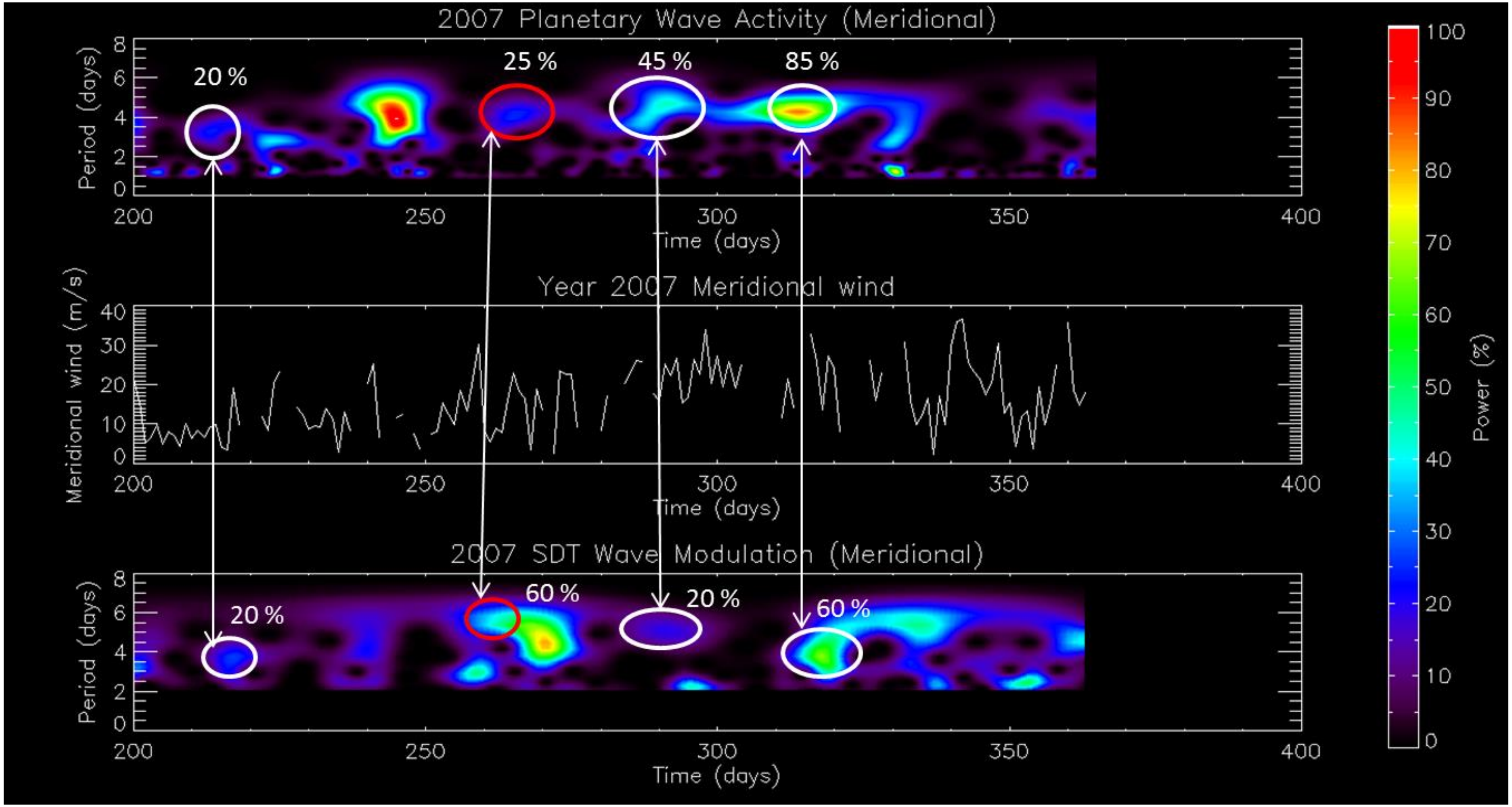

Figure 4.6 (b): Same as Figure 4.4 (b) but for year 2007.

To account for false peaks and the white noise that may be visible in the presented wavelet contour plots, a plot illustrating the correlation between raw wind data and linearly interpolated wind data is presented in Figure 4.7. It is apparent that there is close correlation between the raw wind data and interpolated data with instances where real data is absent barely contributing 20 % of the variation. However, the linear interpolation technique applied in this work presents room for the manifestation of false peaks and white noise as it computes interpolation between two points at any given time. This presents as a potential future perspective, the need to explore a more suitable technique to perform interpolation in similar studies.

Now that the first part towards supporting the proposition (non-linear interaction between p-waves and SDT waves) has been investigated; Chapter 5 employs bispectral analysis to identify peaks and looks for the formation of secondary waves upon possible non-linear interaction between primary waves. Chapter 5 only investigates days where SDT modulation by p-waves was suspected to have occurred.

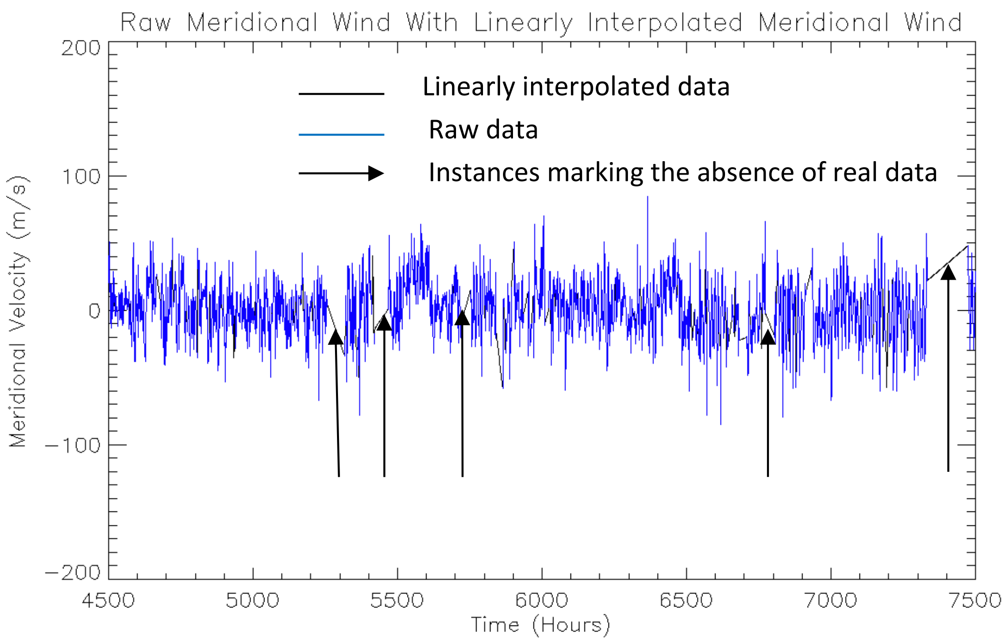

Figure 4.7: A plot showing the actual observed meridional wind data and linearly interpolated meridional wind data to complete the data gap.

Chapter 5

Tides and Planetary Wave Interaction

5.1. Introduction

To further strengthen the previously stated proposition, bispectrum analysis is employed so as to expose possible interactions between p-waves and atmospheric tides. Bispectrum approach germinates from the theoretical suggestion that if there are two or more primary waves interacting non-linearly, secondary waves which are either sums or differences of primary waves will be formed (Spizzichinico, 1969; Tietelbaun and Vial, 1991 etc). Clark and Bergin (1996) defined the bispectrum as the convoluted average of three spectral components capable of revealing phase information of the individual components. Clarks and Bergin (1996) further expounded that the technique works particularly well in revealing the phase coherence of three frequencies where there is a possible summation or subtraction between two frequencies to produce the third. This explanation forms the basis of the case being further investigated in this chapter since there are two primary waves (p-waves and SDT waves) which are assumed to be interacting with each other possibly leading to the formation of secondary waves.

Bispectral analysis finds its applications across many fields because of its ability to simplify complex information. Glass et al. (1997) used the bispectral analysis to measure sedation memory effects of propofol, midazolam, isoflurane and alfentanil in healthy volunteers. They found that the bispectral index (BIS) works well in monitoring levels of responsiveness. They also found that the BIS can predict with a satisfying degree of accuracy the loss of consciousness. In this work bispectral analysis is employed on mesospheric zonal and meridional winds.

The presentation of bispectral plots is divided according to the years being investigated. For each year, the interaction is studied along the zonal component as well as along the meridional component. The data duration for the all the bispectral plots covers the entire 200-300 day range. Signs of a bispectral wave-wave interaction are dispersed throughout the two dimensional plane covering p-waves and atmospheric tides. The study analyses wave-wave interactions which took place a week prior the reported SSW events. The emphasis is on the SDT (tides with 0.5 day periodicity) variability due to the presence of p-waves. The peaks observable in the presented bispectral plots can be assumed to be originating from actual observational data as the applied linear interpolation generates fewer incidences where there is no raw data (see Figure 4.7).

5.1.1. Year 2002 Wave-Wave Interaction

Figure 5.1 shows the possible p-wave-tidal wave interaction occurring during year 2002 along the zonal and the meridional component. The SDT modulation (see section 4.3) showed all the p-wave periods that possibly had an influential modulating effect on SDT variability. In this section, the study tracks these periods and investigates their relationship with SDT waves. The first reported possible p-wave-SDT interaction along the zonal component of 2002 occurred between a 2 day period p-wave and an SDT wave in day 230. The circled peak labelled ‘1’ in the zonal component subplot of Figure 5.1 indicates evidence for this possible interaction. SDT modulation also showed signs of a possible modulation along the zonal component between a 3 day p-wave in day 250 and an SDT. Close examination of the zonal component subplot in Figure 5.1 shows a time localised patch signifying some relationship between a 3 day p-wave and the SDT. This signature is circled and labelled as ‘2’.

Along the meridional component, a 3 day p-wave was reported to have possibly modulated the SDT during day 230. The circled peak labelled ‘3’ in the bottom subplot of Figure 5.1 is indicative of the possible 3 day wave-SDT wave interference. Another p-wave that possibly modulated the SDT along the meridional component has a 6 day period and the resulting peak is circled and labelled ‘4’ in the bottom subplot of Figure 5.1. These results are consistent with p-wave SDT wave modulation suggested in section 4.3 thus strengthening the assertion that p-waves and SDTs interact non-linearly at high altitudes.

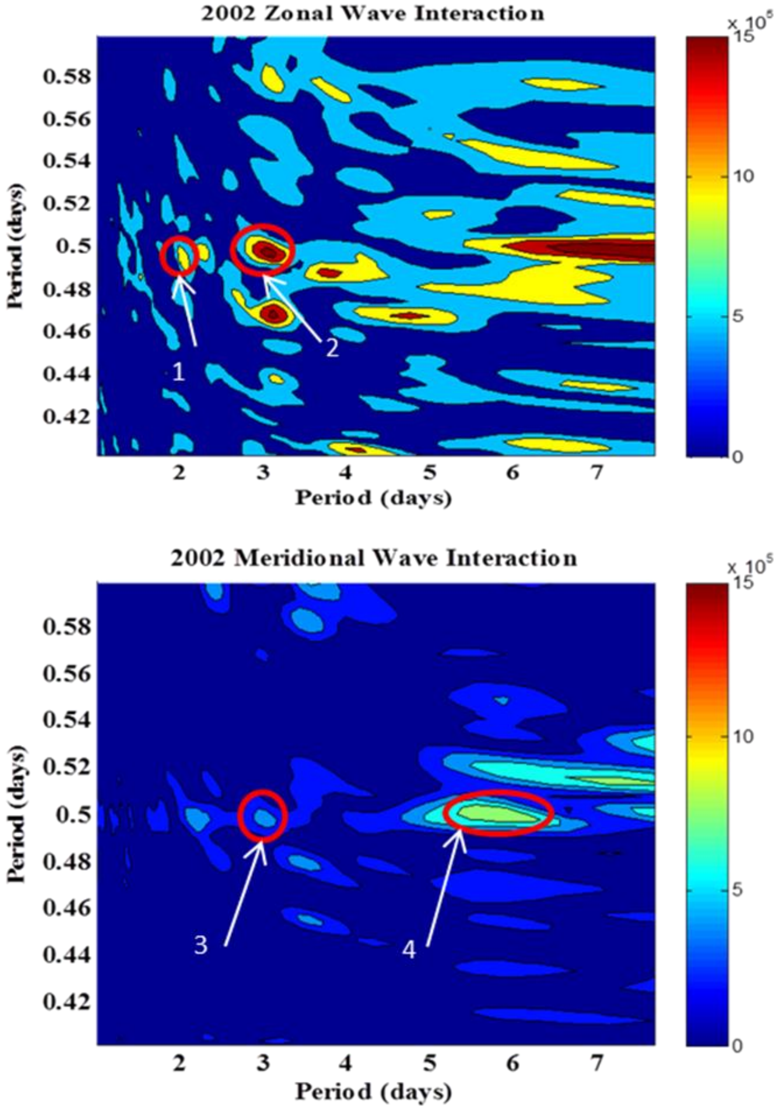

Figure 5.1: The year 2002 p-wave to SDT-wave interaction along the zonal (top subplot) and the meridional (bottom subplot) components. Circled peaks indicate possible interaction between p-waves and SDTs.

5.1.2. Year 2003 Wave-Wave Interaction

A possible wave-wave interaction in the year 2003 along the zonal and meridional components is shown in Figure 5.2. SDT modulation for year 2003 along the zonal component took place near day 290 due to a 4 day active p-wave. This incidence is reported in Figure 4.6 (a) under year 2003 SDT modulation. The zonal component subplot in Figure 5.2 does indicate a well-defined possible interaction signature in the intersection between a 4 day and an SDT periodicity. This signature is circled and labelled ‘1’. The meridional SDT modulation took place during day 280. The 4 day p-wave signature in this day is predicted to have modulated SDT variability. The meridional subplot in Figure 5.2 supports this suggestion by revealing a possible interaction between a 4 day and the SDT. This interaction activity is labelled ‘2’ in the figure. The bispectral analysis results in 2003 are consistent with p-wave-SDT modulation.

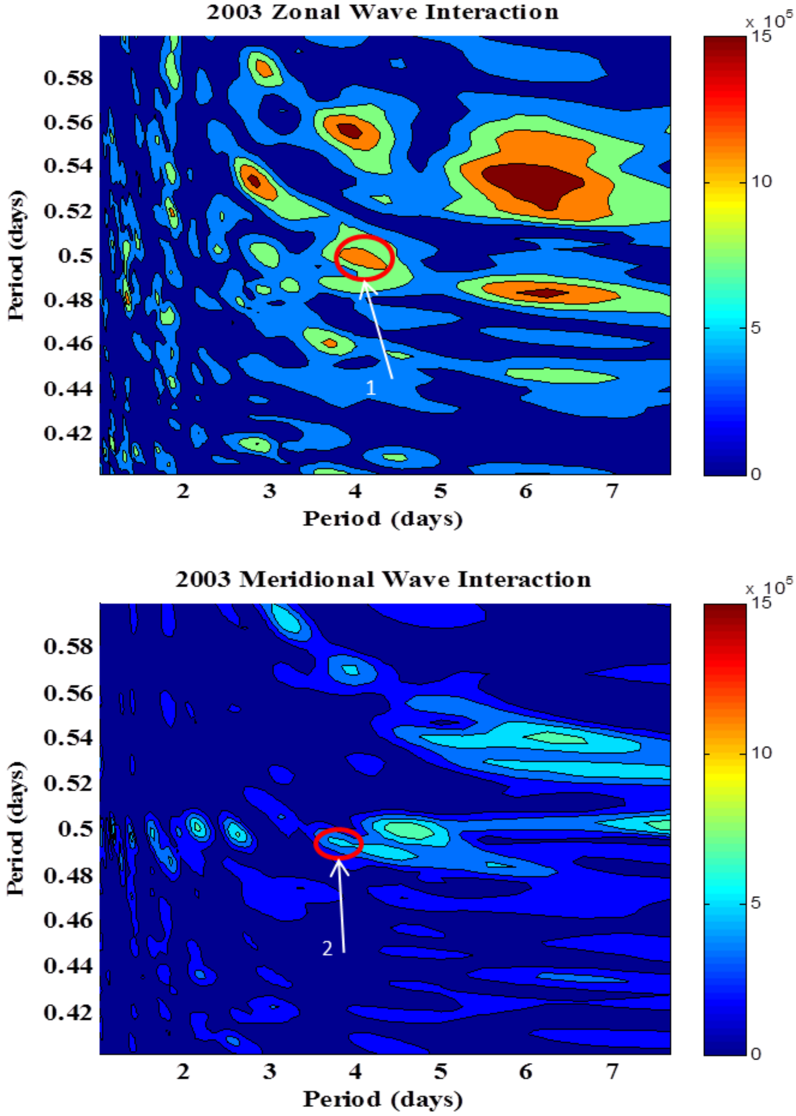

Figure 5.2: Same as Figure 5.1 but for year 2003.

5.1.3. Year 2007 Wave-Wave Interaction

Figure 5.3 presents a possible wave-wave interaction for year 2007. Along the zonal component, the p-wave which possibly modulated an SDT wave had a period of about 6 days and this was in day 255.

The zonal component subplot in Figure 5.3 does display a possible interaction between a 6 day p-wave and an SDT period (see the red circled peak labelled '1' in the figure).

In the meridional component the modulation occurred at approximately day 260. This was a 4 day p-wave modulating an SDT. The circled peak labelled '2' in the meridional component subplot of Figure 5.3 shows the possible interaction between the 4 day p-wave and the SDT. Similar to the results in 2002 and 2003, the findings in 2007 are consistence with p-wave SDT wave modulation. This validates the proposition that p-waves and SDT possibly undergo non-linear interaction with each other.

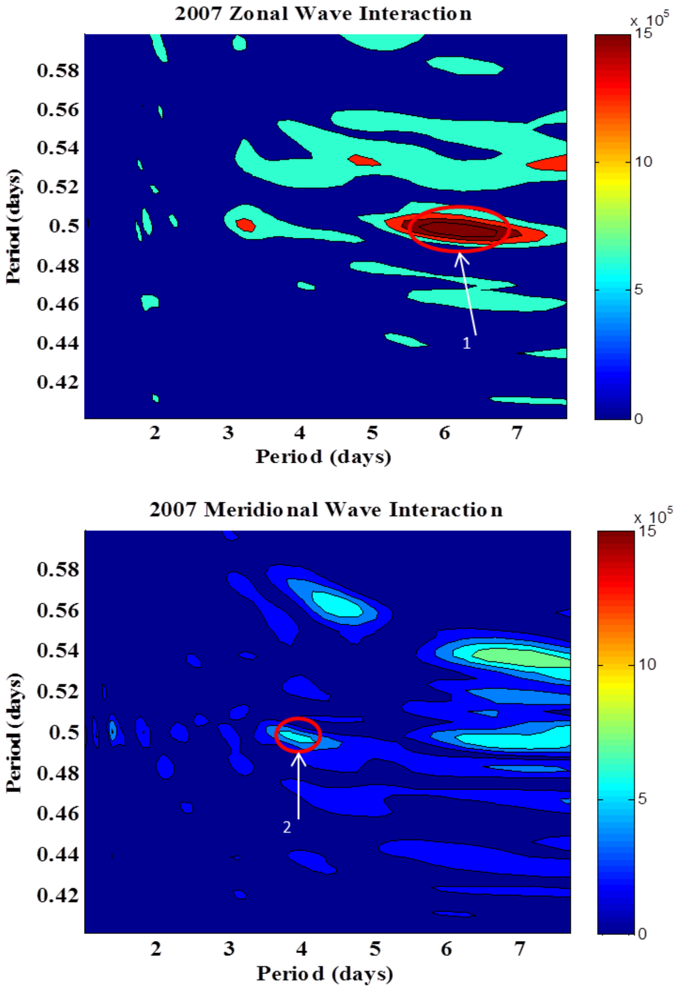

Figure 5.3: Same as Figure 5.1 but for year 2007.

5.2. The Amplitude Spectrum

Wave-wave coupling in Figure 5.1 to Figure 5.3 provides the second step in support of the proposition that there may be a non-linear interaction between p-waves and atmospheric tides. It shows localised wave patches indicating activity between periods which were predicted to undergo modulation in section 4.3. The third step in validating the stated assertion is to search for secondary waves which may be the outcome of a possible interaction between p-waves and SDT waves. For this, the study uses the same periods which were predicted to have undergone modulation in section 4.3.

The depiction of the amplitude spectrum is the final step in the quest to demonstrate the possibility of the non-linear interaction between planetary waves and atmospheric tides. The period is in hours while the amplitude is in meters per second (m/s). The data considered for investigation under this section stretches from day 200 to day 300 for all the years being investigated (2002, 2003 and 2007), an interval encompassing significant warmings. In the said interval (day 200 to day 300), the SDT and secondary wave periods are extracted simultaneously. The presentation of results begins with year 2002.

5.2.1. Investigation of Secondary Waves for Year 2002

Figure 5.4 shows amplitude spectra for zonal and meridional components for the year 2002. The top subplot is a zonal variation while the bottom subplot shows activity along the meridional component. In both zonal and meridional components, SDT amplitude seems to be dominant. P-waves that possibly modulated SDT behaviour as per the findings in section 4.3 are taken with their periods and are made to interact with SDT waves.

The theoretical approach towards extracting secondary wave frequencies involves taking p-wave frequencies which were shown to have possibly modulated SDT behaviour in section 4.3 and which were shown through bispectral plots in section 5.1 to have undergone some non-linear interaction with SDT and adding or subtracting them to SDT frequency. The sum and difference frequencies then represent formed secondary wave frequencies which upon taking an inverse become secondary wave periods. For a 2 day period p-wave, which was found to have possibly modulated the SDT during the winter of 2002 along the zonal component and shown to have had some non-linear interaction with the SDT, the calculation of sum and difference secondary waves, is as follows:

First primary wave period: 48 hours (2 days)

Second primary wave period: 12 hours (SDT)

Frequency of the sum secondary wave = [(1/12)+(1/48)] per hour

= 0.1042 per hour

Period of the sum secondary wave = 1/0.1042 per hour

= 9.6 hours

Similarly, by subtracting a 2 day p-wave frequency from an SDT frequency, the formed difference secondary wave period is 16 hours. The subsequent task is to identify in the amplitude spectrum the calculated periods (9.6 and 16 hours) thus validating the non-linearity of the interaction. As shown in Figure 5.4, the amplitude spectrum shows in black arrows 9.5 and 16 hour peaks with a difference secondary wave (9.5 hours) slightly deviating from the theoretical value (9.6). Continuing in the same way, the secondary waves formed due to a possible interaction between a 3 day p-wave and the SDT during the winter of 2002 in the zonal component, have 10.3 and 14.5 hour periods for sums and differences respectively. These are observable and represented in Figure 5.4 (see red arrow mark). In the meridional mean wind, a 4 day p-wave-SDT possible interaction resulted in theoretical sum and difference secondary waves with 10.6 and 13.7 hour periods respectively. These are indicated with black arrows and observable in the bottom subplot of Figure 5.4. Another possible interaction between a 6 day p-wave and the SDT yielded theoretical sum and difference secondary wave periods equalling 11.1 and 13.1 hours respectively. These are also observable in the meridional amplitude spectrum in Figure 5.4 (see red arrows in the bottom subplot of Figure 5.4). The blue straight line depicts the 95 % confidence line from which significant peaks are deduced.

Table 5.1 shows a summary of results from Figure 5.4. The first panel of Table 5.1 presents theoretical p-waves predicted to have non-linearly interacted with SDTs. Expected secondary waves formed due to frequency summation and due to subtraction are presented. The second row in the first panel then gives observed periods thus enabling the comparison between calculated periods and ones extracted from the amplitude spectrum. Similarly, the second panel does this but for the meridional mean wind. From these results, it is apparent that there is high correlation between the calculated secondary waves and the observed periods.

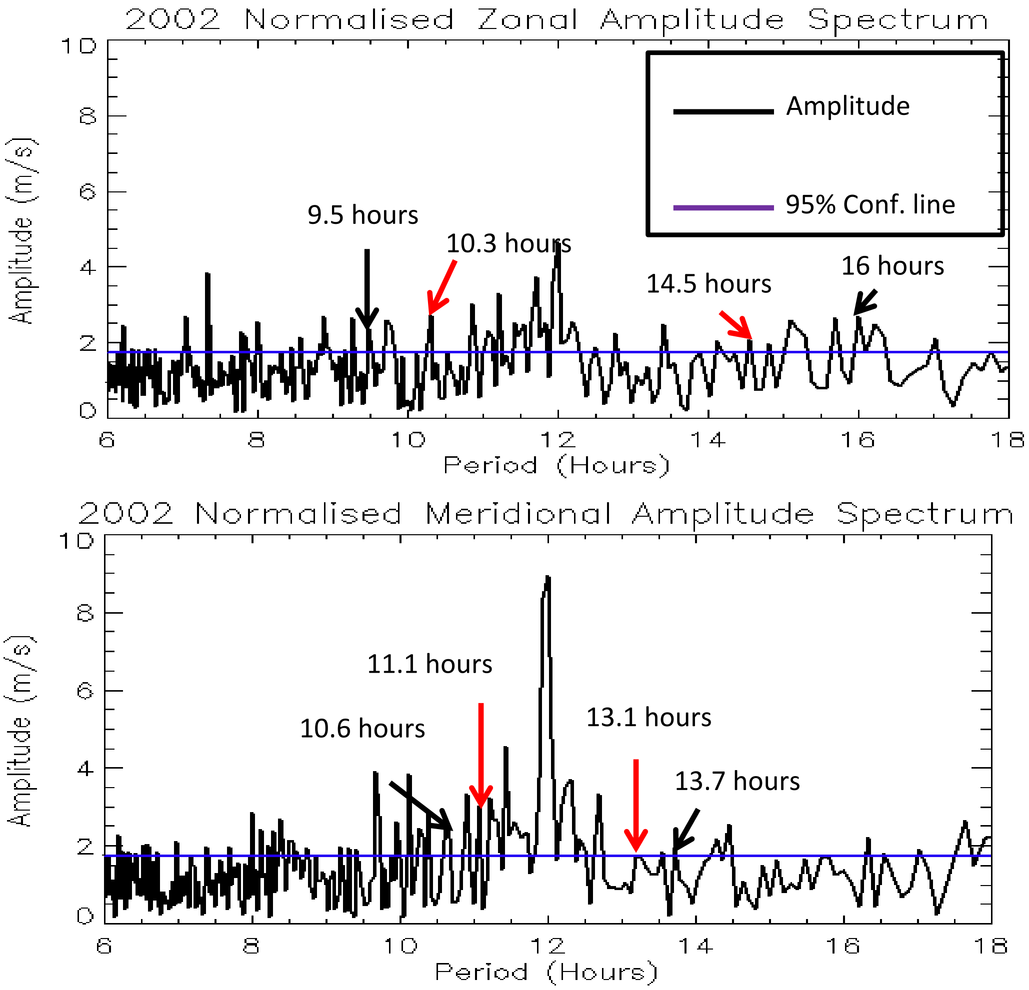

Figure 5.4: The wind amplitude shown as a function of a wave period along the zonal (top subplot) and the meridional (bottom subplot) component for year 2002 together with the 95 % confidence line (blue variation).

Table 5.1: The Table of Theoretical and Observed Periods displaying possible interactions between Planetary and SDT Waves for year 2002 as per the SDT Modulation in Section 4.3.

2002 Zonal Periods					
	Waves	P-Waves	SDT	Secondary Waves	
				Sums	Differences
Period (hours)	Theoretical Values	48	12	9.6	16
	Observation	-	12	9.5	16
Period (hours)	Theoretical Values	72	12	10.3	14.4
	Observation	-	12	10.3	14.5
2002 Meridional Periods					
	Waves	P-Waves	SDT	Secondary Waves	
				Sums	Differences
Period (hours)	Theoretical Values	96	12	10.6	13.7
	Observation	-	12	10.6	13.7
Period (hours)	Theoretical Values	144	12	11.1	13.1
	Observation	-	12	11.1	13.1

5.2.2. Investigation of Secondary Waves for Year 2003

The investigation of the formation of secondary waves in year 2003 follows the same format as for year 2002. The plot depicting the amplitude spectrum is shown in Figure 5.5. Secondary wave peaks are observed before and after the SDT (12 hour period) in Figure 5.5. The extraction of secondary wave periods is informed by the possible p-wave SDT modulation as reported in section 4.3. According to the indications from section 4.3, possible modulation in both the zonal and meridional components during the winter of 2003 was between a 5 day (120 hours) period and an SDT wave. Similar to the analysis for year 2002 and for both zonal and meridional components, the theoretically formed sum secondary wave periods and difference secondary wave periods are 10.9 and 13.3 hours respectively. These are observable in Figure 5.5 along both zonal and meridional components. The interesting observation in the 2003 zonal amplitude spectrum is the absence of a defined larger SDT peak at 12 hours. This is not realistic and may be due to data gaps causing an error in analysis. Table 5.2 presents periods derived from frequency sums and differences that were produced from the interaction between theoretical p and SDT waves. The presented results depict a strong agreement between theoretical secondary wave periods and periods observed from the amplitude spectrum thus enhancing the view that there is non-linear interaction between p-waves and atmospheric tides.

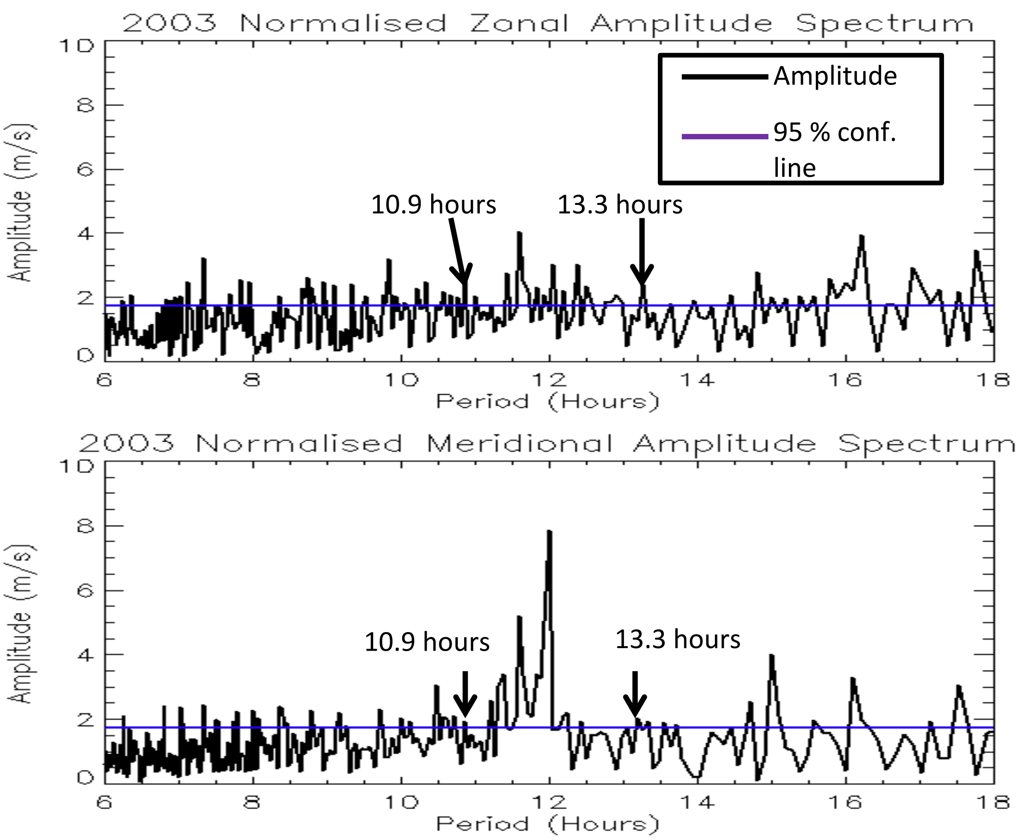

Figure 5.5: Same as Figure 5.4 but for year 2003.

Table 5.2: Same as Table 5.1, but for Year 2003

2003 Zonal Periods					
	Waves	P Waves	SDT	Secondary Waves	
				Sums	Differences
Period (hours)	Theoretical Values	120	12	10.9	13.3
	Observation	-	11.6	10.9	13.3
2003 Meridional Periods					
	Waves	P Waves	SDT	Secondary Waves	
				Sums	Differences
Period (hours)	Theoretical Values	120	12	10.9	13.3
	Observation	-	12	10.9	13.3

5.2.3. Investigation of Secondary Waves for Year 2007

The evaluation of the formation of secondary waves upon possible p-wave-SDT wave interaction for year 2007 is similar to the secondary wave formation of year 2002. The study begins with the presentation of the amplitude spectrum in Figure 5.6. The amplitude variation is along both the zonal and the meridional component. Noticeable amplitude peaks at 12 hour periods are seen along both zonal and meridional components symbolising SDT dominance. Some evidence of secondary waves is notable throughout the 6-18 hour period range in Figure 5.6. In the zonal component, a theoretical interaction between a 6 day p-wave and the SDT was performed as per the reported possible SDT modulation. Theoretical sum secondary wave periods and difference secondary waves were calculated to be 11 and 13 hours respectively. After simultaneously extracting secondary waves and SDTs from the 200 – 300 day interval, the amplitude spectrum in Figure 5.6 shows the 11 hour mode agreeing with the theoretical prediction and a 12.9 hour mode corresponding to a 13 hour theoretically suggested period. In the meridional component, a 4 day p-wave yielded, upon interaction with the SDT, 10.6 and 13.7 hour modes which are all confirmed by observations in the amplitude spectrum in the bottom subplot of Figure 5.6. The 13.7 hour mode is slightly below the 95 % confidence line while all other secondary peaks are above. Similar to Table 5.1 and Table 5.2, Table 5.3 compares the theoretical values formed due to predicted SDT modulation to observed periods extracted from the amplitude spectrum. Results for year 2007 show in the same way as the results for year 2002 and 2003 a strong correlation between predicted secondary wave periods and observed ones thus validating the proposition that there is a non-linear interaction between p-waves and atmospheric tides.

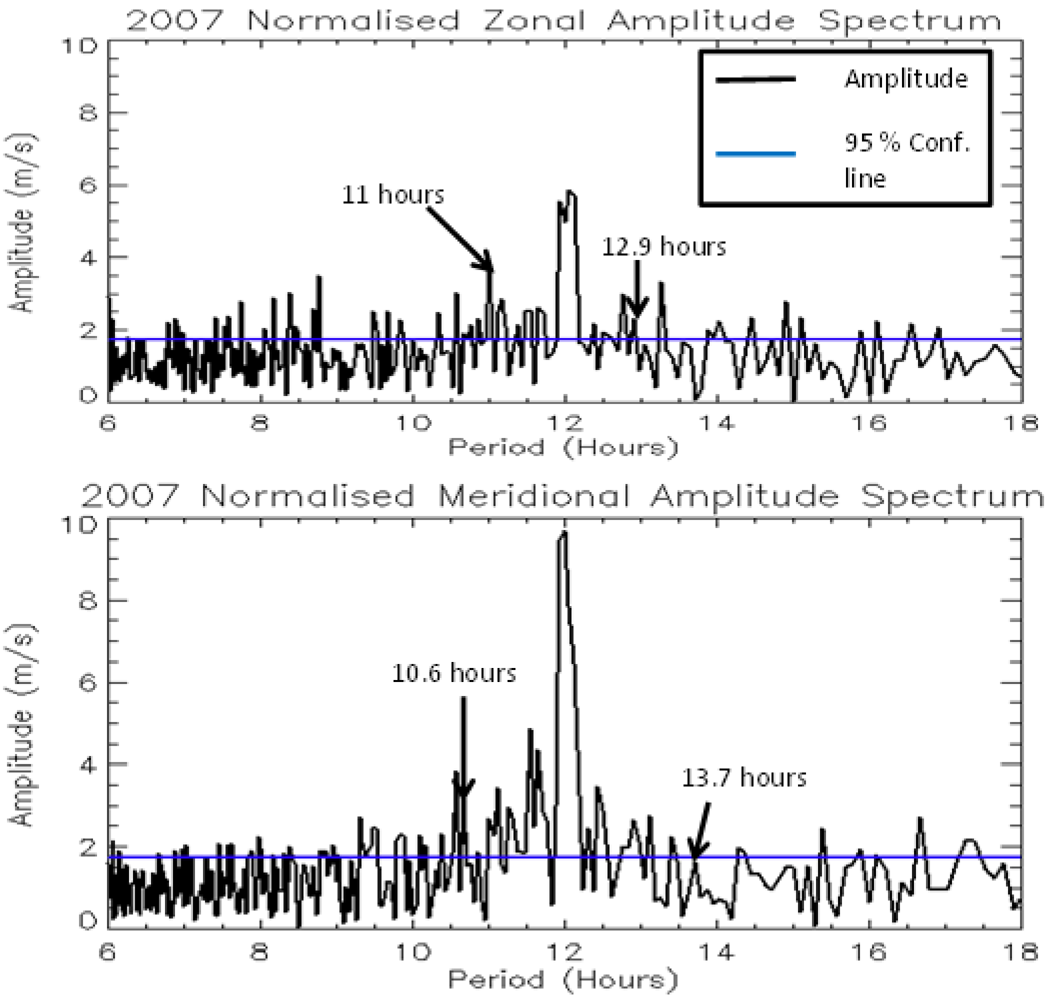

Figure 5.6: Same as Figure 5.4 but for year 2007.

Table 5.3: Same as Table 5.1, but for Year 2007

2007 Zonal Periods					
	Waves	P Waves	SDT	Secondary Waves	
				Sums	Differences
Period (hours)	Theoretical Values	144	12	11	13
	Observation	-	12	11	12.9
2007 Meridional Periods					
	Waves	P Waves	SDT	Secondary Waves	
				Sums	Differences
Period (hours)	Theoretical Values	96	12	10.6	13.7
	Observation	-	12	10.6	13.7

The results shown in section 5.2 represented the third and final technique in support of the assertion that there is a non-linear interaction between p-waves and atmospheric tides during SSW events. From Chapter 4 to Chapter 5, evidence in support of the said proposition has been provided.

According to Spizzichinico (1969), when non-linear interaction between primary waves occurs, a secondary wave is formed. The frequency and phase of the formed secondary wave equals the sum or a difference of the individual frequencies and phases of the primary waves. Pancheva and Mitchell (2004) in their quest to find evidence of non-linear coupling of p-waves in the MLT region, used the above mentioned theory to observe formed secondary period modes upon 15 day wave- SDT interaction. Their theoretical calculations yielded a sum secondary wave with a period equalling 11.6 hours and a difference secondary wave period of 12.4 hours. Kai et al., (2013) in their investigation of the non-linear coupling between a quasi 2 day wave and tides at Mauni observed the presence of quasi 16 hour modes (15.8 hours and 16.2 hours) which were an outcome of a possible interaction between a quasi 48 hour wave and an SDT. Mthembu et al., (2013) also used the above mentioned theory to extract the amplitude of the secondary wave with a period of 11.75 hours formed due to the interaction between an SDT and the 23 day wave in the 2005 zonal mean wind. Mthembu et al., (2013) also extracted 10.9, 11.4 and 11.6 hour modes which were outcomes of an interaction between SDT wave and 5, 10 and 16 day waves respectively. In a method similar to the above mentioned studies, this work extracts secondary waves formed due to a possible non-linear interaction between p-waves established in section 4.3 and SDTs. The study focused on secondary waves formed around an SDT wave, with a period range stretching from 6 to 18 hours.

The significant outcome that can be drawn from the presented results, is that formed secondary waves occur before and after the SDT amplitude peak as previously reported in the literature (see Beard et al., (1999); Pancheva and Mitchell (2004); Mthembu et al., (2013) and others). This is in agreement with the above mentioned theoretical stipulation by Spizzichinico (1969). The possible interactions presented in this work occur close to a week prior the occurrence of minor SSW events (see section 4.3) thus hinting a possible relationship between the p-wave-SDT interaction and the manifestation of significant warmings. The objective analysis employed during the investigation of secondary wave periods in this work displays high level of precision. This is supported by good agreement between theoretical and observed periods with the highest deviation equalling 0.1 hours. This study also revealed the role that p-waves with 3, 4 and 6 day periods play prior the formation of SSW events and in the p-wave-SDT non-linear interaction. The existing literature mainly reported on quasi 2 day waves, 5 day waves and larger period waves such as waves in the 10-16 day range as possible triggers of stratospheric warming events and wave-wave non-linear interaction occurring in the MLT region (see Dowdy et al., (2004); Pancheva and Mitchell (2004); Mthembu et al., (2013); Kai et al., (2013) and others).

Techniques employed to investigate the non-linear interaction between p-waves and atmospheric tides in this work have been applied by a number of researchers including Teitelbaum and Vial (1991), Clark and Bergin (1996), Beard et al. (1997), Beard et al. (1999), Angelatsi and Forbes (2001), Pancheva and Mitchel (2004), Mthembu (2013) and others. Teitelbaum and Vial (1991) suggested that upon wave-wave interaction, an ensemble of secondary waves will be formed from which two will be a sum and a difference of a particular p-wave and tidal wave interaction. Clark and Bergin (1996) investigated the non-linear interaction between primary waves using bispectral analysis. Beard et al. (1999) used, in a way similar to this study both the bispectrum and the formation of a secondary wave to demonstrate evidence of non-linear interaction between p-waves and a semi-diurnal tide. Beard et al. (1999) however observed that p-wave SDT interaction is not the only source of SDT modulation. They called for further research on p-wave activity to clarify some ambiguities. Angelatsi and Forbes (2001) looked at the non-linear interactions in the upper atmosphere. Mthembu (2013) used the bispectral analysis to illustrate the possible non-linear interaction between a 10 day p-wave and an SDT that took place in the vicinity of a 2002 major SSW event.

The research done in this dissertation contributes to the above mentioned work and to the efforts of many other researchers to understand in depth, the global manifestation of p-waves and tidal variability in the MLT region. The next chapter summarises the obtained results and future perspectives.

Chapter 6

Summary and Future Work

6.1. Summary

The main goal of this work was to map out the planetary wave activity in the mesosphere lower thermosphere region during minor SSW events. The emphasis was on the planetary waves (p-waves) with a period range of 2 to 6 days. It was also intended to investigate how the formation and manifestation of these short term p-waves modulates the atmospheric tidal wave activity. The data which was to be considered stretched from year 1998 to the year 2008. It then became necessary that a criterion to establish years of interest had to be designed. The criterion was informed by a finding by Matsuno (1971) that planetary wave activity induces an arbitrary rise in atmospheric temperature. The procedure included searching for years with significant warmings and selecting intervals with minor warming events. The atmospheric wave dynamic behaviour corresponding to those time intervals was then studied. The uniqueness of this work originates from the understanding that no or very few studies on the p-wave behaviour have been carried out specifically looking at short term periods during minor SSW events.

The study through the utilization of NCEP data showed that years with significant temperature enhancements were 2002, 2003 and 2007. Zonal and meridional mean winds for the respective years were then investigated using signal processing techniques which constitute the application of a Fourier Transform. The first revelation was that semi-diurnal tides are the most dominant tidal waves and they were more likely to interact with planetary waves. This was illustrated through STFT plots in Chapter 4 and it was the case for all three years in consideration. Amplitudes corresponding to an SDT frequency were then extracted so as to study how SDTs interact with planetary waves. The duo-facet task which includes displaying short term p-wave activity and checking for a possible non-linear interaction with tides was dealt with simultaneously. This means that while viewing active p-waves during minor warmings, we were also studying their interaction with atmospheric tides. To establish with confidence, the possible existence of non-linear interaction, a three step procedure was followed. The first step was to check for modulation between p-waves and atmospheric tides. This was performed using wavelet analysis in section 4.3. The second step involved the visualisation of the wave to wave interaction and this was done using bispectral analysis in Chapter 5. The third and final step to demonstrate possible non-linearity in interaction was to plot amplitude versus period for all the years of interest along the zonal and meridional components.

The study succeeded in displaying planetary wave activity that takes place during minor warmings in the MLT region. The challenge was in year 2003 were data gaps were prevalent. For all three years considered (2002, 2003 and 2007), some indications of a possible modulation were shown to exist. This can be seen in the wavelet plots produced using SDT amplitudes in comparison with p-wave activity in the SDT modulation under section 4.3. The modulation was further supported by wave to wave interaction plots that were produced using bispectral analysis. At this stage it was apparent that there is some kind of an interaction between p-waves and atmospheric tides. Amplitude spectrum made a case that the interaction is non-linear for all the years that were studied. This was made visible by the formation of secondary waves associated with interactions between p-waves and atmospheric tides in section 5.2.

6.2. Future Work

This study should set precedence for a similar investigation in the Northern hemisphere. In addition to the established planetary wave activity during minor SSW events, it would be interesting to see the temperature structure or envelope that accompanies the short term p-wave behaviour. Also, one is interested in knowing whether or not short term wave activity and minor warmings influence the occurrence of major SSW events. Limitations introduced by the application of the linear interpolation technique when completing data gaps increase the need to adopt a better interpolation technique when carrying out similar studies in future.

References

Andrews, D. G., Halton, J. R, and Leovy, C. B.: Middle Atmospheric Dynamics, 489 pp, Elsevier, New York, 1987

Baldwin, M., Hirooka, T., O'Neill, A., and Yoden, S.: Major stratospheric warming in the Southern Hemisphere in 2002: Dynamical aspect of the ozone hole split, 2003

Beard, G. A., N. J. Mitchelle, P. J. S. Williams and M. Kunitake.: Non-linear interaction between tides and planetary waves resulting in periodic tidal variability. J. Atmos. Solar-Terr. Phys. 61, 1999

Butchart, N., Scaife A. A, Bourqus M., de Grandpre, J., Hare, S. H. E., Kettleborough, J., Langematz, U., Manzini, E., Sassi, F., Shibata, K., Shindell, D., Sigmond, M.: Simulations of anthropogenic change in the strength of the Brewer Dobson circulation, 2006

Brook, D. And Wayne, R. J.: Signal processing: Principles and applications, Edward Arnold London, 1988

Chang, L. C., Scott E. P. and H. –L. Liu.: Short term variation of the s = 1 nonmigrating semidiurnal tide during the 2002 stratospheric warming. J. Geophys. Res. 114, 2009: DO3109

Chapman, S. and R. S. Lindzen. Atmospheric tides. Holland: Riedel, 1970

Chau, J. L., Fejer, B. G. and Goncharenko, L. P.: Queit variability of equatorial $E \times B$ drifts during a sudden stratospheric warming event, 2009

Chihoko Yamashita, Han-Li Liu and Xinzhao Chu: Gravity wave variations during the 2009 stratospheric sudden warming as revealed by ECMWF-T799 and observations, Geophys. Res. Letters, Vol. 37, L22806, doi:10.1029/2010GL045437, 2010

Clark, R. R. and Bergin, J. S.: Bispectral analysis of mesospheric winds. Journal of Atmosphere and Solar-Terrestrial Physics 59, 1997: 629-639

Day, A. K., Taylor, M. J., and Mitchell, N.: Mean winds, temperatures and the 16 and 5-day planetary waves in the mesosphere and lower thermosphere over Bear Lake Observatory (42˚ N, 111˚ W), 2012

Espy, P.J and R.E. Hibbins: Mesospheric planetary waves over Antarctica during 2002, Colorado Research Associates, North West Research Associates, Boulder, Colorado, USA, 2005

Fritts, D. C. and Vincent, R. A. "Mesospheric momentum flux studies at Adelaide Australia: Observations and a gravity wave/tidal interaction model." J. Atmos. Sci, 44, 1987: 605-619

French, W. J. R., G. B. Burns, and P. J. Espy (2005), Anomalous winter hydroxyl temperatures at 69_S during 2002 in a multiyear context, Geophys. Res. Lett., 32, L12818, doi:10.1029/2004GL022287

Goncharenko, L. P., Chau, J. L., Liu, H. L. and Coster, A. J.: Unexpected connections between the stratosphere and ionosphere, 2010

Greenwald, R. A., Baker, K. B., Dudeney, J. R., Pinnock, M., Jones, T. B., Thomas, E. C., Villain, J. -P., Cerisier, J. -C., Senior, C., Hanuise, C., Hunsucker, R. D., Sofko, G., Koehler, J.,Nielsen, E., Pellinen, R., Walker, A. D., Sato, N, and Yamagishi, H.: DARN/SuperDARN: A global view of the dynamics of high latitude convections, Space Sci. Rev, 71, 761-796, 1995

Hagan, M. E., Forbes, J. M. and C. McLandress.: Diurnal tidal variability in the 1 upper mesosphere and lower thermosphere. Ann. Geophys. 15, 1997: 1176-1186

Hall, G. E., MacDougall, J. W., Moorcroft, D. R., St-Maurice, J. P., Manson, A. H., and Meek, C.E.: Super dual auroral radar network observations of meteor echoes, Journal of Geophysical Research, 102, 14603-14614, 1997

Hibbins, R. E., Espy, P. J. and Jarvis, M. J.: Quasi-biennial modulation of the semidiurnal tide in the upper mesosphere above Halley, Antarctica. Geophys. Res. Lett. 34, 2007: L21804

Hoffmann, P.: Latitudinal and longitudinal variability of mesospheric winds and temperatures during stratospheric warming events. J. Atmos. Solar Terr. Phys. 69, 2007

Holton, J. R.: The role of gravity wave induced drag and diffusion in the momentum budget of the mesosphere, Journal of the Atmospheric Science, 39, 791-799, 1982

Hussey, G.C., C.E. Meek, A.H. André, A.H. Manson, G.J., Hall and C.M. Sofko.: A comparison of Northern hemisphere wind using SuperDARN meteor trail and MF radar wind measurements. J. Geophys. Res. 105 (2000): 18053–18066.

Jacobi, Ch.: Non-linear interaction of planetary waves and semidiurnal tide as seen from midlatitude mesopause region winds measured at Collm, Germany. Meteorol. Z., 1999: 28-35

Jenkins, B. and M. J. Jarvis.: Mesospheric winds derived from SuperDARN HF radar meteor echoes at Halley, Antarctica. Earth space 51, 1999

Johnson, R. M. and Killeen, T. L.: The Upper Mesosphere and Lower Thermosphere: A Review of Experiment and Theory. American Geophysical Union, 1995

Labitzke, K. and B. Naujokat.: The lower arctic stratosphere in winter since 1952. SPARK Newsletter, 15, 2000: 11-14

Labitzke, K., and H. Van Loon: The Stratosphere: Phenomena, History, and Relevance, Springer-Verlag, New York, 1999

Lester, M.: The Super Dual Auroral Radar Network (SuperDARN): An overview of its development and science. Dept of Physics and Astronomy, University of Leicester, Leeicester LEI, United Kingdom, J. Geophys. Res. Space Physics, 2013

Lima, L. M., Alves, E. O., Batista, P. P., Clemesha, B. R., Medeiros, A. F. and Burit, R. A.: Sudden stratospheric warming effects on thermospheric tides and 2-day wave dynamics at 7° S. J. Atmos. Solar-Terr. Phys. 2012

Lindzen, R. S.: Atmospheric tides. Annual Review of Earth and Planetary Sciences, 1979: 199-225.

Lovell A. C. B., and Clegg, J. A.: Characteristics of radio echoes from meteor trails, Proc. Phys. Soc. 60, 1948

Malinga, S. B. and Poole, L. M. G.: The 16-day variation in the mean flow at Grahamstown (33.3° S, 26.5° E), Annales geophysicae, 20, 2027-2032, 2002

Malinga, S. B. And Ruohoniemi, J. M.: The quasi two-day wave studied using the Northern Hemisphere SuperDARN HF radars, Annales Geophysicae, vol. 25, pp. 1767-1778, 2007

Mak, M.,: Atmospheric dynamics. Cambridge University Press, 2011

Matsuno, T.: A dynamical model of the stratospheric sudden warming. J. Atmos. Sci. 28, (1971): 1479-1494

Matthews, D.M., M.L. Parkinson, P.L. Dyson and J.C. Devlin.: Optimising estimates of mesospheric neutral wind using the TIGER SuperDARN radar. Adv. Space Res. 38 (2006): 2353–2360

Mbatha, N., Sivakumar, V., Malinga, S. B., Bencherif, H., and Pillay, S. R.: Study on the impact of sudden stratosphere warming in the upper mesosphere-lower thermosphere regions using satellite and HF radar, Atmos. Chem. Phys, 10, 1-8, 2010

Mbatha, N. B.: Study on 2002 Sudden Stratospheric Warming, Mesosphere-Lower Thermospheric wind structure and dynamics and middle atmospheric temperature structure, based on SuperDARN HF RADAR, LIDAR, Riometer, Satellites and Models, PhD thesis, University of KwaZulu Natal, 2012

Misiti, M., Y Misiti, G. Oppeinheim and J. Poggi. Wavelet Toolbox. The MathWork, 1996

Mthembu, S. H.: An investigation of Ultra Low Frequency (ULF) pulsations using radar data and solar wind data. Durban: University of KwaZulu-Natal, 2007

Mthembu, S. H, V. Sivakumar, N. J. Mitchelle, and S. B. Malinga.: Studies on planetary waves and tide interaction in the mesosphere/lower thermosphere region using meteor RADAR data from Rothera (68° S, 68° W), Antarctica. J. Atmos. Solar-Terr. Phys. 63, 2013

Mthembu, S. H.: Studies on atmospheric tides and planetary waves in the mesosphere-lower thermosphere (MLT) region using SuperDARN HF radars and meteor radar. PhD thesis, University of KwaZulu Natal, 2013

Murphy, D. J., W. J. R. French and R. A. Vincent.: Long-period planetary waves in the mesosphere and lower thermosphere above Davis, Antarctica. Atmos. Solar-Terr Phys. 69, 2007

Nakamura, T, T Tsuda and M Tsutsumi.: Meteor wind obsevation with the MU radar. Radio Sci 26 (1991): 875-869.

Ortland, D. A. and M. J. Alexander. "Gravity wave influence on the global structure of the diurnal tide in the mesosphere and lower thermosphere." J. Geophys. Res. 111, 2006: A10S10

Pancheva, D.: Evidence for non-linear coupling of planetary waves and tides in the lower thermosphere over Bulgaria. J. Atmos. Terr. Phys. 62, 2000

Pancheva, D. V., N.J. Mitchell.: Planetary waves and variability of the semidiurnal tide in the mesosphere and lower thermosphere over Esrange 68 degrees N, 21 degrees E during winter. J. Geophys. Res. 109, 2004

Pancheva, D.: Evidence of non-linear coupling of planetary waves in the mesosphere and lower thermosphere. Phys. Chem. Earth PT C 26, 2001: 411-418

Schlatter, T. W.: Atmospheric composition and vertical structure, 2009

Sridharan, S., Sathishkumar, S. and Gurubaran, S.: Variabilities of mesospheric tides and equatorial electrojet strength during major stratospheric warming events. Ann Geophys. 27, 2009

Randel, W. J.: Global variations of zonal mean ozone during stratospheric warming events. J. Atmos. Sci. 50, 1993

Riggin, D. M., Fritts D. C., Jarvis, M. J. and G. O. L., Jones.: Spatial structure of the 12-hour wave in the Antarctic as observed by radar. Earth Planets Space 51, 1999

Saha, K.: The Earth's atmosphere (Its physics and dynamics), University Park, USA, 2008

Sandford, D.J., C.L. Beldon, R.E. Hibbins and N.J. Mitchell.:Dynamics of the Antarstic ans Arstic mesosphere and lower thermosphere: 1. Mean winds. Atmos. Chem. Phys. 10 (21) (2010): 10273-10289.

Schoeberl, M. R.: Stratospheric warmings: observations and theory. Rev. Geophys. 16, 1978: 521-238

Spizzichinico, A.: Etude des interactions entre les differentes composantes du vent dans la haute atmosphere: 3. Theorie des interactions non linearities entre les ondes atmospheriques. Ann. Geophys. 25, 1969: 773-783

Torrence, C. and Compo, G. P.: A practical guide to wavelet analysis, Bulletin of the American Meteorological Society, 79, 61-78, 1998

Tietelbaum, H. and F. Vial.: On the tidal variability induced by non-linear interaction with planetary waves. J. Geophys. Res. 96, 1991: 14 169-14 178

Tsutsumi, M., Murphy, D. J., Aso, D. C., Fritts, R. E., Hibbins A. J., McDonald, D. M., Riggin, M., and R. A. Vincent,: Source regions for Antarctic MLT non-migrating semidiurnal tides. 2009

Volland, H.: Atmospheric tidal and planetary waves. Springer, 1988

Walterscheid, R. L., Sivjee G.G., Roble, R. G.: Mesospheric and Lower Thermospheric manifestations of a stratospheric warming event over Eureka, Canada (80˚ N), Geophysical research letters, Vol. 27, No. 18, p 2897-2900, 2000